C
83
27
Jy 2

UNIVERSITY OF MICHIGAN
JUN 28 1955
SCIENCE LIBRARY

PR

MONTHLY WEATHER REVIEW

VOLUME 83 NUMBER 3

MARCH 1955

CONTENTS

	Page
On the Numerical Prediction of Precipitation. J. Smagorinsky and G. O. Collins	53
A Nomogram Based on the Theory of Extreme Values for Determining Values for Various Return Periods. Leonard L. Weiss	69
The Weather and Circulation of March 1955—A Month of Extreme Heat and Cold over the United States. William H. Klein	72
Damaging Cold Wave of March 23–31, 1955. C. L. Kibler and R. H. Martin	78
Charts I–XV	

U. S. DEPARTMENT OF COMMERCE • WEATHER BUREAU

PUBLICATIONS OF THE U. S. WEATHER BUREAU

As the national meteorological service for the United States, the Weather Bureau issues several periodicals, serials, and miscellaneous publications on weather, climate, and meteorological science as required to carry out its public service functions. The principal periodicals and serials are described on this page and on the inside of the back cover. A more complete listing of Weather Bureau publications is available upon request to Chief, U. S. Weather Bureau, Washington 25, D. C.

Orders for publications should be addressed to the Superintendent of Documents, Government Printing Office, Washington 25, D. C.

MONTHLY WEATHER REVIEW

First published in 1872, the Monthly Weather Review serves as a medium of publication for technical contributions in the field of meteorology, principally in the branches of synoptic and applied meteorology. In addition each issue contains an article descriptive of the atmospheric circulation during the month over the Northern Hemisphere with particular reference to the effect on weather in the United States. A second article deals with some noteworthy feature of the month's weather. Illustrated. Annual subscription: Domestic, $3.00; Foreign, $4.00: 30¢ per copy. Subscription to the *Review* does not include the *Supplements* which have been issued irregularly and are for sale separately.

WEEKLY WEATHER AND CROP BULLETIN

Issued on Wednesday of each week, the bulletin covers the weather of the week and its effects on crops and farm activities. Short reports from individual States are supplemented by maps of average temperature and total precipitation. In the winter months a chart of snow depth is included. Subscription: Annual, Domestic $3, Foreign $4; 10¢ per copy. For period December through March: Domestic $1.00, Foreign $1.50.

CLIMATOLOGICAL DATA—NATIONAL SUMMARY

This monthly publication contains climatological data such as pressure, temperature, winds, rainfall, snowfall, severe storms, floods, etc., for the United States as a whole. A short article describing the weather of the month over the United States, tables of the observational data, and a description of flood conditions are supplemented by 15 charts. An annual issue summarizes weather conditions in the United States for the year. More detailed local data are provided in the Climatological Data (by sections) for 45 sections representing each State or a group of States and Hawaii, Alaska, and the West Indies. Subscription price for either the National Summary or for a Section: $4.00 per year (including annual issue) domestic, $5.50, foreign; 30¢ per monthly issue; 50¢ for annual issue alone

(Continued on inside back cover)

The Weather Bureau desires that the *Monthly Weather Review* serve as a medium of publication for original contributions within its field, but the publication of a contribution is not to be construed as official approval of the views expressed.

The issue for each month is published as promptly as monthly data can be assembled for preparation of the review of the weather of the month. In order to maintain the schedule with the Public Printer, no proofs will be sent to authors outside of Washington, D. C.

The printing of this publication has been approved by the Director of the Bureau of the Budget, February 9, 1955.

DEPARTMENT OF COMMERCE
SINCLAIR WEEKS, Secretary

WEATHER BUREAU
F. W. REICHELDERFER, Chief

MONTHLY WEATHER REVIEW

JAMES E. CASKEY, JR., Editor

Volume 83
Number 3

MARCH 1955

Closed May 15, 1955
Issued June 15, 1955

ON THE NUMERICAL PREDICTION OF PRECIPITATION

J. SMAGORINSKY[1]
Numerical Weather Prediction Unit, U. S. Weather Bureau, Washington, D. C.
and
G. O. COLLINS[1]
Short Range Forecast Development Section, U. S. Weather Bureau, Washington, D. C.

[Manuscript received March 14, 1955]

ABSTRACT

With the three-dimensional field of velocity predicted by numerical methods it is possible to predict the moisture distribution and hence the occurrence of large-scale saturation. A three-parameter model was used to predict the 12-hour precipitation for the early stages of the storms of November 24, 1950 and November 5, 1953, neglecting cloud storage, supersaturation, a possible lack of condensation nuclei, evaporation from falling droplets, and moisture sources. Large-scale orographic influences were taken into account.

A quantitative comparison of the predicted rainfall with the correspondingly large-scale smoothed observed precipitation indicates a skill comparable to that of the predicted flow. An examination of the small-scale observed rainfall indicates that in these cases convective instability resulted in large standard deviations from the large-scale average. Numerical prediction of regions of convective instability, which is also shown, could for the time being be utilized for subjective interpretation.

CONTENTS

	Page
Abstract	53
1. Introduction	53
2. Condensation	54
3. Vertical motion	55
4. Specialization to a three-parameter model	56
5. The experiment	58
6. Discussion of results	59
November 24, 1950	59
November 5, 1953	59
7. Prediction of related elements	65
8. Frictional vertical velocity	66
9. Concluding remarks	67
References	67

1. INTRODUCTION

Workers in the field of numerical prediction have concerned themselves almost exclusively with the prediction of changes in the three-dimensional mass field and hence, as a direct consequence, changes in the large-scale velocity and temperature fields. The prediction of these elements is necessary though not sufficient for the prediction of the large-scale precipitation fields. Thus one finds in the literature (e. g. [7, 10]), for the most part only qualitative comparisons between numerically predicted vertical motion fields and observed precipitation.

The prediction of precipitation is a difficult task mainly for two reasons: (i) a lack of detailed knowledge of the physics of formation of cloud particles and their precipitation; (ii) the fact that, unlike the normal situation with the other meteorological elements such as pressure,

[1] Present affiliation: Joint Numerical Weather Prediction Unit, Federal Office Building No. 4, Suitland, Md.

341003—55——1

temperature, and wind, small-scale precipitation often is of much greater magnitude than the large-scale precipitation.

Our object will be to devise a dynamical large-scale precipitation model which by the application of numerical methods will enable us to predict. In what follows we will circumvent (i) by assuming [14] (a) there are always sufficient condensation nuclei, (b) no supersaturation, (c) no supercooling, (d) no non-adiabatic processes aside from those resulting from changes of state, and (e) and (f) cloud storage and evaporation from falling droplets are both negligible compared with significant amounts of precipitation. Furthermore, we will assume no moisture source outside of the atmosphere, i. e., no evaporation from the surface of the earth. The justification, for shorter periods, lies in the fact that evaporation as a function of space is generally of much smaller amplitude and much more uniform than condensation, although in the large the two must balance.[2] It is obvious that the present laminar lower boundary condition used in numerical prediction is incapable of permitting the transport of moisture across the lower boundary. In order to take evaporation sources into account we must ultimately assume a turbulent boundary layer to make possible eddy diffusion normal to the boundary.

Difficulty (ii) will, for quantitative purposes, be ignored, but will be discussed again later. It must be pointed out that as a consequence of the large non-linear interaction, even the large-scale precipitation calculations must be in error.

2. CONDENSATION

If r is the mixing ratio, then during the condensation process $dr/dt<0$, so that the condensation rate per unit volume is $-\rho_d dr/dt$, where ρ_d is the density of the dry air. Thus the rate of precipitation reaching the ground is

$$P=\int_{p_0}^{0}\frac{1}{g\rho_w}\frac{dr}{dt}\,dp \tag{1}$$

$$\frac{dr}{dt}=\begin{cases}0, & r<r_s\\ \dfrac{dr_s}{dt}, & r=r_s\end{cases} \tag{2}$$

ρ_w being the density of liquid water (1 gm. cm.$^{-3}$), p_0 the pressure at the earth's surface, and r_s the saturation mixing ratio, a function only of p, the pressure and T, the temperature. In the absence of evaporation processes, the integral is different from zero only where $dr/dt<0$. The precipitation accumulated over a period Γ is thus given by

$$\bar{P}=\int_t^{t+\Gamma}P\,dt \tag{3}$$

[2] W. F. Libby has reported [9] that raindrops from hurricanes and stratiform clouds are on the average 3 weeks old.

Equation (1) may be transformed to

$$P=\frac{1}{g\rho_w}\int_D\omega\,dr, \qquad D:\begin{cases}\omega<0\\ r=r_s\end{cases} \tag{4}$$

where $\omega\equiv dp/dt$ and D is the domain of integration. A schematic typical plot of $\omega/g\rho_w$ vs r is shown in figure 1. Only the shaded area thus contributes to the integral. Hence the precipitation may be computed if r, ω, T and p, are known.

In order to predict precipitation it is thus necessary to predict the moisture field as well as the three-dimensional mass field. This may be accomplished by the requirement of continuity of r:

$$\frac{\partial r}{\partial t}\equiv\frac{dr}{dt}-\mathbf{V}\cdot\nabla r-\omega\frac{\partial r}{\partial p} \tag{5}$$

where $\mathbf{V}$ is the horizontal wind vector and the velocity components and partial derivatives are taken with respect to a coordinate system in which x is positive eastward, y is positive northward, and p is positive downward. Thus with $\mathbf{V}$, ω, and r known as functions of x, y, and p, the transport terms may be computed. To calculate dr/dt, which under our assumptions is the condensation rate, we must look to thermodynamic principles.

The mixing ratio may be defined in terms of the vapor density (or absolute humidity) ρ^* by

$$\rho^*=r\rho_d \tag{6}$$

Assuming the water vapor to behave as a perfect gas we have that

$$\rho^*=\frac{e}{R^*T},\quad R^*=\frac{mR}{m^*} \tag{7}$$

where e is the vapor pressure over water or ice depending on whether T is $\geq 0°$ C. or $<0°$ C., respectively, m^* is the molecular weight of water vapor, m the molecular

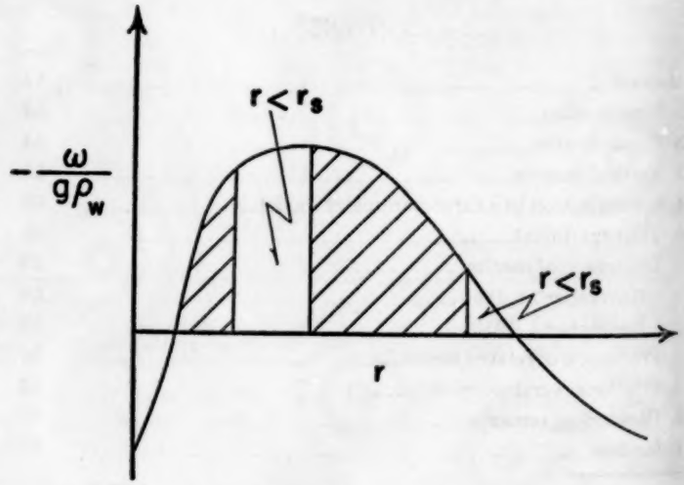

FIGURE 1.—A schematic plot of $-\omega/(g\rho_w)$ vs. r.

weight of dry air, R is the gas constant for dry air, and hence $R^*=1.608\ R$. It is assumed that the temperature of the vapor is the same as that of the dry air. Under saturated conditions $r=r_s$, and hence

$$\frac{d\ln r_s}{dt}=\frac{d\ln (e_s/T)}{dt}-\frac{d\ln \rho_d}{dt} \tag{8}$$

where e_s is the saturation vapor pressure.

The Clausius-Clapeyron equation to good approximation may be written as

$$d\ln e_s-\gamma d\ln T=0,\quad \gamma\equiv\frac{L}{AR^*T} \tag{9}$$

in which L is the latent heat of condensation and A^{-1} the mechanical equivalent of heat. For $T<0$°C. L should be replaced by the latent heat of sublimation.
Thus (8) becomes

$$\frac{d\ln r_s}{dt}=(\gamma-1)\frac{d\ln T}{dt}-\frac{d\ln \rho_d}{dt} \tag{10}$$

During the condensation process the equivalent potential temperature, θ_E, is a conservative property.

$$\frac{d\ln \theta_E}{dt}=0 \tag{11}$$

where

$$\left.\begin{aligned}&\ln\theta_E=\text{const}-\kappa\ln\rho_d+(1-\kappa)\ln T+\alpha,\\ &\alpha\equiv\frac{Lr_s}{c_pT}=\frac{\kappa m}{m^*}\gamma r_s,\\ &\kappa=\frac{AR}{c_p},\end{aligned}\right\} \tag{12}$$

and c_p is the specific heat of dry air at constant pressure. Equation (11) yields

$$\frac{d\ln T}{dt}=\frac{\alpha\dfrac{d\ln r_s}{dt}-\kappa\dfrac{d\ln\rho_d}{dt}}{\alpha-(1-\kappa)} \tag{13}$$

if the individual change of L is assumed small. Thus the individual change of temperature may be eliminated between (10) and (13) to give

$$\frac{d\ln r_s}{dt}=\Lambda\frac{d\ln\rho_d}{dt} \tag{14}$$

$$\Lambda\equiv\frac{\kappa\gamma-(1-\alpha)}{\alpha(\gamma-2)+(1-\kappa)} \tag{14a}$$

Since in these considerations the air is saturated, Λ is purely a function of p and T. Hence, as one expects, the condensation rate is proportional to the compressibility. For $p=700$ mb. and $T=0$°C.: $\alpha=.0493$ and $\gamma=19.7$. One is then justified in assuming $\alpha<<1$ and $\gamma>>2$, so that

$$\Lambda\approx\frac{\kappa\gamma-1}{\alpha\gamma+1-\kappa} \tag{15}$$

Both for small- and large-scale motions $d\rho_d/dt$ is given to good approximation by

$$\frac{d\rho_d}{dt}\approx\omega\frac{\partial\rho_d}{\partial p}$$

thus

$$\frac{d\ln r_s}{dt}\approx\Lambda\frac{\partial\ln\rho_d}{\partial p}\omega,\quad \omega<0 \tag{16}$$

Since Λ and $\partial\ln\rho_d/\partial p>0$, the side condition in (16) is required to insure that $d\ln r_s/dt<0$ for the condensation process.

Equations (1), (2), (5), and (16) taken together with a knowledge of $\mathbf{V}$ and ω suffice for the prediction of precipitation, given as initial conditions the spatial distribution of mass and mixing ratio.

With the approximation that $\omega\approx w\partial p/\partial z$, where w is the vertical velocity when the height, z, is a vertical coordinate, that $\dfrac{\partial p}{\partial z}\approx-g\rho_d$ by the hydrostatic approximation, and that the lapse rate is moist adiabatic, (16) reduces to a result deduced by Fulks [8]. Fulks did not intend to use this result prognostically but rather to calculate precipitation by means of an analogue of equation (1) from a known field of r, T, w, and p. However, we have shown equation (4) sufficient to calculate contemporary precipitation.

3. VERTICAL MOTION

The large-scale field of vertical motion is not an observable quantity. However, application of the hydrostatic and geostrophic filtering approximations to the primitive hydrodynamic equations permits one to deduce the vertical motion field given only the three-dimensional mass (or pressure) field and appropriate boundary conditions. This can be seen from the following differential equations [7]:

$$\left(\frac{\partial}{\partial t}+\mathbf{V}\cdot\nabla\right)\eta=\eta\frac{\partial\omega}{\partial p} \tag{17}$$

$$\left(\frac{\partial}{\partial t}+\mathbf{V}\cdot\nabla+\omega\frac{\partial}{\partial p}\right)\ln\theta=0 \tag{18}$$[3]

[3] There is apparent inconsistency in the use of the adiabatic approximation in the thermodynamic energy equation (18) to predict the three-dimensional velocity. By this, we assume that the heat of condensation does not materially alter the field of flow over periods of the order 24-36 hours. However, there is evidence that for longer periods, all non-adiabatic sources and sinks, orography and skin friction result in significant interactions [11]. In the present situation we may regard the approximation as a quasi-linearization with respect to the condensation in analogy with small perturbation theory where one assumes that the basic flow determines the propagation of a disturbance, but that this disturbance does not affect the mean flow to the first order of small quantities.

in which we take

$$\left.\begin{aligned} \mathbf{V}&=\frac{1}{f}\,\mathbf{k}\times\nabla\phi \\ \phi&=g\,z \\ T&=-\frac{p}{R}\frac{\partial\phi}{\partial p} \\ \eta&=\frac{1}{f}\nabla^2\phi+f \\ \ln\theta&=\text{const}+\frac{c_v}{c_p}\ln p+\ln\left(-\frac{\partial\phi}{\partial p}\right) \end{aligned}\right\} \tag{19}$$

f is the Coriolis parameter and c_v is the specific heat of air at constant volume.

In deriving the vorticity equation (17) the vertical advection of vorticity, $\omega\partial\eta/\partial p$, and the turning of the vortex tubes in vertical planes, $\frac{\partial\omega}{\partial x}\frac{\partial v}{\partial p}-\frac{\partial\omega}{\partial y}\frac{\partial u}{\partial p}$, have been neglected.

Since initially z is given as a function of x, y, and p, system (17), (18) and (19) may be regarded as two differential equations in two unknowns: $\partial z/\partial t$ and ω. Customarily ω is eliminated and the system solved for $\partial z/\partial t$. Then ω can be determined explicitly by substituting back either into (17) or (18). However, we may alternatively eliminate $\partial z/\partial t$ and write the differential equation governing ω:

$$\nabla^2\omega-\left(\frac{pf^2}{RS}\right)\frac{\partial^2\omega}{\partial p^2}=\frac{1}{S}\left(\frac{pf}{R}\frac{\partial J}{\partial p}-\nabla^2\Theta\right) \tag{20}$$

in which we abbreviated

$$\left.\begin{aligned} S&\equiv\frac{1}{T}\frac{\partial\ln\theta}{\partial p} \\ \Theta&\equiv\mathbf{V}\cdot\nabla T \\ J&\equiv-\mathbf{V}\cdot\nabla\eta \end{aligned}\right\} \tag{21}$$

For simplicity, we have replaced η by f when η occurs as a coefficient and also have assumed $\partial\theta/\partial p$, the static stability, to be constant in an isobaric surface, an approximation effectively made in all two-parameter models.

This three-dimensional Poisson equation may be solved by relaxation methods, once given the three-dimensional mass distribution which is sufficient to determine the inhomogeneous terms, and also given boundary conditions at $p=p_0$, $p=0$, and at the lateral boundaries. Consistent with a two-parameter model ω may be expressed as a quadratic function of p. Taking

$$\left.\begin{aligned} &\omega=\omega_0,\ p=p_0 \\ &\omega=0,\ \ p=0 \end{aligned}\right\} \tag{22}$$

then ω may be expressed in terms of the vertical motion, ω^*, at the level $p^*=p_0/2$:

$$\omega=[-(2\omega^*-\omega_0)\,p+(4\omega^*-\omega_0)\,p^*]\,\frac{p}{2p^{*2}} \tag{23}$$

Equation (20) may then be written as

$$\nabla^2\omega+\left[\frac{2f^2}{(2p^*-p)RS}\right]\omega=\frac{1}{S}\left[\frac{pf}{R}\frac{\partial J}{\partial p}-\nabla^2\Theta+\frac{pf^2}{p^*(2p^*-p)R}\,\omega_0\right] \tag{24}$$

We have thus reduced the problem to one of the solutions of a two-dimensional Helmholtz equation into which the boundary conditions at the top and bottom of the atmosphere already have been incorporated.

The surface vertical velocity, w_0, is induced by orography or by skin frictional action and is given by [5]

$$w_0\approx\mathbf{V}_0\cdot\nabla h+\sqrt{\frac{K}{2f}}\sin(2\nu)\,\zeta_0 \tag{25}$$

where h is the elevation of the large-scale orography, ζ_0 is the geostrophic relative vorticity in the friction layer, K is the average eddy diffusivity and ν the angle between the wind and isobars.

4. SPECIALIZATION TO A THREE-PARAMETER MODEL

For the purposes of actual calculation, the general prediction equations are reduced to a three-layered model as described in general by Charney and Phillips [7] and in particular by Charney [4]. This model is equivalent to an atmosphere consisting of three divergent barotropic layers.

The vertical velocity may be computed from the thermodynamic energy equation (18) which may be rewritten

$$w\approx\frac{1}{g}\frac{\partial\phi}{\partial p}\,\omega=\left(g\,\frac{\partial\overline{\ln\theta}}{\partial p}\right)^{-1}\frac{D}{Dt}\left(-\frac{\partial\phi}{\partial p}\right) \tag{26}$$

where D/Dt is the horizontal individual time derivative and a bar denotes the standard value. A quasi-linearization has been performed so that when the stability appeared as a coefficient, the standard atmosphere stability is used. This is consistent with the approximations made in deriving the prediction equations for this model.

The numerical integration scheme used here carries the history of the motion in the potential vorticity. Hence $\partial\phi/\partial t$ is never calculated explicitly. It is thus necessary to approximate $\partial\phi/\partial t$ in (26) by finite differences. In numerically integrating the potential vorticity equation, it is necessary to perform the initial time integration noncentrally over one finite difference time interval and thence to proceed by means of centered time differences over double time intervals [7]. The result is that a small oscillation in ϕ with a period of two time intervals is artificially induced.[4] This oscillation is barely detectable; however,

[4] This was observed by one of the writers who participated in the ENIAC calculation of the first barotropic predictions [6]. The hourly forecast data were available for inspection since the internal memory limitations of the ENIAC required the output of all intermediate results.

where time differences of the ϕ field are taken over an odd number of time intervals, a significant error is introduced. In the case of differences over one time interval, the oscillation in some instances completely masks the physically real finite difference approximation to the continuous time derivative. Therefore in the present calculations, all time differences are taken over a double interval.

In finite difference form (i and j are horizontal coordinates, k pressure, and τ time and the corresponding intervals between integral values of these coordinates are Δs, Δs, Δp, and Δt, respectively) equation (26) becomes

$$w^{\tau}_{ij\,k+\frac{1}{2}} = -\frac{\bar{\theta}_{k+\frac{1}{2}}}{g(\bar{\theta}_k - \bar{\theta}_{k+1})}\left(\frac{\mathfrak{D}}{\mathfrak{D}t}\right)^{\tau}_{ij\,k+\frac{1}{2}}(\phi_k - \phi_{k+1})^{\tau}_{ij} \tag{27}$$

where

$$\left.\begin{aligned}\left(\frac{\mathfrak{D}}{\mathfrak{D}t}\right)^{\tau}_{ij\,k+\frac{1}{2}}\sigma^{\tau}_{ij} &\equiv \frac{(\sigma^{\tau+1}-\sigma^{\tau-1})_{ij}}{2\Delta t} - \frac{m^2_{ij}}{4(\Delta s)^2 f_{ij}}\Im_{ij}(\sigma, \phi_{k+1})^{\tau}_{ij}\\ \Im_{ij}(a,b) &\equiv (a_{i+1}-a_{i-1})_j(b_{j+1}-b_{j-1})_i - (a_{j+1}-a_{j-1})_i(b_{i+1}-b_{i-1})_j\end{aligned}\right\} \tag{28}$$

and m_{ij} is the map scale factor. Since the ϕ field is predicted at integral values of k, we approximate $\phi_{k+\frac{1}{2}}$ by $(\phi_k + \phi_{k+1})/2$ giving

$$\left.\begin{aligned}w^{\tau}_{ij\,k+\frac{1}{2}} &= E_{k+\frac{1}{2}}\left[(\phi_{k+1}-\phi_k)^{\tau+1} - (\phi_{k+1}-\phi_k)^{\tau-1} + F\Im(\phi_k, \phi_{k+1})^{\tau}\right]_{ij}\\ E_{k+\frac{1}{2}} &\equiv \frac{\bar{\theta}_{k+\frac{1}{2}}}{2\Delta t g(\bar{\theta}_k - \bar{\theta}_{k+1})}\\ F_{ij} &\equiv \frac{\Delta t}{2(\Delta s)^2}\left(\frac{m^2}{f}\right)_{ij}\end{aligned}\right\} \tag{29}$$

$\Delta s = 300$ km., $\Delta t = \frac{1}{2}$ hr., and m_{ij}^2 is taken to be unity for the latitude span used here on a Lambert conformal projection (see for example [12]), $k = 1, 1\frac{1}{2}, 2, 2\frac{1}{2}, 3$ refer to 200, 350, 500, 675, 850 mb., respectively, and the boundaries $k = \frac{1}{2}$, $k = 3\frac{1}{2}$ are placed at 25 mb. and 1000 mb., respectively.

w can first be computed centrally over a double time interval at $t = \frac{1}{2}$ hour using information at $t = 0$, and $t = 1$ hour. The initial vertical velocities at $t = 0$ are therefore taken to be the same as those at time $t = \frac{1}{2}$ hour. Inspection of the subsequent data showed that changes within a half hour interval are sufficiently small that no serious error is introduced by this assumption.

Since the vertical velocities computed by the model, especially those at 350 mb., are at rather high levels in the troposphere and above the maximum concentration of moisture, it is considered necessary, for the prediction of precipitation, to deduce vertical velocities at lower levels. Predictions with models giving greater definition at lower levels, e. g., a three-layer model with p^2 the vertical coordinate [4] which gives values at about 575 and 825 mb. or perhaps a five-level model, may eliminate this need to interpolate. Given w at four levels: 675, 350 mb. and the boundaries 1000 and 25 mb., one can fit a cubic with respect to pressure, giving a continuous function:

$$^1w(p) = M(p)w_{675} + N(p)w_{350} \tag{30}$$

in which M and N are the interpolation variables, and the anterior superscript denotes first approximation.

As previously pointed out, the computations of vertical velocities in this particular model are based on the assumption that the vertical velocity is zero at 1000 mb., the lower boundary. This assumption may not produce serious errors in the prediction of the geopotential field but does become more detrimental in the prediction of precipitation. Vertical velocities at the surface produced by forced ascent over orographic barriers can contribute considerably to the precipitation [10]. The most logical and consistent way to include the effects of large-scale varying terrain would be to incorporate this lower boundary condition implicitly in the prediction equations. This can be done without great difficulty (see for example eq. (24)). Since the flow prediction equations used here do not take terrain into account, these effects are included a posteriori. Vertical velocities at the lower boundary, 1000 mb., are computed from (see eq. (25))

$$w_0 = \mathbf{V}_0 \cdot \nabla h \approx \mathbf{V}_{900} \cdot \nabla h \tag{31}$$

where $\mathbf{V}_{900}$ is the geostrophic wind at 900 mb. $\mathbf{V}_{900}$ was extrapolated quadratically from information at 200, 500, and 850 mb. For a second approximation to the vertical velocity we define

$$^2w(p) = {}^1w(p) + \frac{p}{1000}w_0 \tag{32}$$

While this procedure is somewhat arbitrary, it has the characteristic, somewhat similar to that of the atmosphere, that the effects of the lower boundary on the flow are damped out approximately linearly with decreasing pressure. Vertical velocities may be calculated in this manner for $p = 400(100)900$mb. denoted by $k' = 1$ to 6, respectively.

In the integration of the finite difference form of the potential vorticity equation the choice of Δt was bounded by the requirement of computational stability with respect to Δs. Since there is no such restriction in using the results of the integration of the potential vorticity equation together with the finite difference form of the system (1), (2), (5), and (16), a time interval, $\Delta' t$, in precipitation equations, may be chosen commensurate only with the time scale of the dependent variables.

The ϕ field at the levels k', may be quadratically interpolated and extrapolated from the values at $k = 1, 2, 3$.

The temperature $\left(T = -\frac{p}{R}\frac{\partial\phi}{\partial p}\right)$ is predicted only at $k = 1\frac{1}{2}$ and $2\frac{1}{2}$. While a linear interpolation for intermediate levels may adequately determine the tempera-

ture, experiments in extrapolating to flanking levels prove inadequate for our purposes. This can be overcome to some extent by making selective use of the observed detail in the initial soundings. The observed initial temperatures at each level k' are smoothed subjectively yielding $T^0_{ijk'}$. The predicted temperature change, ΔT, at $k=1\frac{1}{2}, 2\frac{1}{2}$ over the time interval $\Delta' t$ is then interpolated and extrapolated linearly to give the temperature change at the levels k'. This process may be iterated:

$$\left.\begin{aligned} T^{\tau'}_{ijk'}{}^{+1} &= [T^{\tau'} + (\Delta T)^{\tau'+\frac{1}{2}}]_{ijk'} \\ (\Delta T)^{\tau'}_{ijk'}{}^{+\frac{1}{2}} &= [a_{k'}(\Delta T)_{1\frac{1}{2}} + b_{k'}(\Delta T)_{2\frac{1}{2}}]^{\tau'+\frac{1}{2}}_{ij} \end{aligned}\right\} \tag{33}$$

where $a_{k'}$ and $b_{k'}$ are determined from the interpolation formula. Since $\phi_{k'}$ is determined independently by a much simpler scheme, there will be some hydrostatic inconsistency with the corresponding $T_{k'}$ field. This may be avoided by determining $T_{k'}$ as described, but integrating vertically to obtain $\phi_{k'}$, using as a reference one of the $\phi_{k'}$'s.

The system of prediction equations (1), (2), (3), (5) and (16) in finite difference form is thus:

$$P^{\tau'}_{ij} = \frac{1}{g\rho_w} \sum_{k'} \left(\frac{dr}{dt}\right)^{\tau'}_{ijk'} (p_{k'+\frac{1}{2}} - p_{k'-\frac{1}{2}}) \tag{34}$$

$$\frac{dr}{dt} = \begin{cases} 0, & r < r_s \\ \dfrac{dr_s}{dt}, & r = r_s \end{cases} \tag{35}$$

$$\bar{P}_{ij} = \sum_{\tau'} P^{\tau'}_{ij} \Delta' t \tag{36}$$

$$\left.\begin{aligned} r^{\tau'}_{ijk'}{}^{+1} &= r^{\tau'}_{ijk'}{}^{-1} + \delta \Delta' t \left[\left(\frac{dr}{dt}\right)_{k'} + \frac{m^2}{4(\Delta s)^2 f}\right. \\ &\left. \Im_{k'}(r,\phi)_{k'} - \omega_{k'}\left(\frac{r_{k'+1} - r_{k'-1}}{p_{k'+1} - p_{k'-1}}\right)\right]^{\tau'}_{ij} \\ \delta &= \begin{cases} 1 \text{ and } r^{\tau'-1} = r^0 & \text{for } \tau' = 0 \\ 2 & \text{for } \tau' > 0 \end{cases} \end{aligned}\right\} \tag{37}$$

$$\left(\frac{dr_s}{dt}\right)^{\tau'}_{ijk'} = \left[r_s \Lambda \frac{(\partial \ln \rho_d)}{\partial p} \omega\right]^{\tau'}_{ijk'}, \quad \omega < 0 \tag{38}$$

For computational convenience the density lapse rate is taken to correspond to that of the moist-adiabatic lapse rate, and hence is a function of height only. This approximation is not necessary with numerical prediction models of three or more parameters. In the present three-parameter model the static stability, although constant in the vertical, may vary in time and in the horizontal. Hence the continuous form

$$\frac{d \ln \rho_d}{dt} \approx -\omega \left(\frac{\partial \phi}{\partial p}\right)^{-1} \left(\frac{\partial^2 \phi}{\partial p^2}\right)$$

in finite differences becomes

$$\left(\frac{d \ln \rho_d}{dt}\right)^{\tau}_{ijk} = \left[\frac{2\omega_k}{p_{k+1} - p_{k-1}} \left(\frac{\phi_1 + \phi_3 - 2\phi_2}{\phi_{k+1} - \phi_{k-1}}\right)\right]^{\tau}_{ij} \tag{39}$$

At the upper and lower boundaries $\partial\phi/\partial p$ must be determined non-centrally. In all calculations, for convenience, L is taken as the latent heat of condensation, and e and r are taken with respect to water, irrespective of T. This restriction may easily be removed.

Comparisons of predicted geopotential tendencies with observed 12-hour changes [2] indicate that a time interval, $\Delta' t$, of 12 hours represents an upper limit. However, appreciable error can be introduced by the assumption that the saturation state is constant over so long an interval. It is estimated that $\Delta' t = 3$ hours would result in more tolerable truncation errors. It is possible, however, to use a larger $\Delta' t$ if the truncation error resulting from the constant saturation state approximation is to some extent eliminated. This may be accomplished by estimating the time, t_s, of occurrence of change of saturation state during $\Delta' t$. One can determine from the initial mixing ratio, r^0, the saturation state at that time. In the instance where $r^0 < r^0_s$, then one may determine whether saturation will occur during $\Delta' t$ from the non-central form of (37) between $t=0$ and t_s:

$$t_s = \frac{(r^0_s - r^0)_{k'}}{\left[\dfrac{m^2}{4(\Delta s)^2 f} \Im_{k'}(r,\phi)_{k'} - \omega_{k'}\left(\dfrac{r_{k'+1} - r_{k'-1}}{p_{k'+1} - p_{k'-1}}\right)\right]^0_{ij}} \tag{40}$$

t_s is thus defined and determinable. If $t_s > \Delta' t$ then $dr/dt = 0$ over the entire interval. If not, dr_s/dt computed from (38) is to be weighted by the factor $(1 - t_s/\Delta' t)$. For initially saturated conditions one uses a correspondingly derived criterion for the occurrence of unsaturated conditions during $\Delta' t$. Thompson and Collins [14] used a similar technique for precipitation calculations in which $\Delta' t$ was taken as 12 hours. They did not take horizontal moisture transport into account.

5. THE EXPERIMENT

The situations chosen were the early synoptically unspectacular stages of two cases of rapid cyclogenesis. The initial conditions were taken at 0300 GMT, November 24, 1950, and 1500 GMT, November 5, 1953. The object was to predict the accumulated precipitation over a 12-hour period. For this purpose $\Delta' t$ was first taken as 12 hours. With the scheme outlined in the previous section, the only predictive element is a determination of the time of occurrence of change of saturation state. Otherwise, only the initial ω and r fields are needed. A second calculation was prepared in which $\Delta' t$ was taken as 3 hours and, therefore, the full set of prediction equations were used in 4 iterations for a 12-hour forecast.

Numerical flow forecasts for the same two periods

treated here were performed by the Princeton group using a three-parameter 900–700–400-mb. model [4], but 3-hourly vertical motion fields were not calculated. The fact that these situations were highly baroclinic in the lowest levels meant that the 850–500–200-mb. model was incapable of recognizing the large amount of potential energy available for conversion to kinetic energy. The result is that the predicted development by the 850–500–200-mb. model was inferior to that by the 900–700–400-mb. model in both cases. This is particularly true for the November 5, 1953, case.

6. DISCUSSION OF RESULTS

For the purposes of verifying the forecasts of large-scale precipitation accumulating over 12-hour periods, observations from all hourly precipitation reporting stations were utilized. This of course gives a relatively fine-grained picture of the actual precipitation—with stations having an average separation of roughly 30 miles. The observations were taken from *Climatological Data for the United States* [15] and from specially prepared listings supplied by the National Weather Records Center in Asheville, N. C.

NOVEMBER 24, 1950

A comparison of the 850-mb. maps at initial time 0300 GMT (fig. 2A) and 12 hours later (fig. 2E) shows that the depression centered south of Lake Superior filled but a secondary trough was forming to the south. This is predicted by the model used (fig. 2E). At 500 mb. the Low centered in Wisconsin (fig. 2B) elongated and moved to southern Lake Michigan (fig. 2F). Again this evolution was adequately predicted (fig. 2F). At 200 mb. the flow forecast was not quite as good, but has less bearing on the present problem and is not shown. The calculated vertical motion fields at the beginning and end of this 12-hour period at 675 mb. and at 350 mb. are shown in figure 2 (C, D, G, and H). The predicted fields of ϕ and w at the intermediate 3-hourly intervals are not shown.

In figure 3A are plotted all non-zero and non-missing 12-hourly precipitation reports to the south and east of the heavy boundary. The results using $\Delta' t=12$ hours (dashed lines) indicate a maximum of .23 inch at Lake Erie. However for $\Delta' t=3$ hours (solid lines) there occurs a double maximum, one at Lake Erie of the same magnitude and another in Tennessee with somewhat larger maximum value. A comparison of non-zero points and predicted precipitation greater than .01 inch indicates a good qualitative forecast for either model and thus a fairly reliable statement of the time of onset and cessation of precipitation. However examination of the individual reports indicates large deviations even from the results using $\Delta' t=3$ hours. Figure 3B summarizes the large-scale average observed precipitation and the standard deviation from this average. This was constructed by averaging all observations within the isohyetal channels of the prediction in which $\Delta' t=3$ hours. These points were computed from over 1,300 observation stations in eastern United States. The model is seen to have over-predicted the large-scale precipitation by a factor of approximately 2 for the intermediate amounts and by a factor of 1.25 for the maximum.

It is also important to bear in mind that the three-parameter model used here (850–500–200-mb.) gives a flow forecast inferior to that of the 900–700–400-mb. model even in the first 12 hours.

It is evident from a comparison of figure 2 (C, D, G, and H) with figure 3A that upward vertical motion is only a necessary though not a sufficient condition for precipitation even for qualitative purposes. For instance one would not have judged from the vertical velocity field alone that the primary precipitation maximum would be in Tennessee.

NOVEMBER 5, 1953

This case deals with a nascent cyclone in the northeast Gulf of Mexico at 850 mb. (fig. 4A) which deepened and traveled up off the east coast to 31° N. latitude in a 12-hour period (fig. 4E). Actually the 850–500–200-mb. model gave a forecast which was quite poor in describing the observed development. No deepening and only slight eastward motion were predicted at 850 mb. (fig. 4E); At 500 mb. the primary trough in northeastern United States (fig. 4B and F) was predicted to move too rapidly to the east and the development of a closed circulation was missed entirely. On the other hand the secondary in the Gulf, associated with the 850-mb. closed Low, was predicted to move to the east at the approximate speed observed.

It should be noted that the anticyclogenesis predicted in north-central United States at 850 mb. and 500 mb. but not observed does not directly affect the area of our precipitation forecasts.

In figure 5A we have, as before, the raw precipitation observations superimposed on forecasts computed using $\Delta' t=12$ and 3 hours.

An essential difference in the observed precipitation between this case and that of November 1950 is the occurrence of large amounts along the Carolina and southern Virginia coasts. The observed 850-mb. flow at the beginning and end of this period shows onshore winds. This coastal effect is well known [1] but is not taken into account by the present theory. Presumably this could be accomplished by an extension of the theory resulting in equation (25) to apply to variable surface roughness.

A significant difference is observed between the predictions using $\Delta' t=12$ hours and 3 hours. For $\Delta' t=12$ hours the maximum is only half as large as that for $\Delta' t=3$

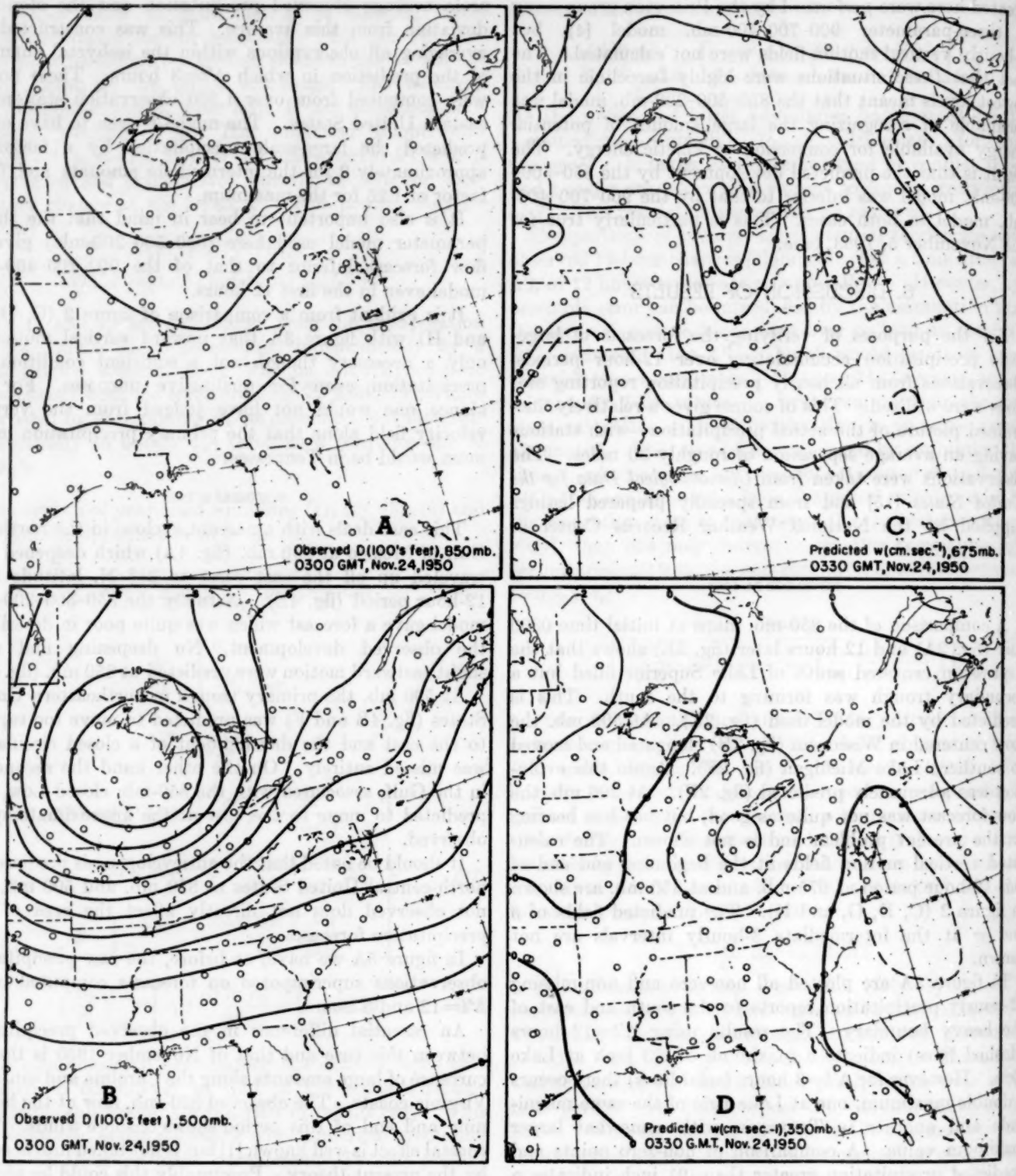

FIGURE 2.—November 24, 1950 case: initial, predicted, and verifying horizontal flow (A, B, E, F,); initial and predicted vertical flow (C, D, G, H) for the 12-hour period 0300–1500 GMT, November 24, 1950.

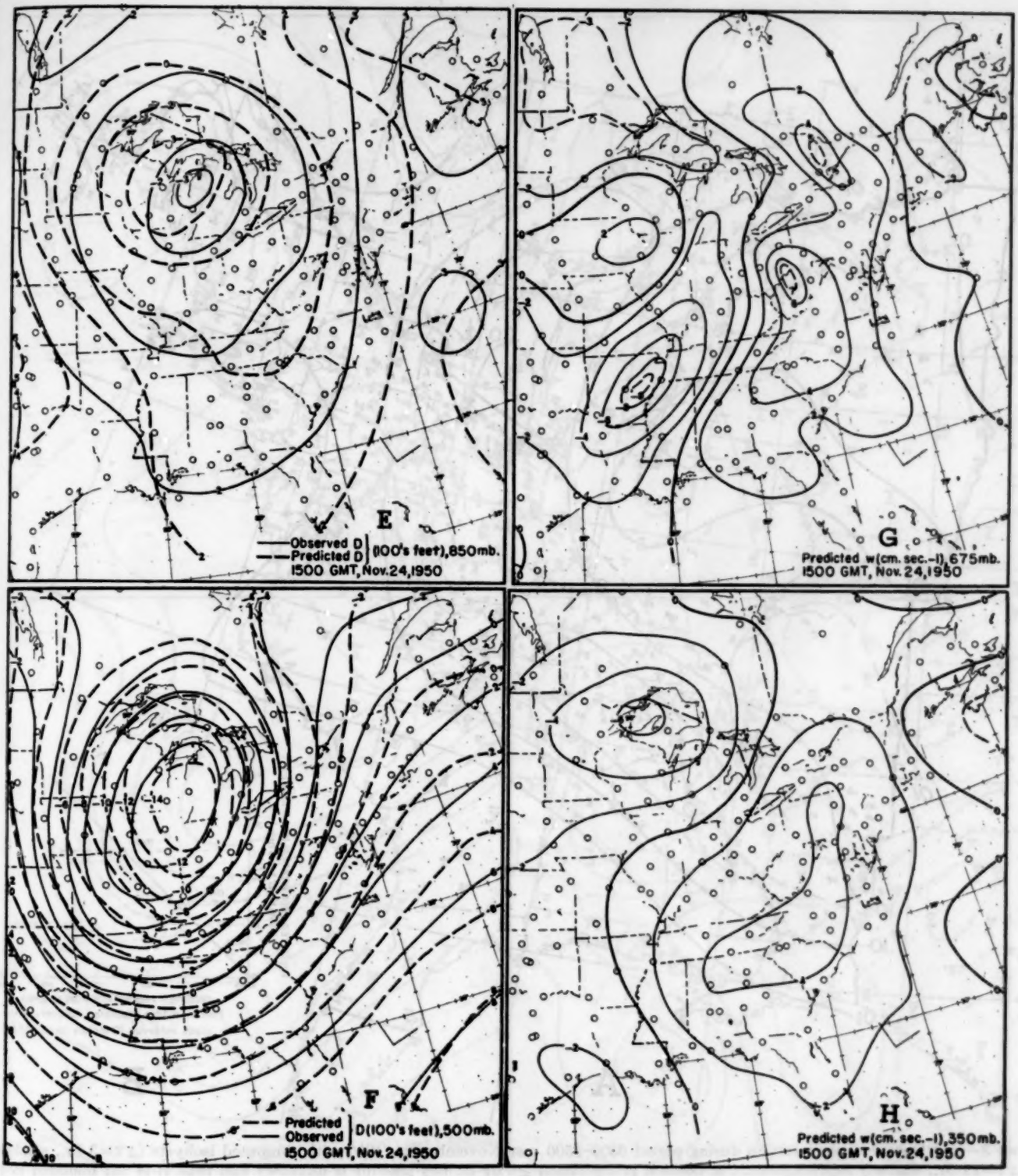

Figure 2—Continued

341693—55——2

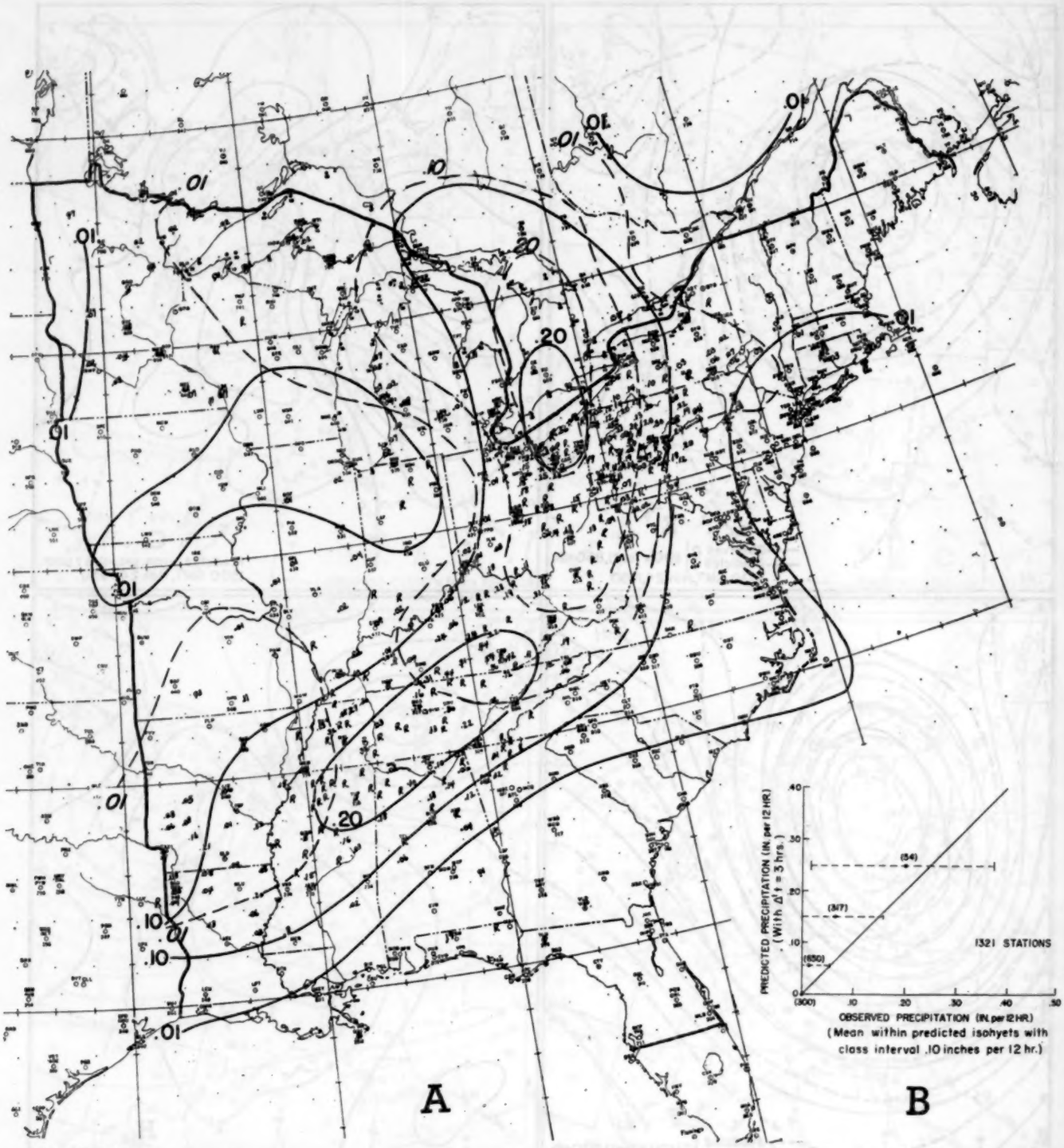

FIGURE 3.—(A) Observed precipitation during period 0300–1500 GMT November 24, 1950 with computed isohyets ($\Delta' t = 3$ hr., solid and $\Delta' t = 12$ hr., dashed) superimposed. R denotes precipitation ≥ 0.01 in. but amount is unknown and thus R is not included in the numerical verification. Missing reports and zero precipitation are not shown. (B) Summary of results with observations smoothed for large-scale verification. Numbers in parentheses at plotted points give number of stations averaged in the respective isohyetal channel. Dashed lines indicate standard deviation of observations in the respective channel.

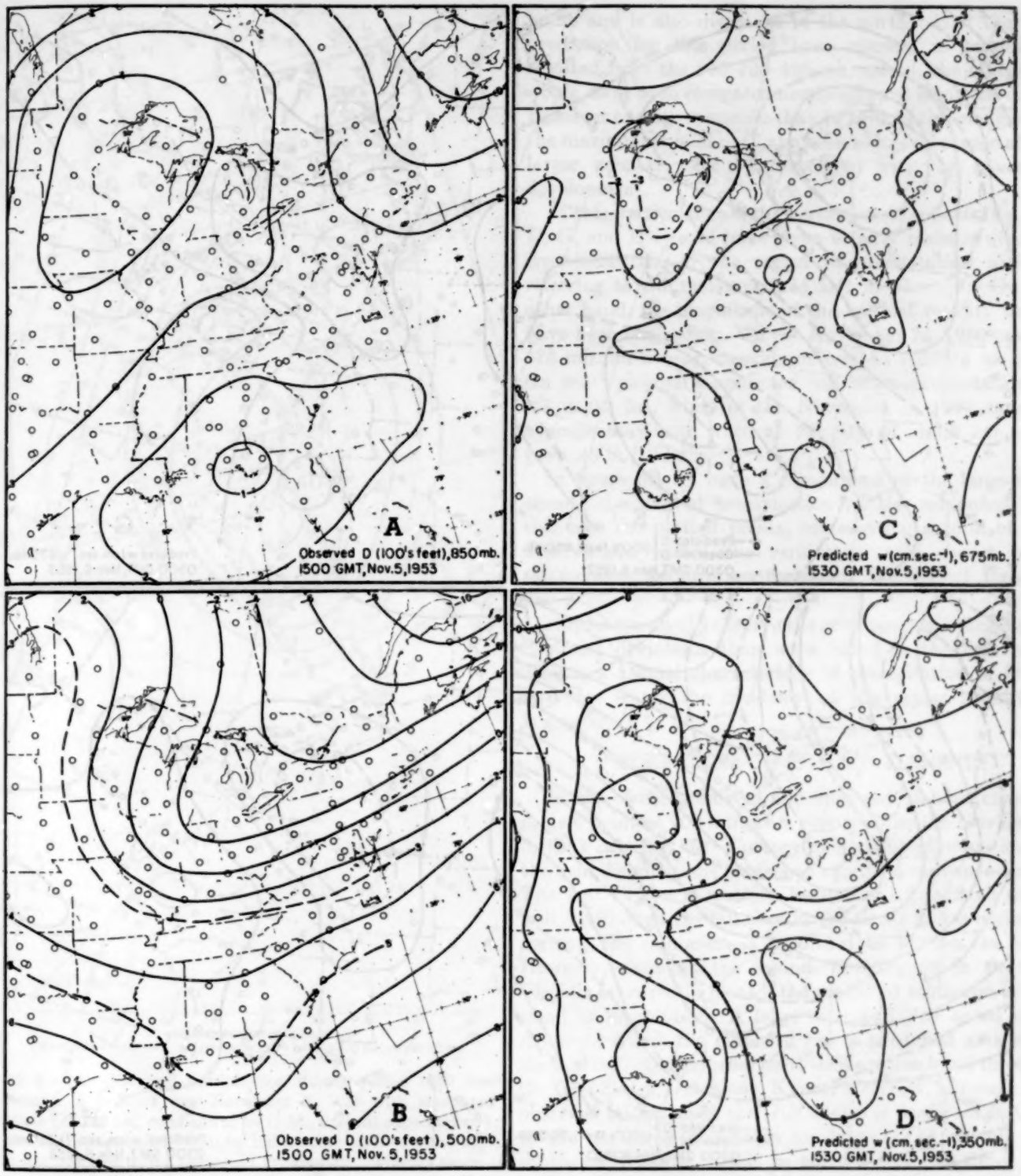

FIGURE 4.—November 5, 1953 case: initial, predicted, and verifying horizontal flow (A, B, E, F); initial and predicted vertical flow (C D, G, H) for the 12-hour period 1500 GMT November 5 to 0300 GMT November 6, 1953. See p. 64 for parts E, F, G, H.

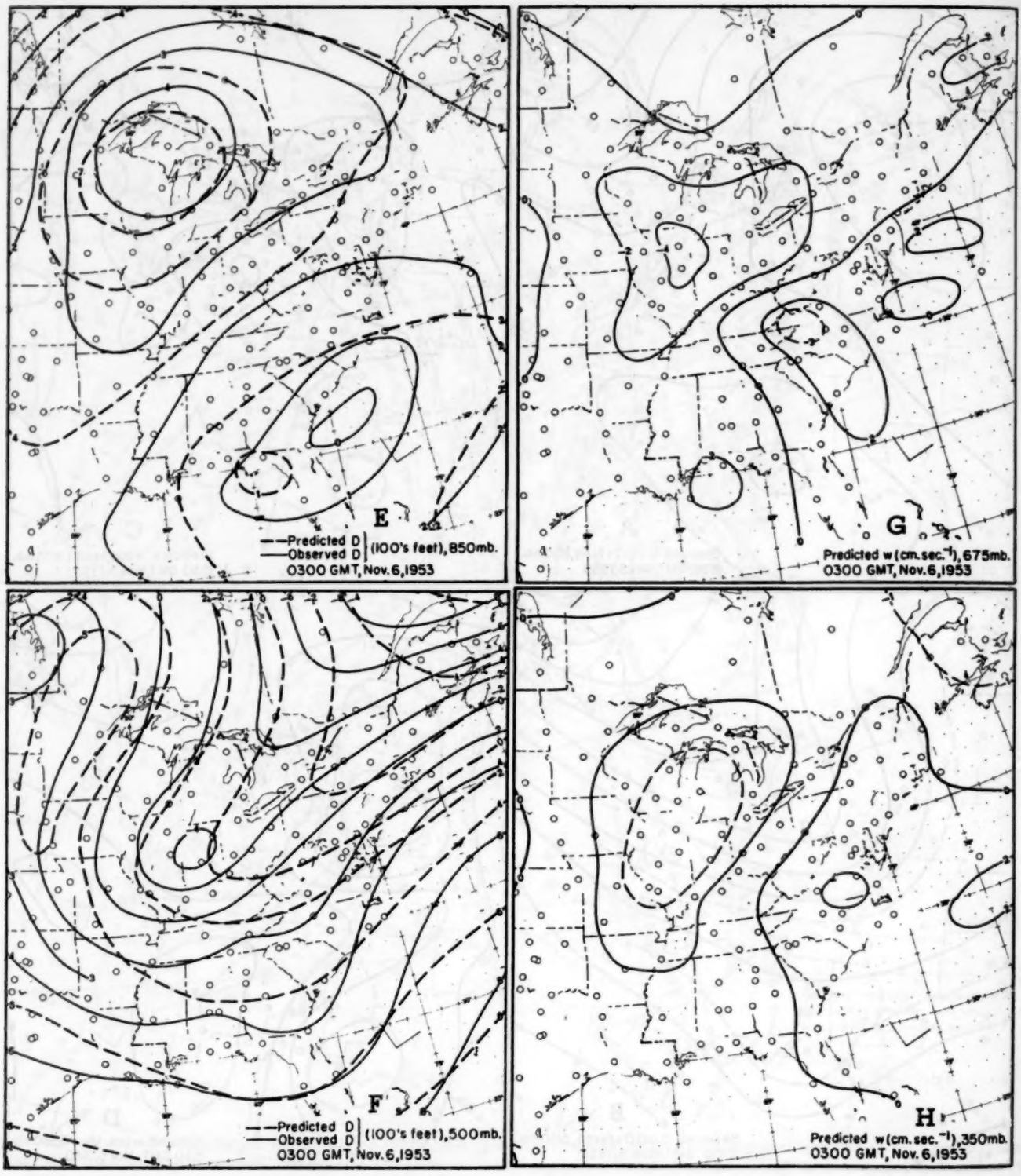

FIGURE 4.—(Continued) November 5, 1953 case: initial, predicted, and verifying horizontal flow (A, B, E, F); initial and predicted vertical flow (C, D, G, H) for the 12-hour period 1500 GMT November 5, 1953 to 0300 GMT November 6, 1953. See p. 63 for parts A, B, C, D.

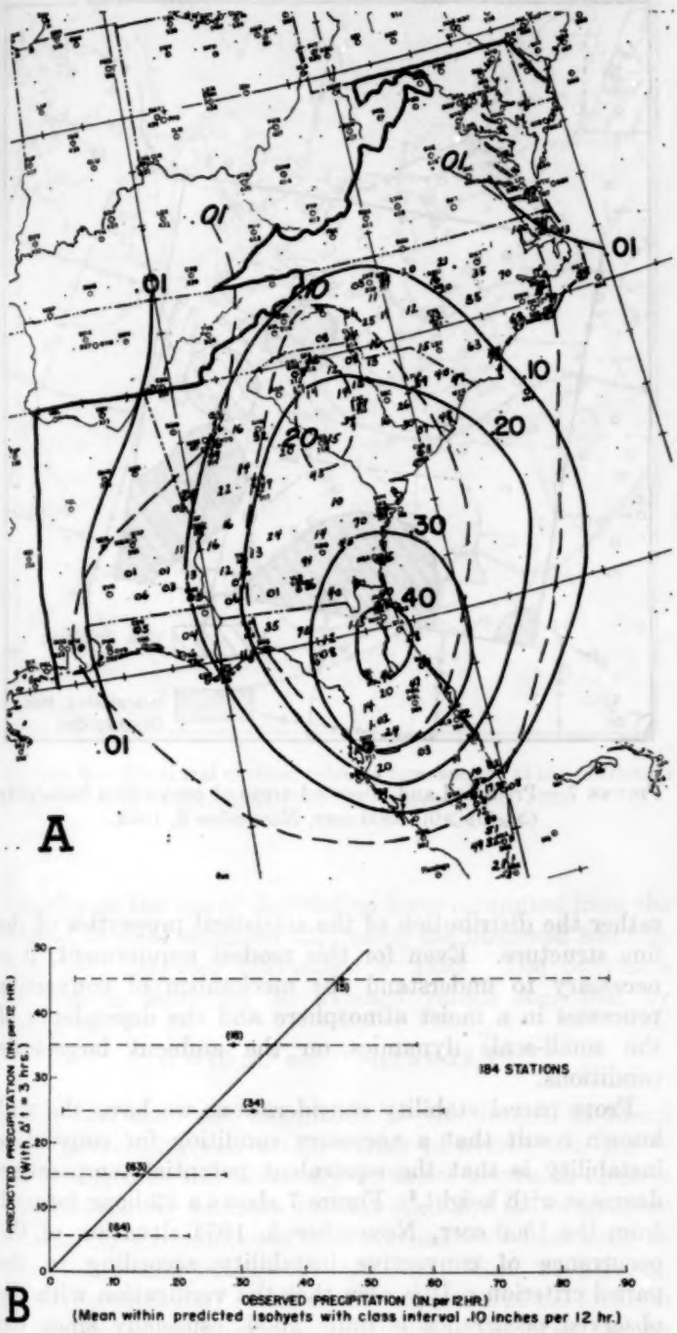

FIGURE 5.—(A) Observed precipitation during period 1500 GMT November 5 to 0300 GMT November 6, 1953 with computed isohyets ($\Delta' t = 3$ hr., solid and $\Delta' t = 12$ hr., dashed) superimposed. R denotes precipitation ≥ 0.01 in. but amount unknown and thus R is not included in the numerical verification. Missing reports and zero precipitation are not shown. (B) Summary of results with observations smoothed for large-scale verification. Numbers in parentheses at plotted points give number of stations averaged in the respective isohyetal channel. Dashed lines indicate standard deviation of observations in respective channel.

hours and is also displaced to the north. Had the flow prediction for this period been correct, as essentially resulted from the 900–700–400-mb. model, the maximum would have been elongated northeastward along the coast. However one can speculate that, in spite of this elongation, the maximum would not have been reduced because of the larger vertical velocities associated with the increased development.

In this particular case the vertical motion fields (fig. 4C, D, G, and H) would have given a fairly realistic qualitative indication of the region of precipitation without referring to the moisture field and its changes. On the other hand, the magnitude of the vertical velocity would have been misleading. In the November 24, 1950 case at 675 mb. an average maximum vertical velocity of +6.5 cm sec^{-1} yielded a predicted maximum precipitation of .23 in./12 hr., while in the November 5, 1953 case an average maximum vertical velocity of +2.5 cm sec^{-1} gave .43 in./12 hr.

In figure 5B we have a comparison of the large-scale smoothed observed precipitation vs. the computed. In this case the plotted points, representing a total of 184 observations within the verification area chosen have more-or-less uniform scatter about the perfect forecast line.

It is interesting to observe the occurrence of much larger standard deviations than were found in the first case. This is a normal characteristic of precipitation at lower latitudes where the incidence of convective instability is greater.

7. PREDICTION OF RELATED ELEMENTS

Charts of the predicted and observed 12-hour changes in dew point at 900 mb. were prepared for the November 5, 1953 case (fig. 6). Cursory qualitative examination of the field distributions reveals an excellent correspondence. The 7.5° C. rise in western Kentucky is predicted quite well. Although the fall area in the Great Lakes region is correct, the minimum is predicted to be too far east. However, although the secondary minimum in western Virginia is correctly placed, the predicted minimum is too small in magnitude. A large discrepancy is noted over Arkansas where the observed rise is predicted as a substantial fall. On the other hand the negative band through the Gulf States, Oklahoma, Kansas is correct, although the observed minimum in the Gulf States is predicted farther to the northwest and twice too large. The rise off the southeast Atlantic Coast is correct but one-third the observed magnitude. Fortunately the discrepancies pointed out above do not greatly affect the precipitation calculations.

The details of the moisture prediction calculations show

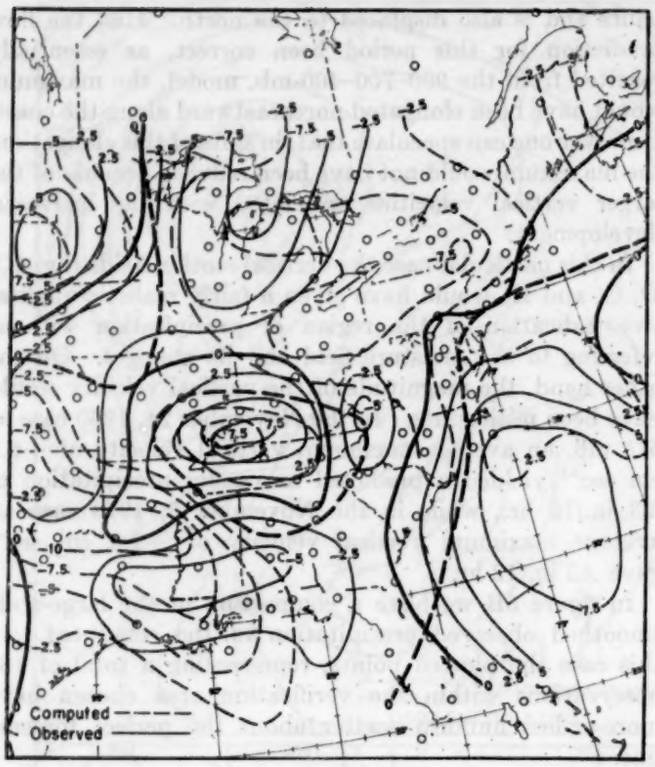

FIGURE 6.—Predicted and observed 12-hour change of dew point (°C.) at 900 mb. between 1500 GMT, November 5 and 0300 GMT, November 6, 1953.

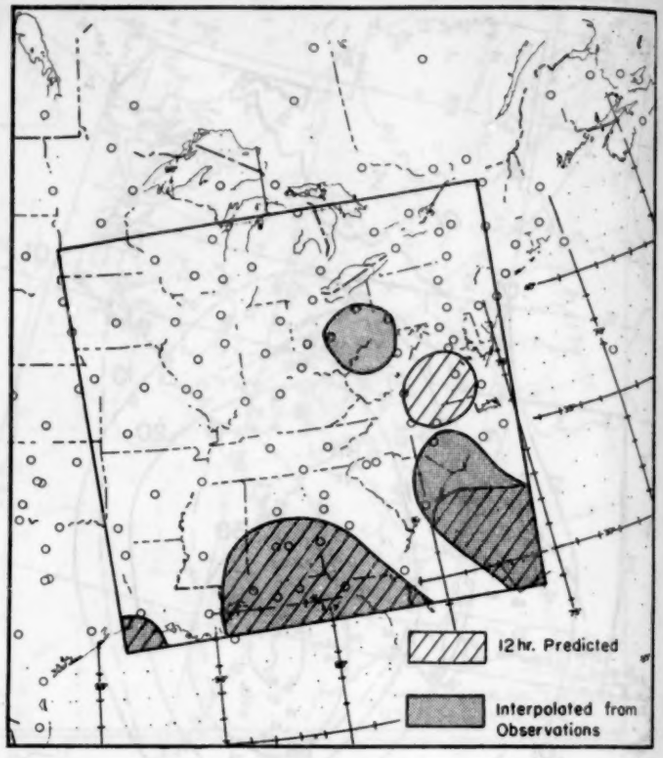

FIGURE 7.—Predicted and observed areas of convective instability ($\partial\theta_E/\partial p>0$), 0300 GMT, November 6, 1953.

that on the average, the condensation, the local time derivative of mixing ratio, and the horizontal and vertical transports of mixing ratio are all of the same magnitude. Hence any approximation neglecting one of these would be invalid.

We see that the large-scale average precipitation is on the whole predicted correctly. Thus one could expect to be able quantitatively to predict total precipitation over large watersheds the scale of a unit mesh area—approximately 35,000 sq mi. The fine structure due to small-scale instability is not capable of being predicted by the models used. For a wholly dynamical prediction, small-scale non-linear theory of the type utilized by Tepper [13] would be required. The obvious difficulty is that an extremely fine network of surface and aerological observations would be required in order to adequately specify initial conditions. For the time being this is not economically feasible operationally, even if the theory were adequately developed. For most purposes it might be sufficient if statistical moments of precipitation higher than the mean (such as the standard deviation) were somehow attainable by dynamical methods.

Thus, what suggests itself, is a statistical-mechanical approach such as is used in other branches of physical science. The fine structure itself is not predicted but rather the distribution of the statistical properties of the fine structure. Even for this modest requirement, it is necessary to understand the mechanism of convective processes in a moist atmosphere and the dependence of the small-scale dynamics on the ambient large-scale conditions.

From parcel stability considerations we have the well known result that a necessary condition for convective instability is that the equivalent potential temperature decrease with height.[5] Figure 7 shows a 12-hour forecast from the 1500 GMT, November 5, 1953 situation of the occurrence of convective instability according to the parcel criterion. It is seen that the verification with the observed occurrence is quite good, especially since the flow prediction at this time was already beginning to degenerate. The release of this instability could be accomplished, theoretically, by sufficient lifting.

8. FRICTIONAL VERTICAL VELOCITY

Although the influence of frictional divergence is not included in the prediction model, it is of interest to study the magnitude of the vertical velocity so produced in one of the cases treated. Figure 8 shows the frictional vertical

[5] Parcel dynamics have often been viewed critically, and with good reason. The most recent is an article by C. H. B. Priestley, "Buoyant Motions and the Open Parcel", *The Meteorological Magazine*, vol. 83, No. 982, April 1954, pp. 107-114.

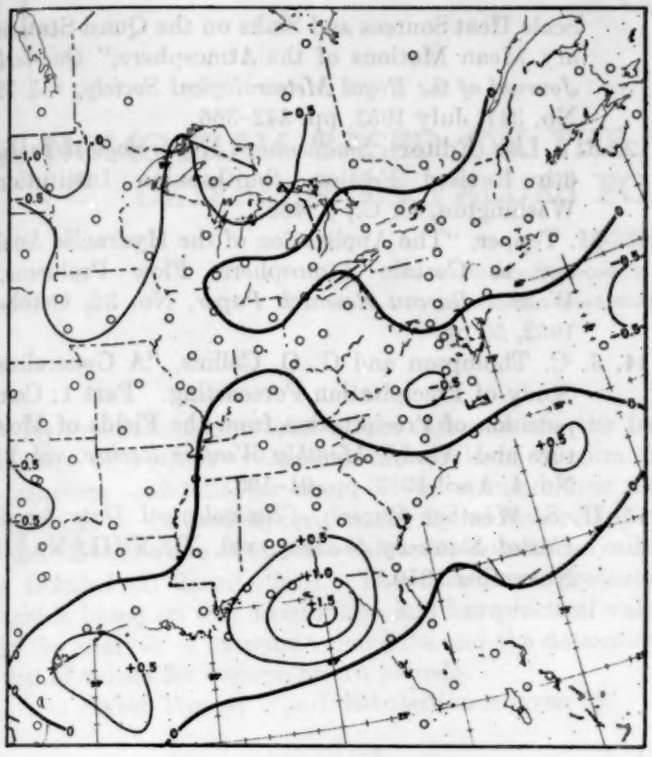

FIGURE 8.—Frictional vertical velocity (cm. sec. $^{-1}$) at top of friction layer computed at 1500 GMT, November 5, 1953.

velocity at the top of the friction layer computed from the second term of equation (25) using the observed 850-mb. flow at 1500 GMT November 5, 1953. The constants are chosen according to average values suggested by Brunt [3]:

$$K \approx 10 \text{ m.}^2 \text{ sec.}^{-1} \text{ and } \nu \approx 22.5°.$$

We see that the magnitude of the forced frictional vertical velocity can attain values of over 1 cm. sec.$^{-1}$. Assuming that this boundary influence decreases linearly with decreasing pressure (as was done for the orographic influence), the computed free vertical velocities even at 675 mb. would change by not more than 25 percent. However there may result significant shifts in the location of centers of maximum or minimum. For example the frictional maximum of +1.5 cm. sec.$^{-1}$ south of Tallahassee would result in shifting the free maximum at 675 mb. to the west over the northern Florida peninsula with little change in magnitude.

On the other hand, fields of free vertical velocity not associated with large-scale storms, and which are thus more of the magnitude of frictional vertical velocities, could undergo large percental changes, conceivably changing sign. Under proper moisture conditions this could make the difference as to whether or not small amounts of precipitation would result over large areas.

9. CONCLUDING REMARKS

The foregoing represents a rudimentary physical framework by which the occurrence of precipitation may be predicted. The reality of the results may be thought of as depending in part on the goodness of the numerical three-dimensional flow prediction and in part on the physical model accounting for moisture changes and the precipitation process.

We have seen that the precipitation calculations were not too sensitive to the failings of the flow prediction in the two cases studied. To some extent this must be due to the time-wise integrating process (eq. (3)). Since these were only 12-hour predictions, it is difficult to surmise the influence of a continually deteriorating flow prediction over a 24-hour period. On the other hand the predictions of dew point and convective instability, which do not involve such an integration, apparently have not suffered inordinately.

The approximations regarding the condensation process discussed in the Introduction do not appear to be crucial in these cases. A more comprehensive study for a larger number of cases should disclose any systematic effect on the predictions. Relaxation of the constraints introduced by these approximations depends on progress in the field of cloud physics. Without these constraints it should in principle be possible to distinguish between large-scale cloudiness and clear skies.

The approximations which were made only for computational convenience in that portion of the calculations done by hand, may of course be eliminated in programming the entire problem for a high-speed computing machine.

Judging the results of the two cases chosen by the subjective standards normally used for precipitation verification, we conclude a skill comparable to that of the predicted flow.

REFERENCES

1. T. Bergeron, "The Problem of Artificial Control of Rainfall on the Globe, II. The Coastal Orographic Maxima of Precipitation in Autumn and Winter," *Tellus*, vol. 1, No. 3, August 1949, pp. 15–32.
2. B. Bolin and J. G. Charney, "Numerical Tendency Computations from the Barotropic Vorticity Equation," *Tellus*, vol. 3, No. 4, November 1951, pp. 248–257.
3. D. Brunt, *Physical and Dynamical Meteorology*, Cambridge University Press, Cambridge, 1939.
4. J. G. Charney, "Numerical Prediction of Cyclogenesis," *Proceedings of the National Academy of Sciences*, vol. 40, No. 2, February 1954, pp. 99–110.
5. J. G. Charney and A. Eliassen, "A Numerical Method for Predicting the Perturbations of the Middle Latitude Westerlies," *Tellus*, vol. 1, No. 2, May 1949, pp. 38–54.

6. J. G. Charney, R. Fjørtoft, and J. von Neumann, "Numerical Integration of the Barotropic Vorticity Equation," *Tellus*, vol. 2, No. 4, November 1950, pp. 237–254.
7. J. G. Charney and N. A. Phillips, "Numerical Integration of the Quasi-Geostrophic Equations, for Barotropic and Simple Baroclinic Flows," *Journal of Meteorology*, vol. 10, No. 2, April 1953, pp. 71–99.
8. J. R. Fulks, "Rate of Precipitation from Adiabatically Ascending Air," *Monthly Weather Review*, vol. 63, No. 10, October 1935, pp. 291–294.
9. W. F. Libby, Address to American Chemical Society, September 12, 1954.
10. J. S. Sawyer, "A Study of the Rainfall of Two Synoptic Situations," *Quarterly Journal of the Royal Meteorological Society*, vol. 78, No. 336, April 1952, pp. 231–246.
11. J. Smagorinsky, "The Dynamical Influence of Large-Scale Heat Sources and Sinks on the Quasi-Stationary Mean Motions of the Atmosphere," *Quarterly Journal of the Royal Meteorological Society*, vol. 79, No. 341, July 1953, pp. 342–366.
12. R. J. List (Editor), *Smithsonian Meteorological Tables*, 6th Revised Edition, Smithsonian Institution, Washington, D. C., p. 485.
13. M. Tepper, "The Application of the Hydraulic Analogy to Certain Atmospheric Flow Problems," *Weather Bureau Research Paper*, No. 35, October 1952, 50 pp.
14. J. C. Thompson and G. O. Collins, "A Generalized Study of Precipitation Forecasting. Part 1: Computation of Precipitation from the Fields of Moisture and Wind," *Monthly Weather Review*, vol. 81, No. 4, April 1953, pp. 91–100.
15. U. S. Weather Bureau, *Climatological Data for the United States by Sections*, vol. XXXVII, No. 11, November 1950.

A NOMOGRAM BASED ON THE THEORY OF EXTREME VALUES FOR DETERMINING VALUES FOR VARIOUS RETURN PERIODS

LEONARD L. WEISS

Hydrologic Services Division, U. S. Weather Bureau, Washington, D. C.

[Manuscript received March 14, 1955, revised April 15, 1955]

Hydrometeorologists and others interested in the frequency of extreme values of meteorologic or climatic quantities—rainfalls, for example—have found their distribution to be well approximated by a Fisher-Tippett type I distribution of extreme values [1] (sometimes called a Gumbel [2] distribution). The nomogram presented here is based on this distribution and has practical value in the analysis of extreme-value data and the determination of values for various return periods.

The Fisher-Tippett type I distribution is given by

$$P=e^{-e^{-y}} \tag{1}$$

where P is the probability that an extreme value will be less than X, e is the base of the natural logarithms and y is a reduced variate defined following equation (5). $1-P$ is, therefore, the probability that an extreme value will equal or exceed X; and the return period T, is the reciprocal of this probability, i. e.,

$$T=1/(1-P) \tag{2}$$

and

$$y=-\ln \ln(1/P) \tag{3}$$

In this case, the general formula, as given by Chow [3], for frequency analysis can be written,

$$X_T=\overline{X}+S_xK \tag{4}$$

where

$$K=(y-\overline{y}_n)/S_n \tag{5}$$

X=individual item in series of extreme values.
X_T=magnitude of item with return period T.
$\overline{X}$=mean of the extreme values.
S_x=standard deviation of the series of extreme values.
$\overline{y}_n$, S_n=mean and standard deviation of the reduced variate y for the particular sample size n.
y=reduced variate=$(X-u)(S_n/S_x)$.
u=mode of extreme values=$\overline{X}-S_x(\overline{y}_n/S_n)$.

The values of $\overline{y}_n$ and S_n, used in the construction of the graph are shown in table 1. These values are calculated from equation (3), setting $P=m/(n+1)$, where $m=1, 2, 3, \ldots . n$.

TABLE 1.—*Computed values of* $\bar{y}_n$ *and* S_n *for selected years of record* n

n	10	15	20	30	40	60	100	∞
$\bar{y}_n$	0.4967	0.5128	0.5236	0.5362	0.5436	0.5521	0.5600	0.5772
S_n	.9573	1.0206	1.0628	1.1124	1.1413	1.1747	1.2065	1.2826

The values of the reduced variate, y, for particular values of T, calculated from equations (2) and (3) and used in constructing the graph are shown in table 2, and the values of K calculated from equation (5) and the values in tables 1 and 2, are shown in table 3. Tables 1, 2, and 3 are similar to previously published ones [3, 4] but are extended to lower values of n.

TABLE 2.—*Computed values of* y *for selected return periods* T *(years)*

T	2	5	10	25	50	100
y	0.3665	1.4999	2.2504	3.1986	3.9019	4.6002

TABLE 3.—*Computed values of* K *for selected years of record* n, *and return periods,* T

T	n						
	10	15	20	30	40	60	100
2	−.1361	−.1433	−.1479	−.1525	−.1552	−.1580	−.1604
5	1.0479	.9672	.9186	.8663	.8379	.8068	.7790
10	1.8319	1.7026	1.6247	1.5410	1.4955	1.4457	1.4010
25	2.8224	2.6316	2.5160	2.3934	2.3263	2.2529	2.1860
50	3.5570	3.3207	3.1786	3.0256	2.9425	2.8516	2.7699
100	4.2865	4.0049	3.8357	3.6534	3.5544	3.4461	3.3486

The relationship given in equation (4) can be put in graph form as shown in figure 1. The nomogram is used in the following way: When the mean and standard deviation of a series of extreme values have been computed, the graph is entered at the desired return period T, thence horizontally to the right to the line of the number of items in the series, thence downward to the line of the standard deviation, thence horizontally to the right to the scale marked D. The value of D read there is added to the mean, $\overline{X}$, to give the value for the required return period T. The graph can be read to within about one percent of the values computed in the usual way.

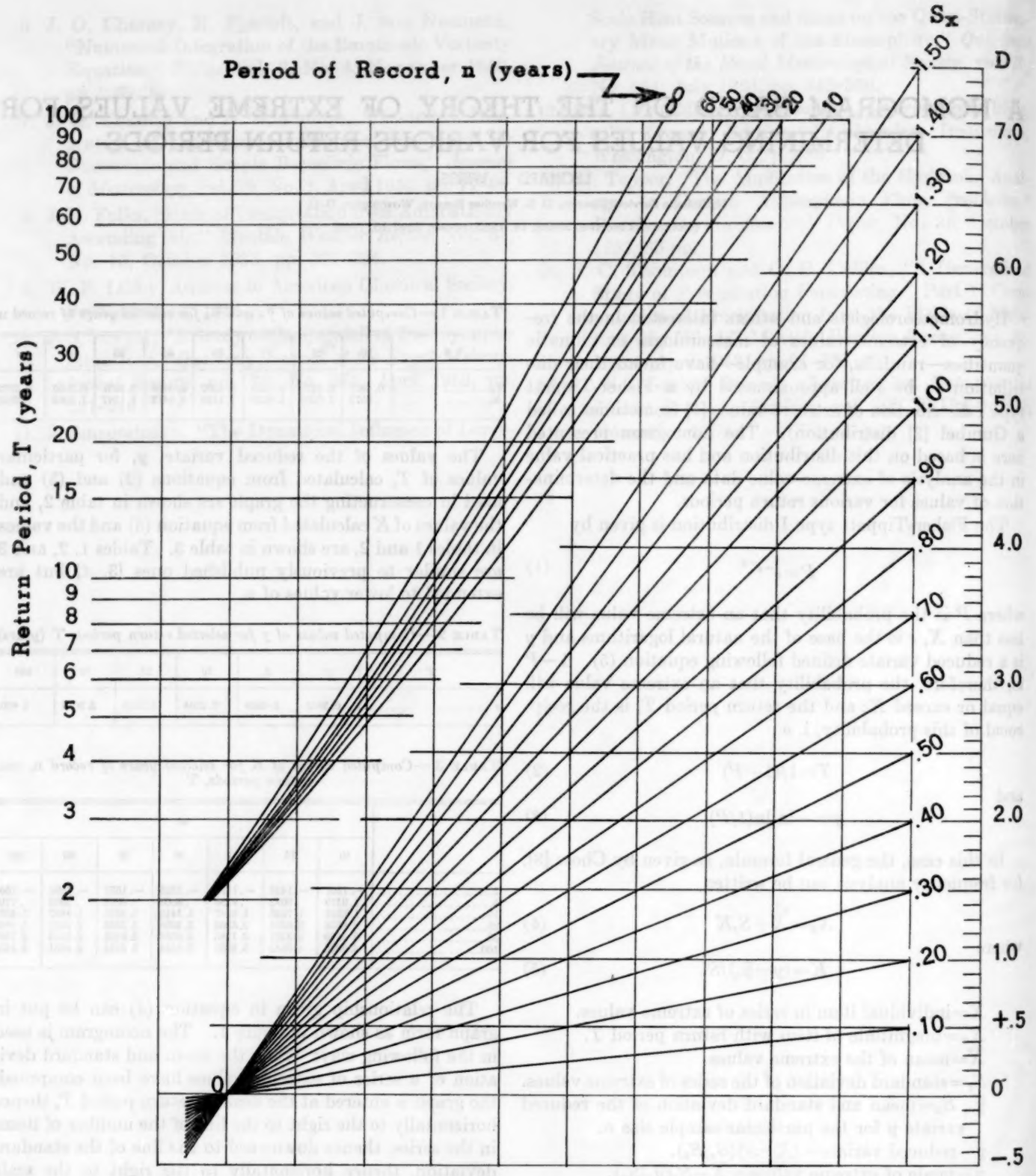

FIGURE 1.—Nomogram to determine D, the amount to be added to the mean of the series of extreme values to get the value for any return period T. The S_x and D scales are relative, i. e., for S_x=4.00 use the line labeled .40 and multiply the D value obtained by 10, etc.

Example: Given the mean value of 3.0 and standard deviation of .50 for the series of 40 extremes, required to determine the value that will be equalled or exceeded on the average once in 10 years (i. e., will have a return period of 10 years). Enter left of diagram at $T=10$, move horizontally to line $n=40$, thence downward to line $S_x=.50$, thence horizontally to the right to scale D to read .75, which added to 3.0 gives the answer 3.75.

REFERENCES

1. R. A. Fisher, and L. H. C. Tippett, "Limiting Forms of the Frequency Distribution of the Largest or Smallest Members of a Sample," *Proceedings of the Cambridge Philosophical Society*, vol. 24, part 2, 1928, pp. 180–190.
2. U. S. Department of Commerce, National Bureau of Standards, "Probability Tables for the Analysis of Extreme-Value Data," *Applied Mathematics Series* 22, July 6, 1953.
3. Ven Te Chow, "The Log-Probability Law and Its Engineering Applications," American Society of Civil Engineers, *Proceedings Separate No. 536*, vol. 80, November 1954.
4. Arnold Court, "Some New Statistical Techniques in Geophysics," from *Advances in Geophysics*, vol. 1, Academic Press, New York, 1952, pp. 45–86.

THE WEATHER AND CIRCULATION OF MARCH 1955 [1]

A Month of Extreme Heat and Cold Over the United States

JAY S. WINSTON

Extended Forecast Section, U. S. Weather Bureau, Washington, D. C.

1. MARKED TEMPERATURE VARIATIONS

The pattern of average temperature anomaly in the United States for March 1955 was essentially simple—cold weather in the North and West and warm weather over the South and East (Chart I–B). However, in many sections of the country temperatures varied in such an extreme manner during March that mean temperature anomalies for the month as a whole do not provide sufficient information about the basic character of the temperature regime. The broad-scale variations in temperature during the month are more clearly revealed by a set of weekly temperature anomaly charts covering most of March (fig. 1).

Figure 1A illustrates the great contrasts in temperature that existed between various parts of the country during the first week of the month. Temperatures over the Northern Plains and the Far West were close to normal values for *January* while those in the East and South were like the normals for *May*. During the second week of the month (fig. 1B) warm weather became dominant over

[1] See Charts I–XV following p. 82 for analyzed climatological data for the month.

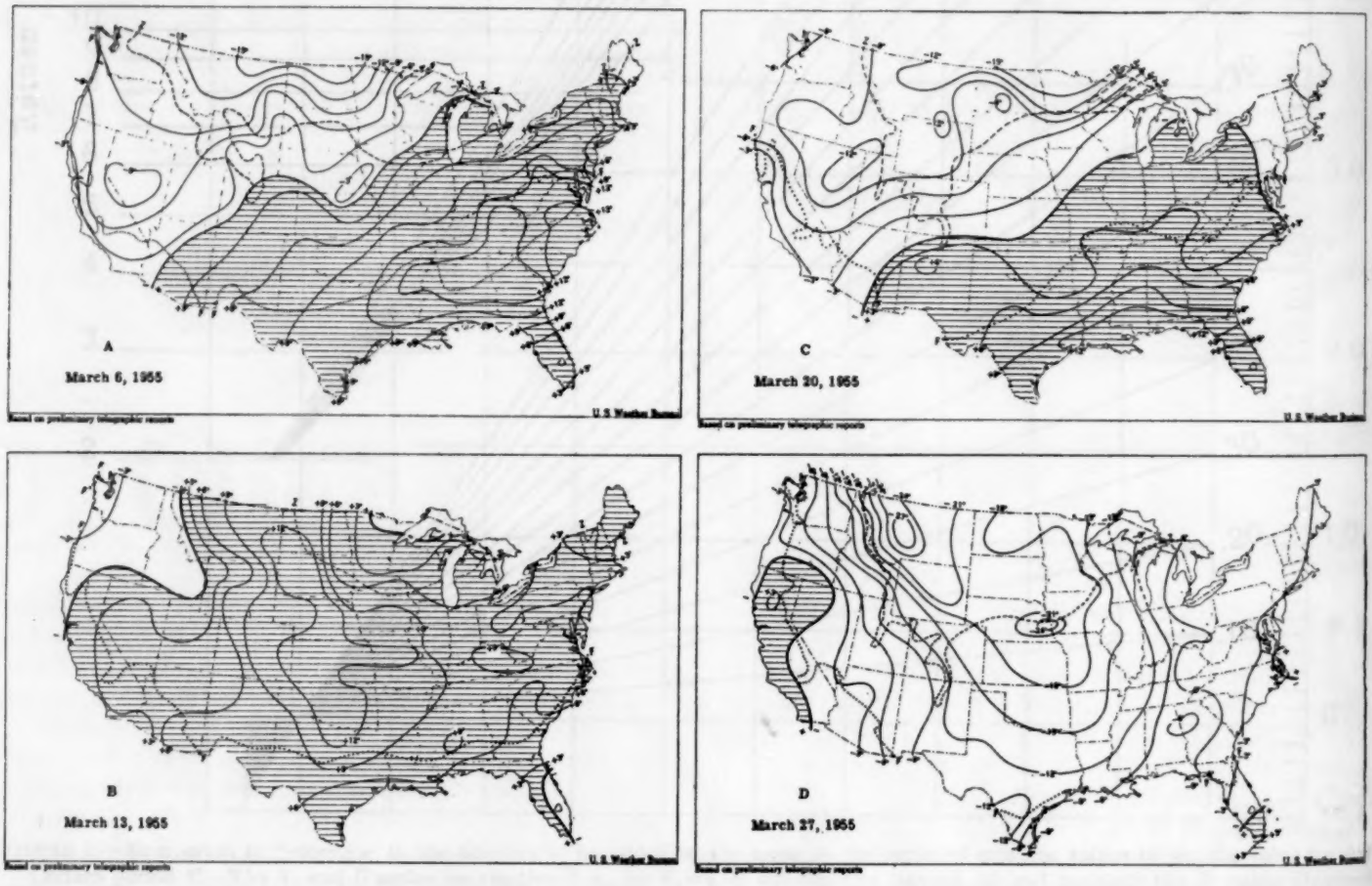

FIGURE 1.—Departure of average temperature from normal (°F.) for the weeks ending at midnight, local time, on the dates shown. Shading indicates temperatures of normal or above; dotted line shows southern limit of freezing temperatures; dashed line, southern limit of zero degrees. Note general containment of cold air in northern and western portions during first three weeks and then the ensuing outbreak of extremely cold air in the week ending March 27.

almost the entire country. The biggest change from the first week was in the Northern Plains and the Southwest, where temperatures were almost as far above normal as they had been below normal the week before. But this rapid emergence of spring in these areas was quickly terminated by new invasions of cold air in the third week (fig. 1C). Some cooling also set in over middle and northeastern sections of the country by the third week, but temperatures remained well above normal in the South. The fourth week was essentially the climax of the month, temperature-wise, as extremely frigid air swept through virtually the entire country (fig. 1D). Temperatures characteristic of midwinter prevailed almost everywhere, and record-low temperatures for this late in the season were observed at most stations in the South and Midwest. Some statistics of this cold wave are given in table 1 of the adjoining article by Kibler and Martin [1].

The fact that the cold wave followed almost directly on the heels of a major March heat wave added to its remarkable and damaging nature. For, during the second and third weeks of March new records for early-season warmth were set at many locations in the middle and eastern sections of the country. This prevailing warmth caused early blooming of fruit trees and other crops in middle, southern, and southeastern portions of the country. Thus plants and trees in these areas were especially vulnerable to the severe frost that accompanied the cold wave even as far south as the Gulf Coast. Preliminary estimates of crop loss due to the cold wave ran as high as $50 million.

2. CONTROLLING CIRCULATION FEATURES

The struggle for dominance between warm and cold air over the United States in March was governed by some fundamental changes in the planetary wave pattern as the month progressed. Fifteen-day mean charts for the two halves of March conveniently portray these events (fig. 2).

During the first half of March (fig. 2A) the circulation pattern at middle and higher latitudes from the Asiatic coast eastward to the central Atlantic consisted of waves of rather large longitudinal dimensions. The key features of this pattern—a trough along the Asiatic coast, a ridge over the eastern Pacific, and a trough over Canada—were all displaced well to the west of the positions of corresponding troughs and ridges found on the normal 700-mb. chart for March [2]. The ridge was located farthest from its normal counterpart—some 20° to 25° of longitude west of the normal ridge over western Canada. Its position over the Gulf of Alaska was very unusual since this area has been found (according to studies now going on in the Extended Forecast Section) to be a zone of minimum frequency of occurrence of both 5-day and 30-day mean ridges at this season in recent years. This ridge, incidentally, was in virtually the same position as during the second half of February [3], when a strong northwesterly

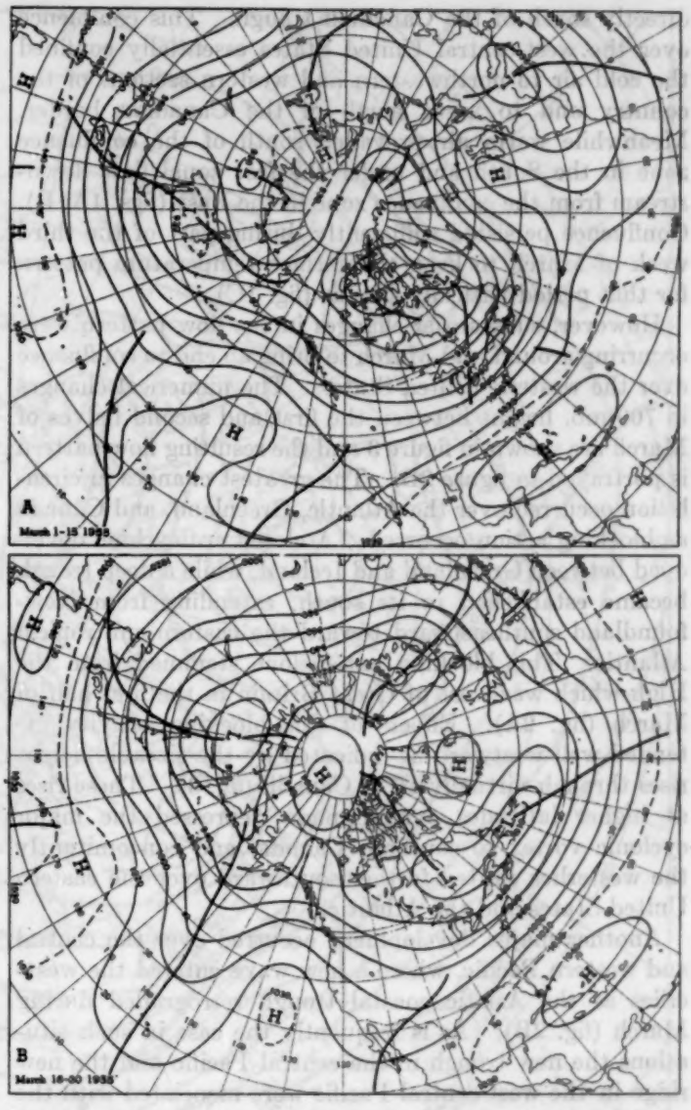

FIGURE 2.—Mean 700-mb. contours (tens of feet) for (A) March 1–15 and (B) March 16–30, 1955. Confluence over west-central United States in first half of March was weakened and shifted to southeastern United States by second half as new wave in Pacific caused eastward motion of middle and lower latitude wave train, while blocking action over Atlantic and Canada depressed westerlies southward.

flow of cold air became established over western North America. Although the ridge decreased in amplitude somewhat during the first half of March, anomalous northwesterly flow persisted over western Canada and Northwestern United States.

Over the west-central United States this cold northwesterly current flowed alongside a warm southwesterly current emanating from relatively low latitudes. This confluence zone was associated with the out-of-phase nature of the wave patterns at higher and lower latitudes. For, a low-latitude trough was situated south-southeast of the eastern Pacific ridge, while a subtropical anticyclone over the southeastern United States and the West Indies was

directly south of the Canadian trough. This confluence over the west-central United States essentially confined the cold air to northwestern and western sections of the country and to areas north of the Canadian border. Meanwhile warm air prevailed south of the confluence zone in the South and under the fast zonal flow downstream from the confluence zone in the East (figs. 1A, B). Confluence persisted sufficiently during part of the third week of March to keep the surface temperature pattern for that period basically similar (fig. 1C).

However, substantial changes in the flow pattern were occurring around mid-March to bring an end to confluence over the western United States. The numerical changes in 700-mb. height between the first and second halves of March are shown in figure 3 and the resulting flow pattern is portrayed in figure 2B. The greatest changes in circulation occurred over the Atlantic, Greenland, and Canada as blocking action occurred. A closed anticyclone developed between Greenland and Iceland, while a deep trough became established to its south, extending from Newfoundland southeastward toward the eastern subtropical Atlantic. This blocking anticyclone stemmed from the High which was west of Great Britain in the first half of March (fig. 2A). Effects of this blocking activity extended well westward as indicated by the sizeable height rises through virtually all of Canada (fig. 3). These rises at higher latitudes over Canada depressed the major cyclonic vortex to southern Canada, and concomitantly the westerlies shifted farther southward over the eastern United States and the Atlantic.

Another major development occurred over the central and western Pacific, where a new wave entered the westerlies as the Asiatic coastal trough retrograded during March (fig. 2B). As is frequently the case in such situations the new trough in the central Pacific and the new ridge in the west-central Pacific were associated with the northward extension of a trough and a ridge which existed earlier in the subtropical Pacific (fig. 2A). Inspection of figure 3 shows that the main height changes associated with this new wave were concentrated exactly in middle latitudes (+36 in the western Pacific and −39 in the east-central Pacific, both at 45° N.). As a result of this shortened wave spacing in the Pacific, the ridge in the eastern Pacific moved some 10° to 15° of longitude eastward between the two halves of March. This progression of the ridge, combined with increased westerlies through the lower latitude portion of the central Pacific trough, resulted in rapid motion of the trough from off California into the southern Plains and the Southwest. Although this trough by strict definition [2] did not build northeastward to join with the Canadian trough over Hudson Bay, maximum cyclonic curvature did extend northeastward across the Midwest and the Great Lakes. Meanwhile the subtropical High over the West Indies also shifted eastward.

[2] Trough and ridge are defined as points of lowest or highest latitude reached by the contours, or minimum or maximum height along latitude circles.

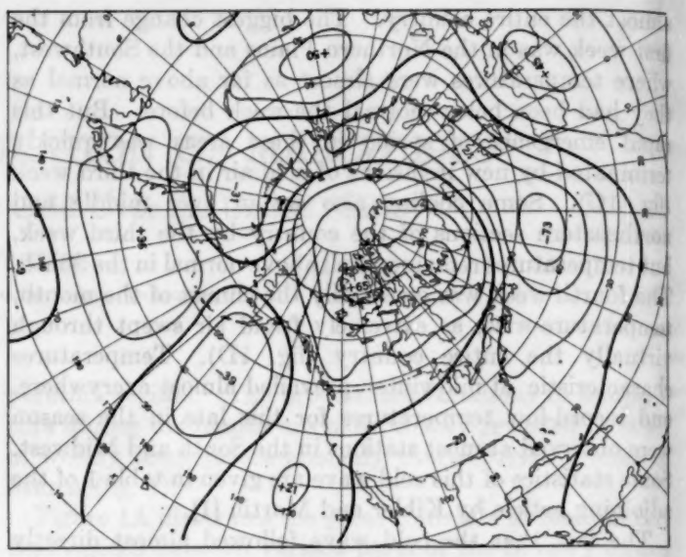

FIGURE 3.—Change in 15-day mean 700-mb. height (tens of feet) from March 1–15 (fig. 2A) to March 16–30, 1955 (fig. 2B). Largest changes occurred in Atlantic and Canada where strong blocking action developed. Note falls in central Pacific and rises in western Pacific associated with new wave development.

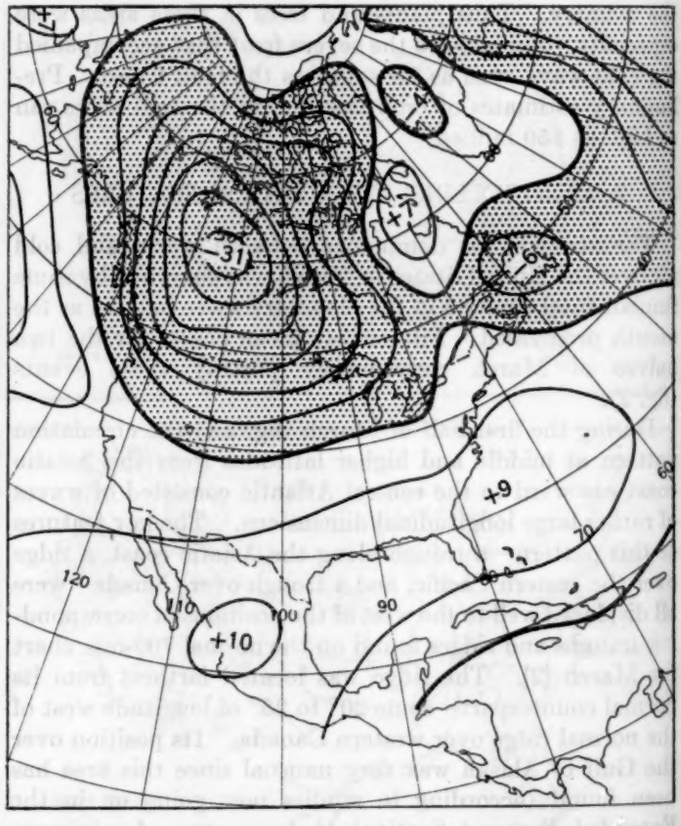

FIGURE 4.—Mean thickness anomaly (tens of feet) for the layer between 1000 and 700 mb. for March 1–30, 1955. Isopleths are drawn at 50-ft. intervals and negative values are shaded. Pool of abnormally cold air in western Canada (310 ft. or 10° C. below normal) was source for extremely cold air which invaded the United States in force late in month.

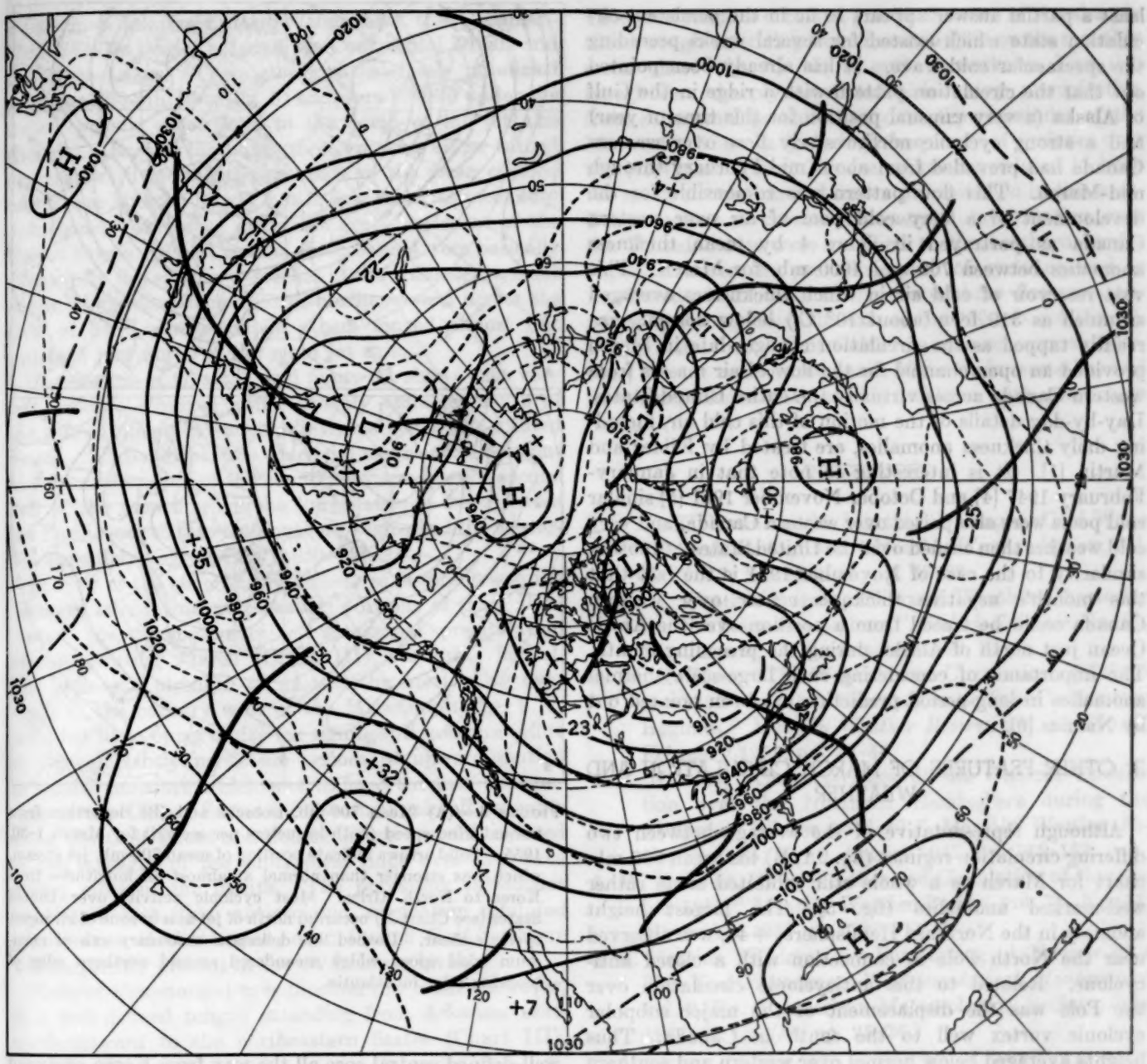

FIGURE 5.—Mean 700-mb. contours and height departures from normal (both in tens of feet) for March 1–30, 1955. Outstanding feature for North America was subpolar cyclonic vortex with associated cyclonic circulation dominating most of Canada and northern half of United States. Stronger-than-normal northwesterly flow west of Mississippi resulted in generally subnormal precipitation over country (see Chart III). Sharply tilted trough between Ohio and Texas produced band of heavy precipitation to its east.

These eastward motions of the waves at middle and lower latitudes, in conjunction with the southward shift of westerlies over the United States, operated to weaken the aforementioned confluence zone over the United States and shift the remnants of it into the Southeast (fig. 2B). The concomitant decrease of zonal flow and increase of northerly flow components over many portions of the United States now began steering cold air masses progressively farther southward in the United States culminating in the final record-breaking outbreak in the fourth week of March (fig. 1D). The increasing frequency of polar Highs invading the United States east of the Continental Divide in the second half of March is evident in Chart IX.

The question naturally arises as to why the cold wave in the latter part of March was so extreme since the observed circulation pattern at the time of the outbreak was certainly not the most abnormal ever observed. At

least a partial answer appears to lie in the persistent circulation state which existed for several weeks preceding the spectacular cold wave. It has already been pointed out that the circulation pattern with a ridge in the Gulf of Alaska (a very unusual position for this time of year) and a strong cyclonic northwesterly flow over western Canada had prevailed from about mid-February through mid-March. This flow pattern was responsible for the development of a very cold pool of air over western Canada as portrayed in figure 4 by mean thickness anomalies between 700 and 1000 mb. for March. This vast reservoir of cold air in which thicknesses averaged as much as 310 feet (about 10° C.) below normal, was readily tapped as the circulation changes late in March provided an open channel for the flow of air masses from western Canada across virtually the entire United States. Day-by-day details of the motion of this cold air, including daily thickness anomalies, are treated by Kibler and Martin [1]. It is interesting to note that in January-February 1947 [4] and October-November 1951 [5] similar cold pools were also poised over western Canada, and very cold weather then ensued over the United States. Another similarity to the case of November 1951 is the fact that this month's negative thickness center over western Canada could be traced from a position over the Arctic Ocean just north of Alaska during the preceding month. The importance of considering such large-scale thermal anomalies in long-period prediction has been pointed out by Namias [6].

3. OTHER FEATURES OF MARCH CIRCULATION AND WEATHER

Although representative of the average between two differing circulation regimes (fig. 2A, B) the mean 700-mb. chart for March as a whole still exhibited some rather well-marked anomalies (fig. 5). The largest height anomaly in the Northern Hemisphere, +44, was observed near the North Pole in connection with a closed anticyclone. Related to this anticyclonic circulation over the Pole was the displacement of the major subpolar cyclonic vortex well to the south in Canada. Thus heights averaged below normal over western and southern Canada and the northern United States. The occurrence of the maximum negative anomaly center in western Canada was also associated with the unusual ridge location in the Gulf of Alaska, which has already been treated in terms of the 15-day mean circulation patterns.

Perhaps the most interesting feature of the cyclonic vortex over Canada was the considerable longitudinal breadth of the cyclonic curvature of the flow, i. e., from western North America to the central Atlantic. Near the southern edge of this cyclonic flow a pronounced monthly mean "jet stream" was located (fig. 6A). Maximum wind speeds in this jet occurred near the Middle Atlantic Coast where values exceeded 20 m./sec. The westerlies were organized in a single belt with a relatively well-defined central core all the way from Korea eastward to the west-central Atlantic. In the eastern Atlantic, however, there was a split in the westerlies in connection with blocking activity, but even in this zone the main branch (the southern one) was a well-organized concentrated current. Figure 6B shows that the winds along this "jet stream" were greater than normal practically all the way from Korea to North Africa. The most extensive region of subnormal wind speeds was in the Pacific at lower middle latitudes, where the maximum westerlies were shifted some 5° to 10° of latitude north of their normal location. This was related to the abnormal strength of the subtropical ridges in the Pacific during the month (fig. 5).

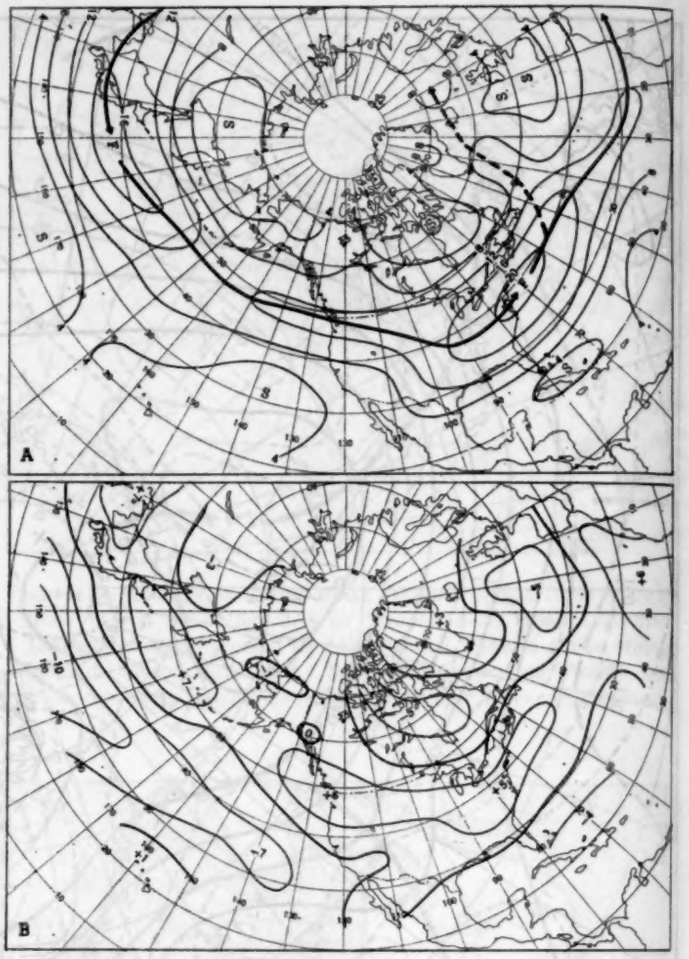

FIGURE 6.—(A) Mean 700-mb. isotachs and (B) departure from normal wind speed (both in meters per second) for March 1–30, 1955. Solid arrows indicate position of mean 700-mb. jet stream, which was stronger than normal at almost all longitudes from Korea to North Africa. Most cyclonic activity over United States (see Chart X) occurred north of jet axis in zone of strongest cyclonic shear. Dashed line delineates secondary axis of maximum wind speed which meandered around northern edge of blocking ridge in Atlantic.

The cyclone tracks for March (Chart X) were concen-

trated in a relatively narrow zone near the Canadian-United States border between the Continental Divide and the Great Lakes. These storm paths closely paralleled the mean 700-mb. flow (fig. 5) and were located under the major cyclonic shear zone to the north of the jet axis (fig. 6A). East of the Lakes these cyclones either turned northeastward around the east side of the mean cyclone center near Hudson Bay or lost their identity as secondary disturbances developed along the northeast coast of the United States. These coastal disturbances were basically affected by the split in westerlies in the Atlantic, as some of the Lows were steered north-northeastward across the Gulf of St. Lawrence while others moved almost due eastward just north of the main jet axis.

Comparison of Chart X and figure 6A shows that very few cyclones occurred either directly under or south of the axis of maximum mean westerlies across the United States. Those few storms which did move across portions of the southern half of the country occurred in the second half of the month when the lower-latitude trough from the Pacific moved into the Southern Plains and the westerlies were displaced farther south (fig. 2).

In view of the general confinement of storminess to the northern border and northeastern portions of the United States, the predominance of subnormal precipitation amounts during March (Chart III) was quite logical. The abnormal strength of west-northwesterly flow over much of the country west of the Mississippi (figs. 5, 6) provided little opportunity for significant moisture influx or for sufficiently persistent periods of upward motion to release moisture which was transported into the confines of the United States. Subnormal rainfall amounts along the Gulf Coast and Southeast were mainly related to the strength of the subtropical ridge over that area during most of the month. The prevailing subsidence associated with this anticyclonic circulation inhibited precipitation in that region, even though Gulf moisture was frequently present in the air in lower levels.

Heavier-than-normal precipitation did occur, however, in a well-defined tongue extending from Arkansas east-northeastward to the northeastern States (Chart III). This precipitation occurred just to the east of the sharply tilted trough extending from Texas to Ohio on the monthly mean chart (fig. 5). It is quite remarkable how this trough line sharply separated this heavy precipitation from subnormal precipitation over the remainder of the Midwest. The relatively high frequency of cyclones over the Northeast (Chart X) was, of course, related to both the mean circulation and heavy precipitation in this area. Other regions of greater-than-normal precipitation over the United States were confined to the northern border region, close to the prevailing path of cyclones, and to the Pacific Northwest where the onshore flow was abnormally strong along the axis of the 700-mb. jet (fig. 6). Precipitation over all of California was subnormal, however, since it was located south of the main westerlies and flow components were mainly offshore with respect to normal (fig. 5).

REFERENCES

1. C. L. Kibler and R. H. Martin, "Damaging Cold Wave of March 23–31, 1955," *Monthly Weather Review*, vol. 83, No. 3, March 1955, pp. 78–82.
2. U. S. Weather Bureau, "Normal Weather Charts for the Northern Hemisphere," *Technical Paper* No. 21, Washington, D. C., October 1952, 74 pp.
3. W. H. Klein, "The Weather and Circulation of February 1955—Another February with Two Contrasting Regimes," *Monthly Weather Review*, vol. 83, No. 2, February 1955, pp. 38–44.
4. J. Namias, "Characteristics of the General Circulation over the Northern Hemisphere during the Abnormal Winter 1946–47," *Monthly Weather Review*, vol. 75, No. 8, August 1947, pp. 145–152.
5. W. H. Klein, "The Weather and Circulation of November 1951," *Monthly Weather Review*, vol. 79, No. 11, November 1951, pp. 208–211.
6. J. Namias, "Thirty-Day Forecasting: A Review of a Ten-Year Experiment," *Meteorological Monographs*, vol. 2, No. 6, American Meteorological Society, July 1953, 83 pp. (see pp. 25–26.)

DAMAGING COLD WAVE OF MARCH 23–31, 1955

C. L. KIBLER and R. H. MARTIN

National Weather Analysis Center, U. S. Weather Bureau, Suitland, Md.

1. INTRODUCTION

The cold wave of March 23–31, 1955, was typical of Arctic outbreaks that occur frequently during the winter season, but was phenomenal for the early spring. The severity of this freeze is evidenced by the many minimum temperature records (see table 1) that were broken as the cold air moved south and east across the United States, and is of special interest because of the extensive freeze damage to crops and shrubbery.

One of the causes of the great damage was the warm weather of the previous week. Departures of average temperature from normal for the weeks ending March 21 and 28 respectively are shown in figure 1C and D of the preceding article by Winston. For the week ending March 21, the Southern, Central, and Southeastern States experienced temperatures above normal. This warm weather permitted the fruits and flowers to advance rapidly, but the early beginning was severely checked as the cold air extended eastward to the Atlantic Coast.

The purpose of this paper is to discuss the weather sequence that was associated with this severe cold wave.

2. THE ARCTIC HIGH OVER CANADA

The synoptic weather picture as it existed on March 23, at 1500 GMT is presented in figure 1. The 1000-mb. chart shows a large complex Low dominating southeastern Canada with a trough from the Great Lakes to a weak cyclonic circulation near St. Cloud, Minn. The High centered over Georgia was a remnant of a weak surge of cold air earlier in the week. The Arctic High centered just north of Alberta, Canada, with a ridge to the east of the Continental Divide, was the surface reflection of the very cold air dome that was destined to push southeastward over the United States.

The 1000- to 500-mb. thickness of 15,800 feet at Edmonton, Alberta, and northward was 400 feet thinner, i. e., colder, than the four-year (1947–1951) March minima as shown by Sutcliffe [1]. From the cold High in Canada to the front near Topeka, Kans., there existed 2,000 feet of 1000- to 500-mb. thickness gradient, indicating the great magnitude of the cold air poised and waiting to move south.

The 500-mb. chart for March 23, 1500 GMT (fig. 1b) indicates moderately strong westerlies throughout the United States with a broad cyclonic flow. There were two closed low cells in southern Canada, one near Montreal, the other near Edmonton, and a sharp ridge line extending inland along the Canadian-Alaskan border from a broader ridge just off the western Canadian coast. A sharp trough in the central Pacific with a closed Low at 47° N., 160° W., completed the 500-mb. picture.

The stagnant cold Low over Alberta at 500 mb. superimposed on the surface High made ideal conditions for the development of extremely cold temperatures. The

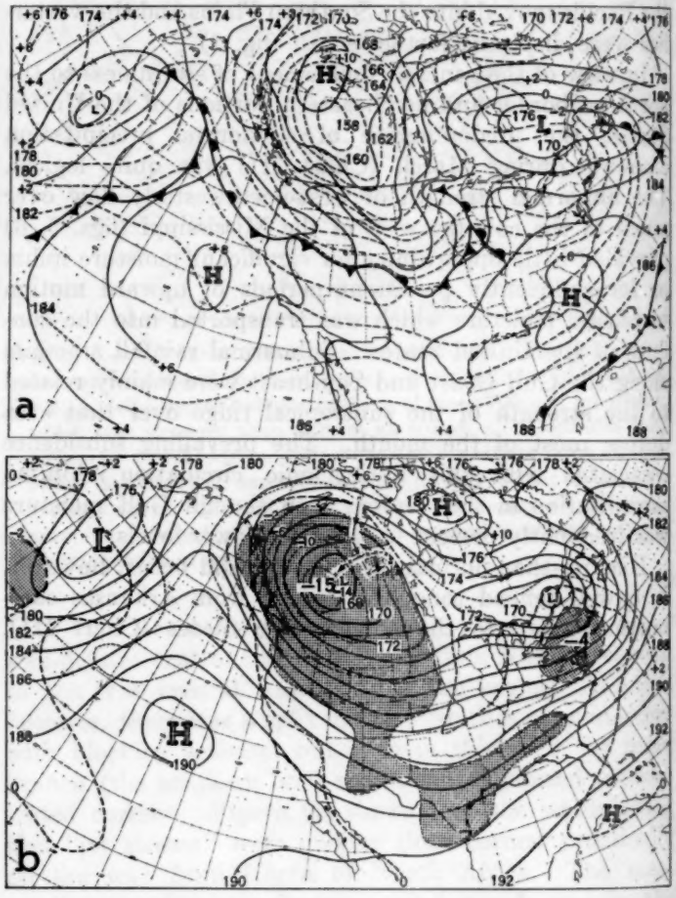

FIGURE 1.—1500 GMT, March 23, 1955. (a) 1,000- to 500-mb. thickness lines (dashed) superimposed on 1,000-mb. contours (solid) and surface fronts. (b) 1,000- to 500-mb. thickness departure from normal (dashed) superimposed on 500-mb. contours (solid) with negative departure of 200 feet or more shaded. All isopleths are labeled in hundreds of feet. Track shows previous 12-hour positions of low center.

−1400-ft. departure from normal 1000- to 500-mb. thickness values over Edmonton were testimony of the extreme nature of the situation.

3. THE ARCTIC HIGH MOVES SOUTH

A deep 500-mb. Low, associated with a deepening surface system in the western Pacific on March 23, moved to the eastern Aleutian Islands by March 25. The strong southwesterly flow in the southeast quadrant of this system may be seen in figure 2. It was also evident by this time that the westerlies would require the central Pacific trough to remain cut off.

Confluence over the area near ship PAPA (50° N., 145° W.) appeared to be building the eastern Pacific ridge into western Canada, joining it with the warm westward-moving Canadian High. The result of this was increased northerly flow over western North America, which in turn could direct the cold air, then in the North Central States, farther south and east. Surface minimum temperatures over the northern United States had started to reflect the intensity of this cold air by the morning of March 25 with Helena, Mont., recording −30° F., the coldest March temperature ever recorded there.

As the weak Low over Iowa, March 23, 1500 GMT, moved northeast through the St. Lawrence Valley, the associated cold front moved east and south. During the 48 hours that elapsed between figures 1 and 2, the Arctic High became more cellular and the first indication of a break-off cell was in evidence near Great Falls, Mont.

The center of the cold air, as indicated by the closed 1000- to 500-mb. thickness line near Edmonton on March 23, had moved to Huron, S. Dak., by March 25, with only slight modification as evidenced by the central thickness value. In this center the 1000- to 500-mb. thickness remained in excess of 1,400 feet thinner than normal (figs. 1b and 2b) during the initial southward movement of the cold air, although the actual thickness indicated air mass warming.

The 1000- to 500-mb. thickness values shown in figure 2a are of record-breaking magnitude over South Dakota, Nebraska, and Iowa. These values are 400 to 600 ft. lower than the March minima prepared by Sutcliffe

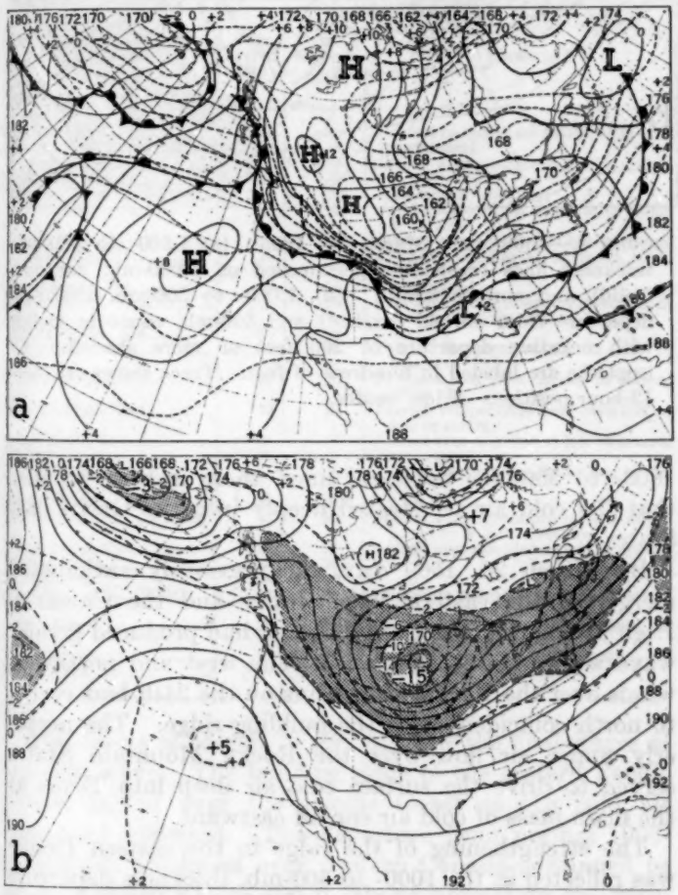

FIGURE 2.—1500 GMT, March 25, 1955. (a) 1,000- to 500-mb. thickness lines (dashed) superimposed on 1,000-mb. contours (solid) and surface fronts. (b) 1,000- to 500-mb. thickness departure from normal (dashed) and 500-mb. contours (solid) with negative departure of 200 feet or more shaded. All isopleths are labeled in hundreds of feet.

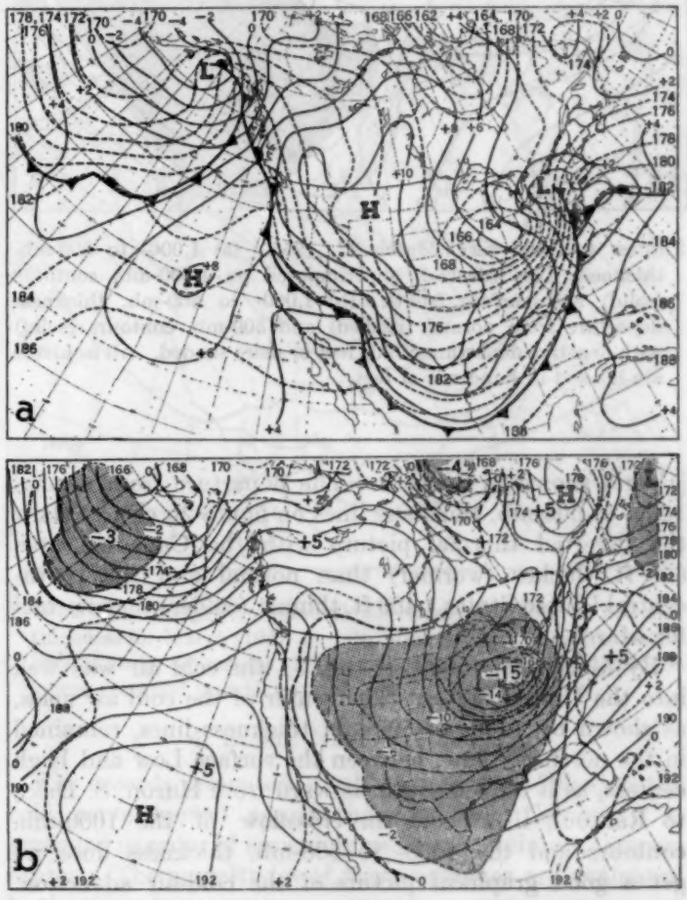

FIGURE 3.—1500 GMT, March 26, 1955. (a) 1,000- to 500-mb. thickness lines (dashed) superimposed on 1,000-mb. contours (solid) and surface fronts. (b) 1,000- to 500-mb. thickness departure from normal (dashed) and 500-mb. contours (solid) with negative departure of 200 feet or more shaded. All isopleths are labeled in hundreds of feet.

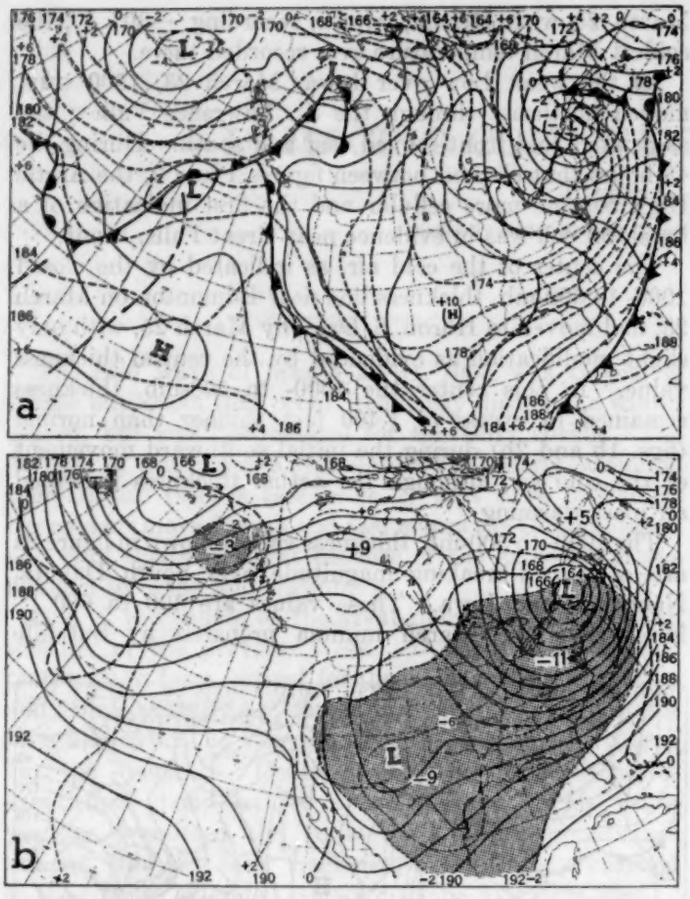

FIGURE 4.—1500 GMT, March 27, 1955. (a) 1,000- to 500-mb. thickness lines (dashed) superimposed on 1,000-mb. contours (solid) and surface fronts. (b) 1,000- to 500-mb. thickness departure from normal (dashed) and 500-mb. contours (solid) with negative departure of 200 feet or more shaded. All isopleths are labeled in hundreds of feet.

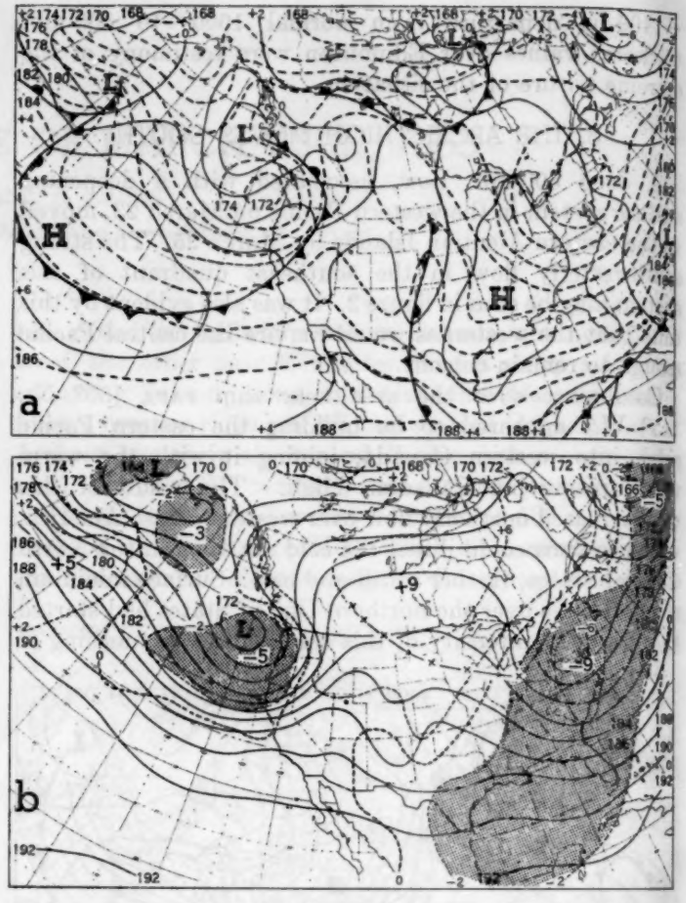

FIGURE 5.—1500 GMT, March 29, 1955. (a) 1,000- to 500-mb. thickness lines (dashed) superimposed on 1,000-mb. contours (solid) and surface fronts. (b) 1,000- to 500-mb. thickness departure from normal (dashed) and 500-mb. contours (solid) with negative departure of 200 feet or more shaded. All isopleths are labeled in hundreds of feet. Track shows previous 12-hour positions of low center.

[1] and shown in figure 6. The departure from normal 1000- to 500-mb. thickness lines on figure 2b clearly show the inverted thermal picture with the Canadian area 600 ft. thicker (warmer) than normal and the north-central United States 1,400 ft. thinner (colder) than normal for March.

By March 26, 1500 GMT (fig. 3), the cold air was well into the United States. The center of the cold air mass, as shown by 1000- to 500-mb. thickness lines, remained in the northerly flow, between the surface Low and High centers, as it moved southeastward from Huron, S. Dak., to Rantoul, Ill. From the crossflow of the 1000-mb. contours and the 1000- to 500-mb. thickness lines we get a good graphical picture of the cold-air advection. From Atlanta, Ga., to Oklahoma City, Okla., there was a gradient of 210 feet at the 1000-mb. level which produced an average northerly flow component of 50 knots. With this strong northerly flow almost perpendicular to the 1000- to 500-mb. thickness lines, there is little wonder that the cold air penetrated deeply into the Gulf Coast States.

By March 26, 1500 GMT, the previously anticipated merger of the eastern Pacific ridge and the Canadian High at 500 mb. was complete, and had produced greater wave amplitude at this level. The west and northwest winds over the Rocky Mountains on the 24th had veered to north coincident with the building ridge. The northerly upper air flow over the Rocky Mountain States served to drive the surface cold air deep into Texas as the main mass of cold air spread eastward.

The strengthening of the ridge in the eastern Pacific was reflected in the 1000- to 500-mb. thickness departure from normal. On the 25th there was an area of positive departure from normal near California and another in northwestern Canada. By March 26, 0300 GMT (not shown), these two areas of positive departure from normal

had merged in the vicinity of Annette, Alaska, and by March 26, figure 3b, the combined area had expanded and was 400 feet above normal. This type of change frequently occurs in advance of a deepening cyclone as it moves into the Gulf of Alaska, and alert forecasters have learned that it is a critical area for forecasting weather over much of North America.

By March 27, 1500 GMT (fig. 4a), the 1000-mb. High was centered near Fort Worth, Tex., with a ridge along the east coast of Mexico that thrust the cold air as far south as Mexico City. The eastward thrust of the High extended the cold air along the Gulf Coast and into the Carolinas with many new minimum temperature records. New Orleans reported the latest spring freeze since 1894 and the lowest temperature for so late in the season for 82 years of record [2]. In 24 hours the 1000- to 500-mb. thickness over the Carolinas changed from 200 ft. above normal to 200–700 ft. below normal, and Cape Hatteras cooled 1,050 ft.

TABLE 1.—*Record-breaking minimum temperatures at selected stations along the path of the Arctic air mass that moved south and east over the United States, March 28–31, 1955*

Location	Date, March 1955	Minimum temperature (° F.)	Remarks
Helena, Mont.	25	−30	Coldest on record for month of March.
International Falls, Minn.	27	−15	Broke record.
Denver, Colo.	26	−4	Lowest ever recorded so late in spring.
Missoula, Mont.	26	−3	Do.
Omaha, Nebr.	26	0	New record.
Des Moines, Iowa.	26	2	Previous record for this late in season 4° on 25th.
Peoria, Ill.	26	5	Lowest ever recorded so late in spring.
Kansas City, Mo.	25	9	Previous record so late in season, 12° in 1894.
Indianapolis, Ind.	26	10	Broke record.
Greenville, N. C.	27	16	Previous lowest temperature so late in spring, 27.4° on April 15, 1907.
Muscle Shoals, Ala.	26	18	
Memphis, Tenn.	26	18	Lowest temperature for so late in season.
Birmingham, Ala.	27	18	Previous record for so late in season, 29° in 1937.
Wichita Falls, Tex.	26	19	Lowest temperature ever recorded so late in spring.
Little Rock, Ark.	26	19	Lowest ever recorded so late in season.
Raleigh, N. C.	27	20	Broke record.
Augusta, Ga.	27	21.6	Lowest temperature for so late in the spring.
Waco, Tex.	26	25.0	Do.
Charleston, S. C. (WBAS).	27	26	Minimum temperature records established for so late in season.
Columbia, S. C.	28	26	Lowest ever recorded so late in spring.
Savannah, Ga.	27	26.4	Do.
Del Rio, Tex.	28	27	Do.
Charleston, S. C. (WBO).	27	28	Minimum temperature records established for so late in season.
New Orleans, La.	27	30	Coldest temperature experienced in city since February 1951.
Lake Charles, La.	27	31	New record for so late in spring.
Laredo, Tex.	28	35	Lowest for so late in spring.

The charts of March 29 (fig. 5) show the final stages of the cold wave. The building ridge of the eastern Pacific moved inland over the Pacific Coast as the cold air continued eastward. The departure from normal 1000- to 500-mb. thickness over western Canada continued to grow, increasing from 400 ft. above normal on the 26th, to 800 ft. above normal on the 27th, with the 800-ft. above normal area expanding slightly by the 29th. With the shift of the ridge onshore, temperatures began to return to normal over the United States.

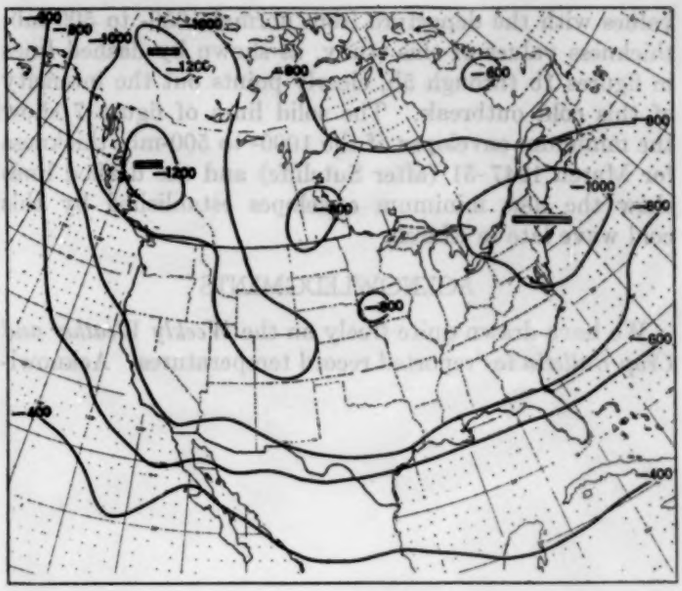

FIGURE 6.—Departure from normal of the southern (minimum) envelopes of 1,000- to 500-mb. thickness for March. (1947–51 data after Sutcliffe [1]).

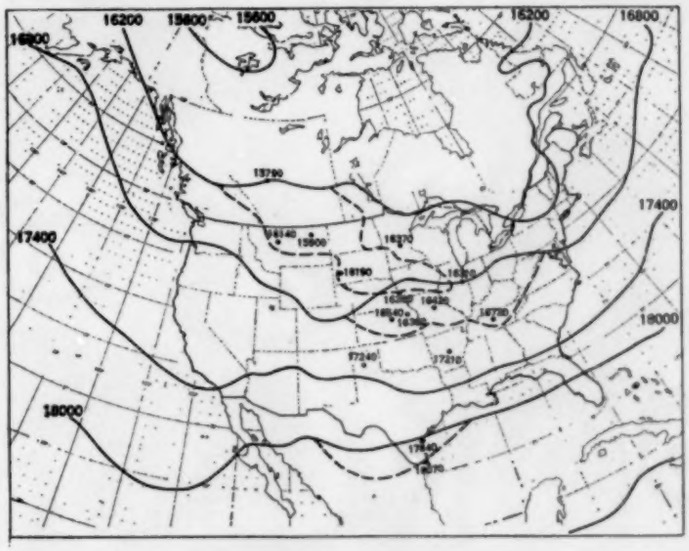

FIGURE 7.—Southern (minimum) envelopes of 1,000- to 500-mb. thickness for March (1947–51 data, after Sutcliffe [1]) with dashed lines showing extensions of the envelopes demanded by thickness values recorded in cold wave of March 1955.

4. SOME NEW RECORDS

The records presented in table 1 were established as the cold wave moved across the country. Column 3 is arranged in order of ascending values of minimum temperatures. The magnitudes of these extremes are evaluated in the remarks.

Figure 6 presents the departure from normal of the southern (minimum) envelopes of 1000- to 500-mb. thickness for March (1947–51) after Sutcliffe [1]. A comparison of these

values with the departure from normal 1000- to 500-mb. thickness values of this study, as shown by dashed lines in figures 1b through 5b, clearly points out the intensity of this cold outbreak. The solid lines of figure 7 show the minimum envelopes of the 1000- to 500-mb. thickness for March 1947–51 (after Sutcliffe) and the dashed lines show the new minimum envelopes established by this cold wave late in March.

ACKNOWLEDGMENTS

We have drawn quite freely on the *Weekly Weather and Crop Bulletin* for reported record temperatures. Acknowledgment is made to senior members of NWAC for review and suggestions.

REFERENCES

1. R. C. Sutcliffe, *Charts of Maximum and Minimum Thickness Lines 1000/500 mb., Northern Hemisphere 1947–1951*, Meteorological Office, Dunstable, England, 24 charts. (Reproduced by U. S. Air Weather Service, Washington.)
2. U. S. Weather Bureau, *Weekly Weather and Crop Bulletin, National Summary*, vol. XLII, No. 13, March 28, 1955.

U. S. GOVERNMENT PRINTING OFFICE: 1955

Chart I. A. Average Temperature (°F.) at Surface, March 1955.

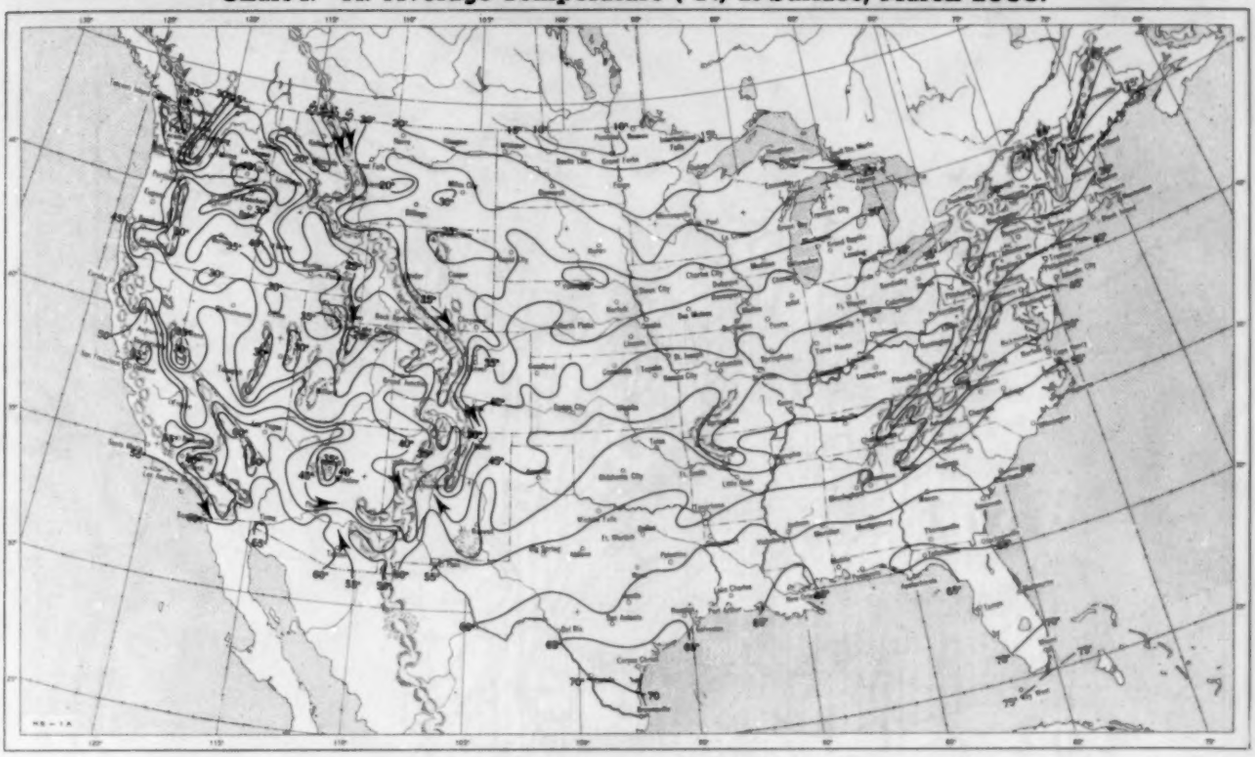

B. Departure of Average Temperature from Normal (°F.), March 1955.

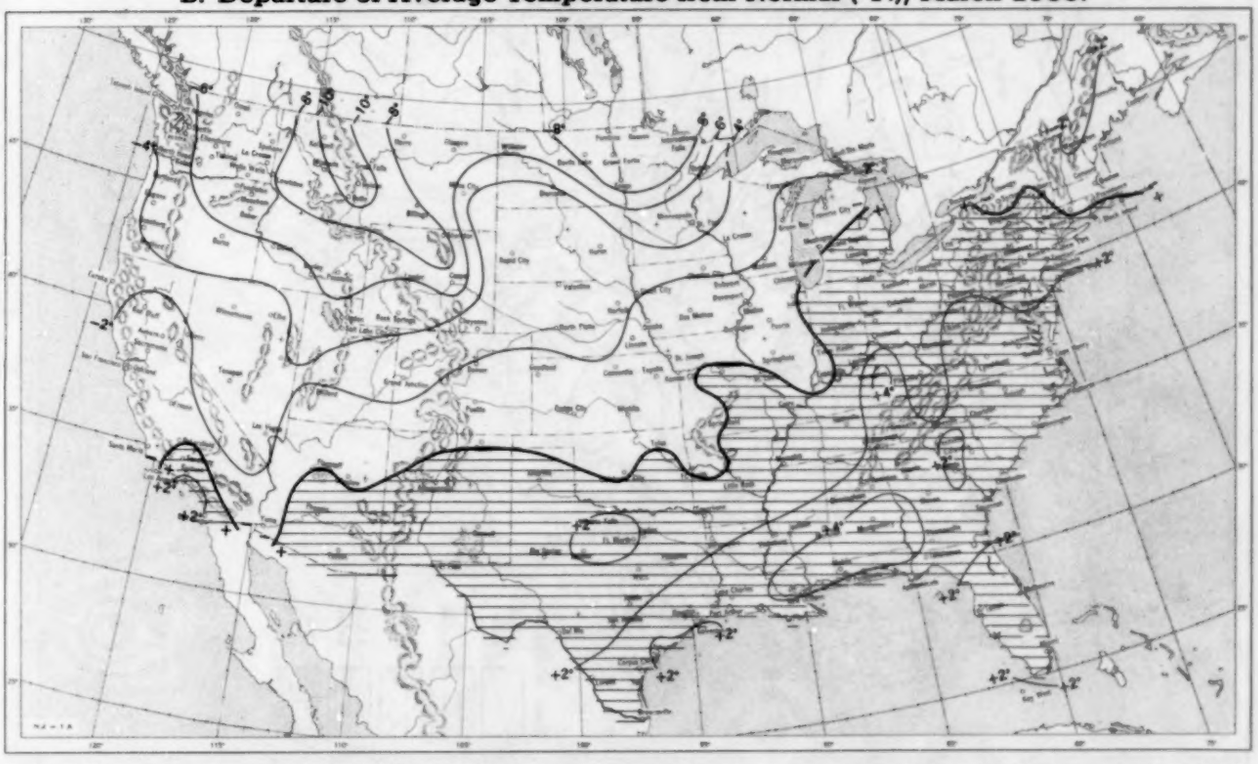

A. Based on reports from 800 Weather Bureau and cooperative stations. The monthly average is half the sum of the monthly average maximum and monthly average minimum, which are the average of the daily maxima and daily minima, respectively.
B. Normal average monthly temperatures are computed for Weather Bureau stations having at least 10 years of record.

Chart II. Total Precipitation (Inches), March 1955.

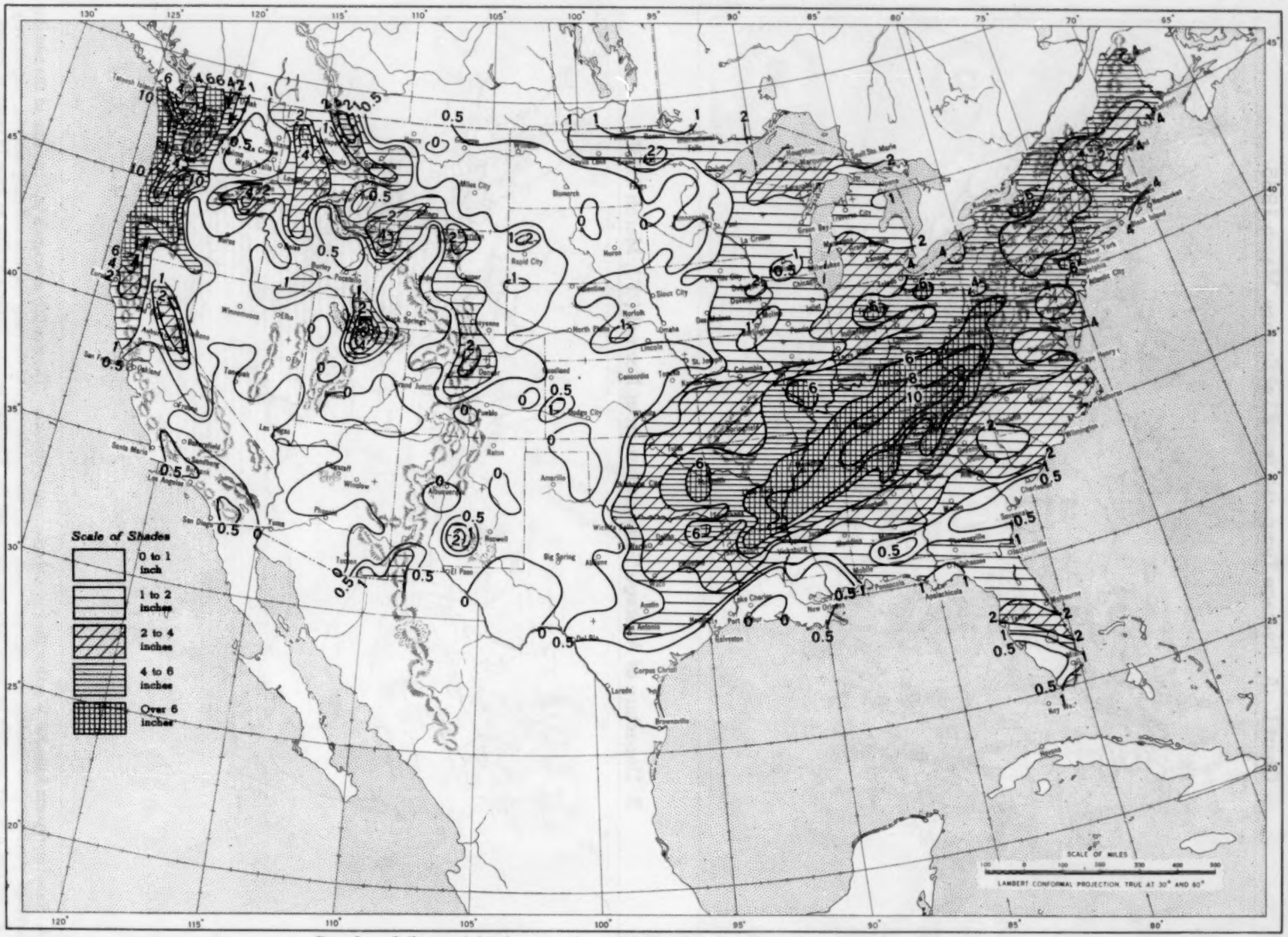
Scale of Shades
0 to 1 inch
1 to 2 inches
2 to 4 inches
4 to 6 inches
Over 6 inches
SCALE OF MILES
LAMBERT CONFORMAL PROJECTION TRUE AT 30° AND 60°

Based on daily precipitation records at 800 Weather Bureau and cooperative stations.

Chart III. A. Departure of Precipitation from Normal (Inches), March 1955.

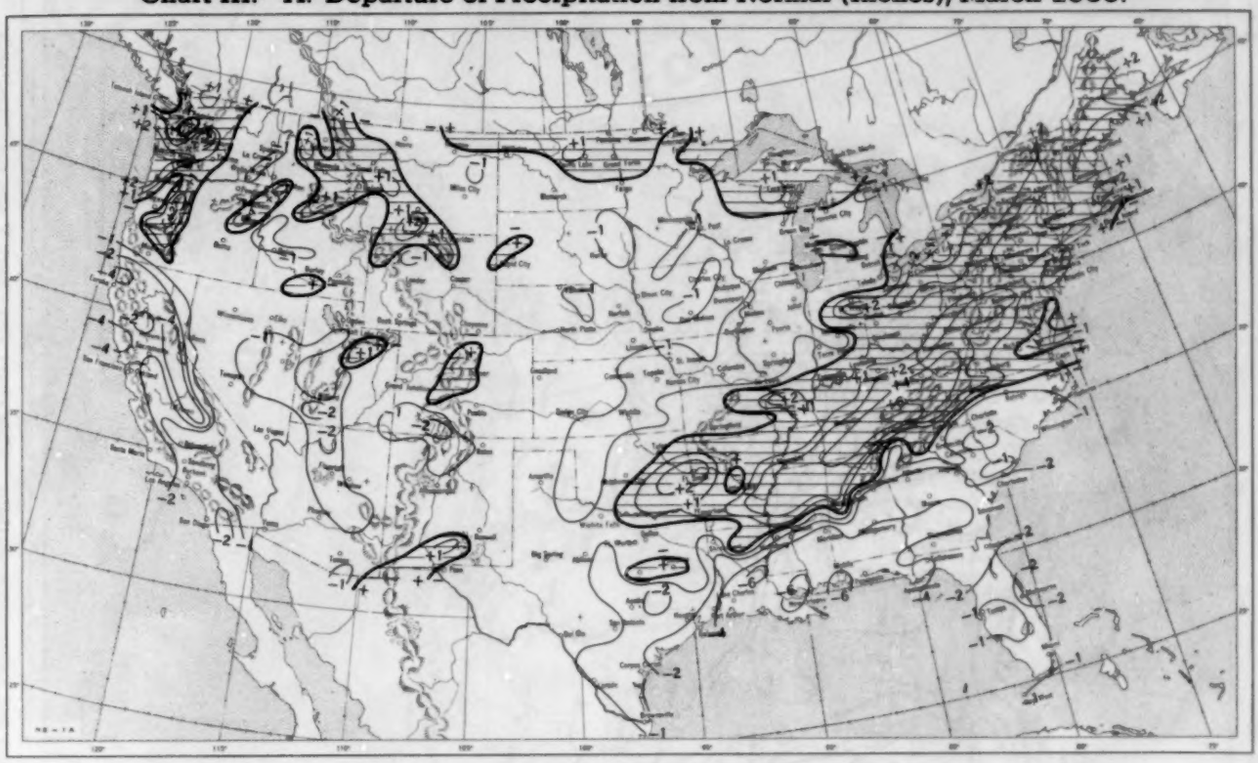

B. Percentage of Normal Precipitation, March 1955.

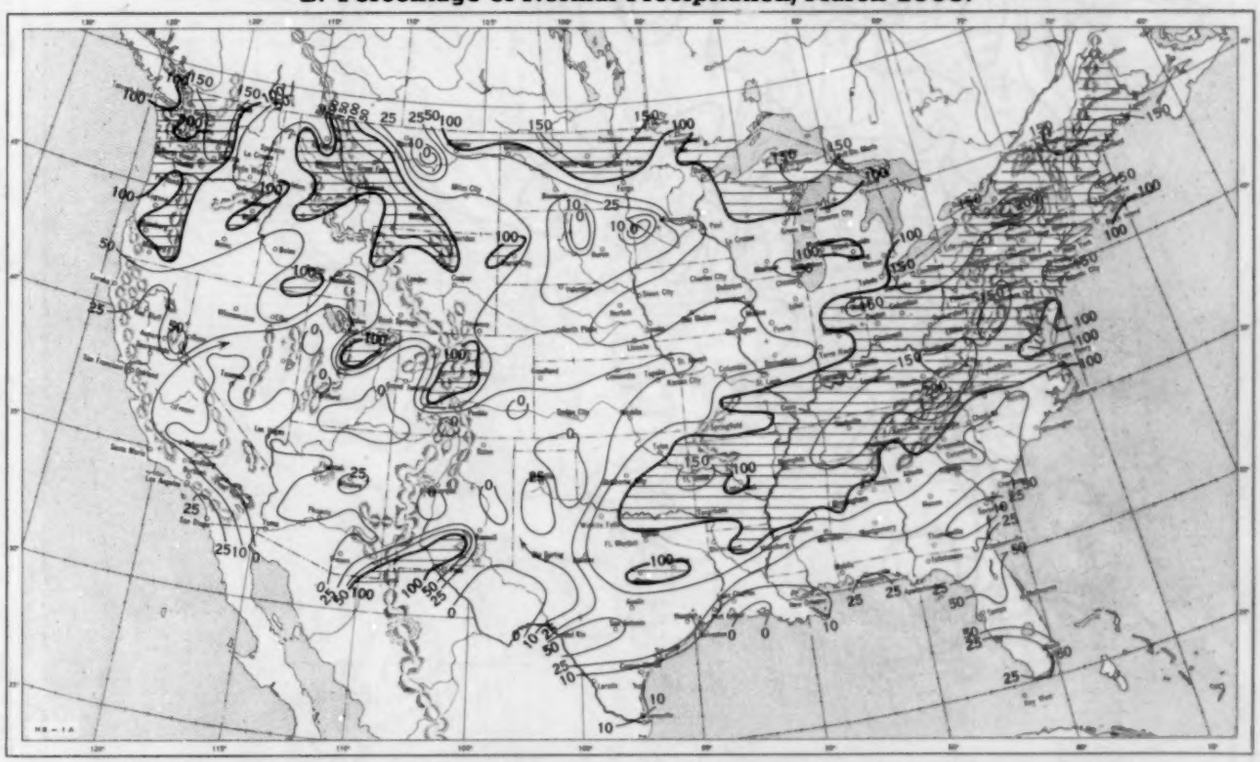

Normal monthly precipitation amounts are computed for stations having at least 10 years of record.

Chart IV. Total Snowfall (Inches), March 1955.

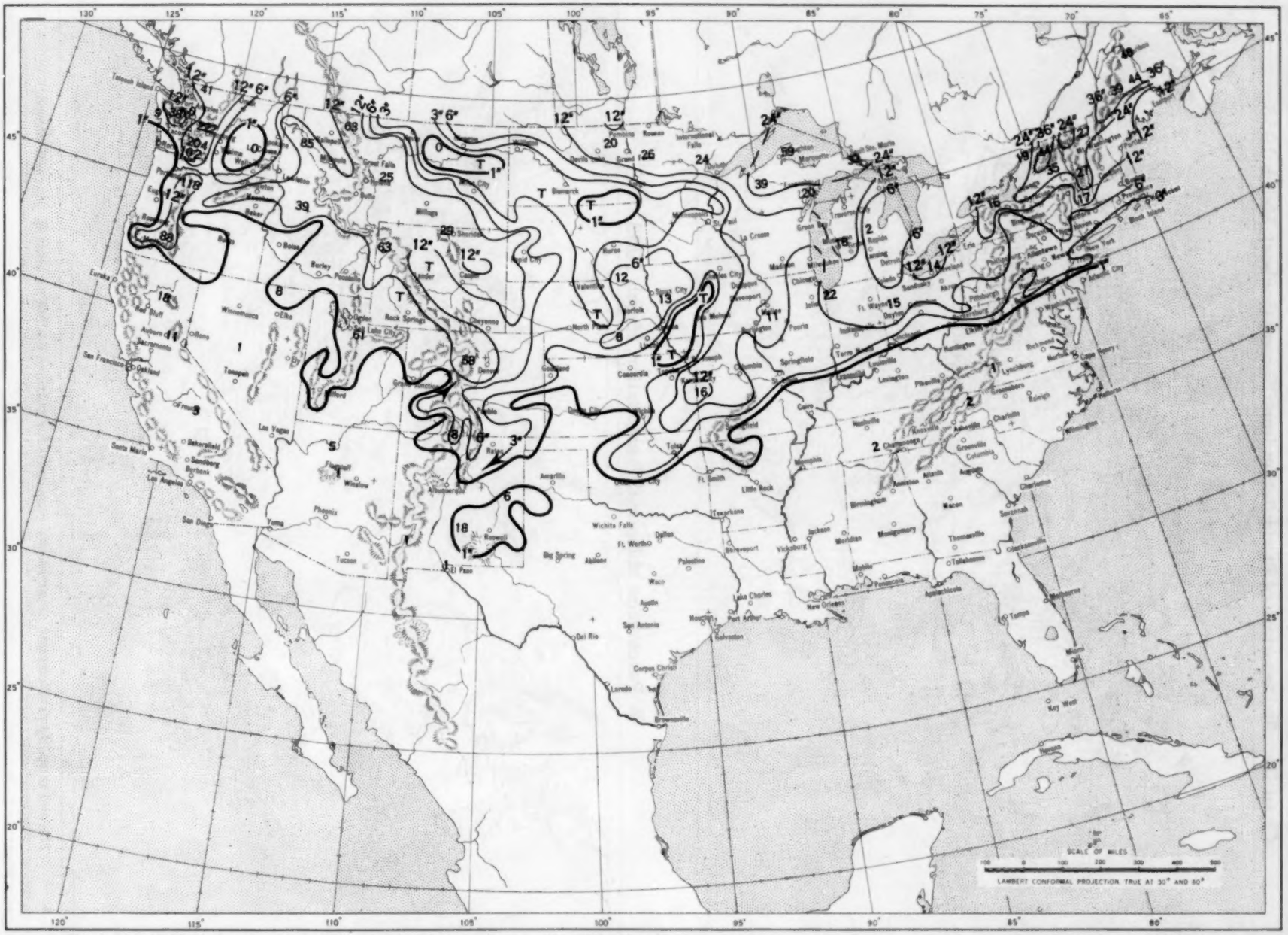

This is the total of unmelted snowfall recorded during the month at Weather Bureau and cooperative stations. This chart and Chart V are published only for the months of November through April although of course there is some snow at higher elevations, particularly in the far West, earlier and later in the year.

Chart V. A. Percentage of Normal Snowfall, March 1955.

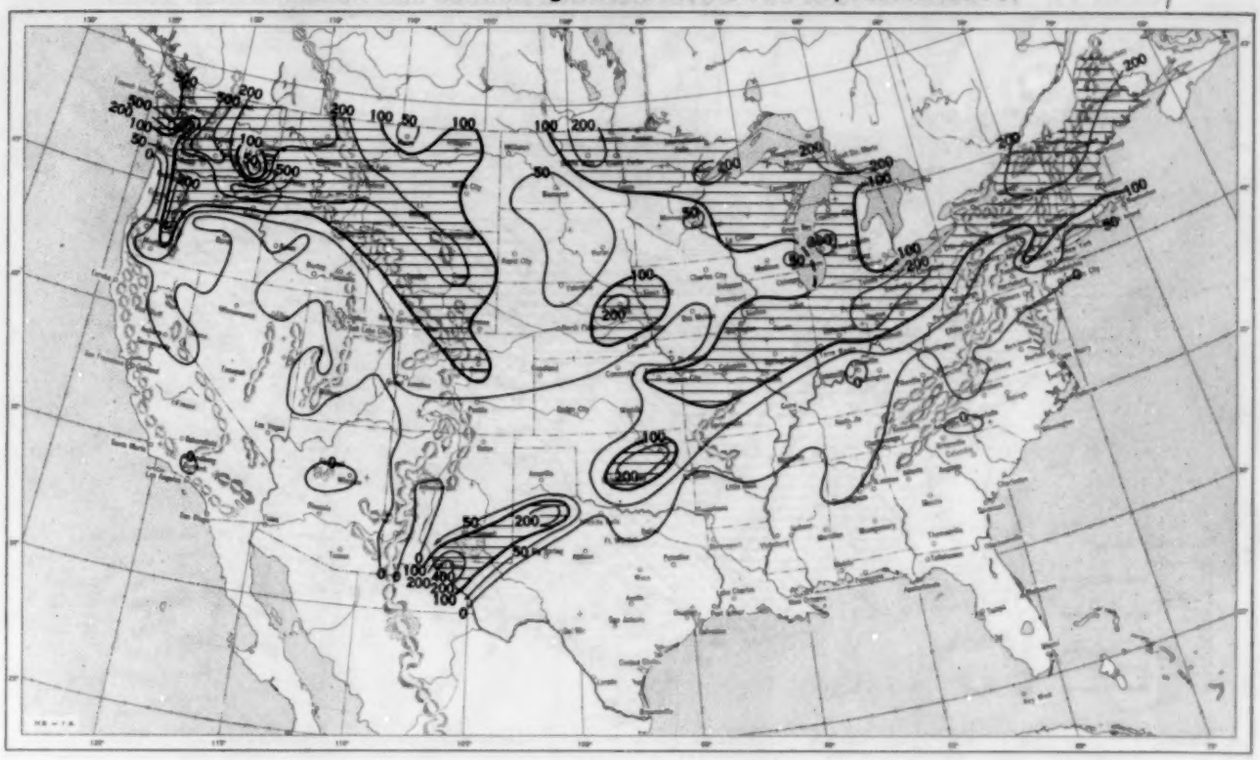

B. Depth of Snow on Ground (Inches). 7:30 a. m. E. S. T., March 28, 1955.

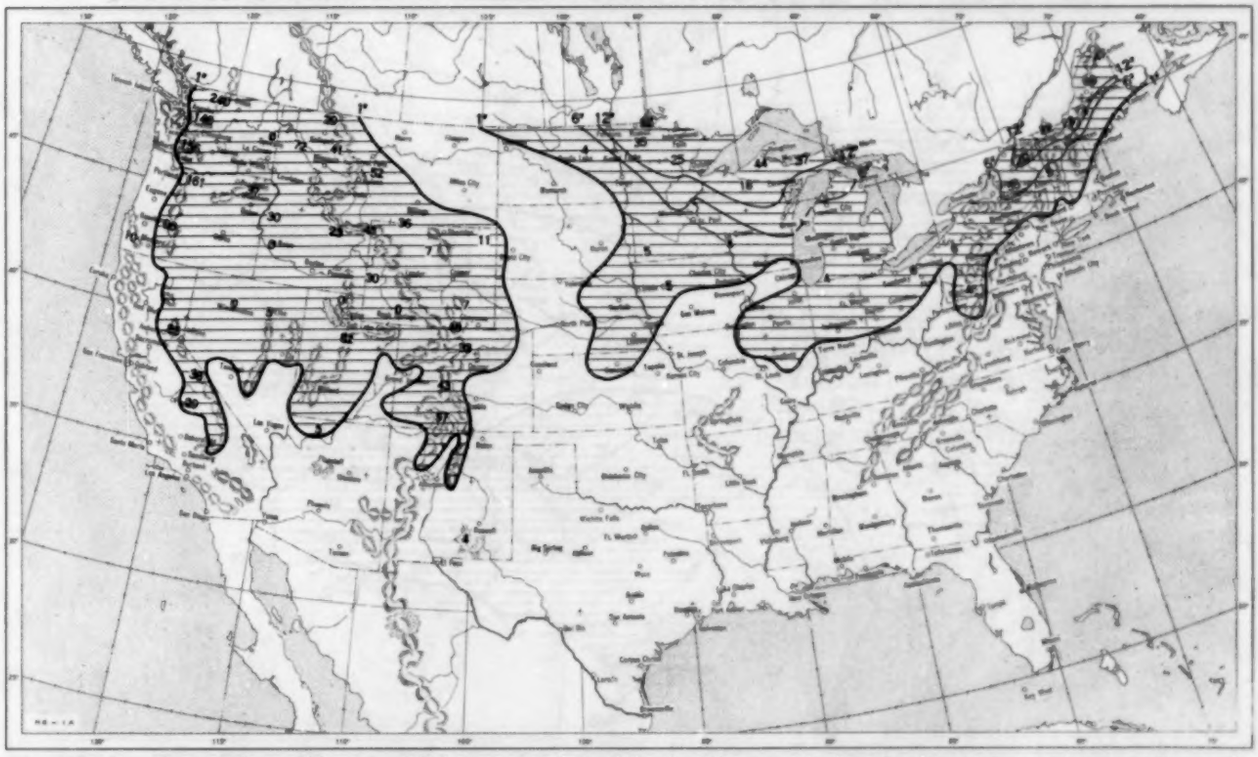

A. Amount of normal monthly snowfall is computed for Weather Bureau stations having at least 10 years of record. B. Shows depth currently on ground at 7:30 a. m. E. S. T., of the Tuesday nearest the end of the month. It is based on reports from Weather Bureau and cooperative stations. Dashed line shows greatest southern extent of snowcover during month.

Chart VI. A. Percentage of Sky Cover Between Sunrise and Sunset, March 1955.

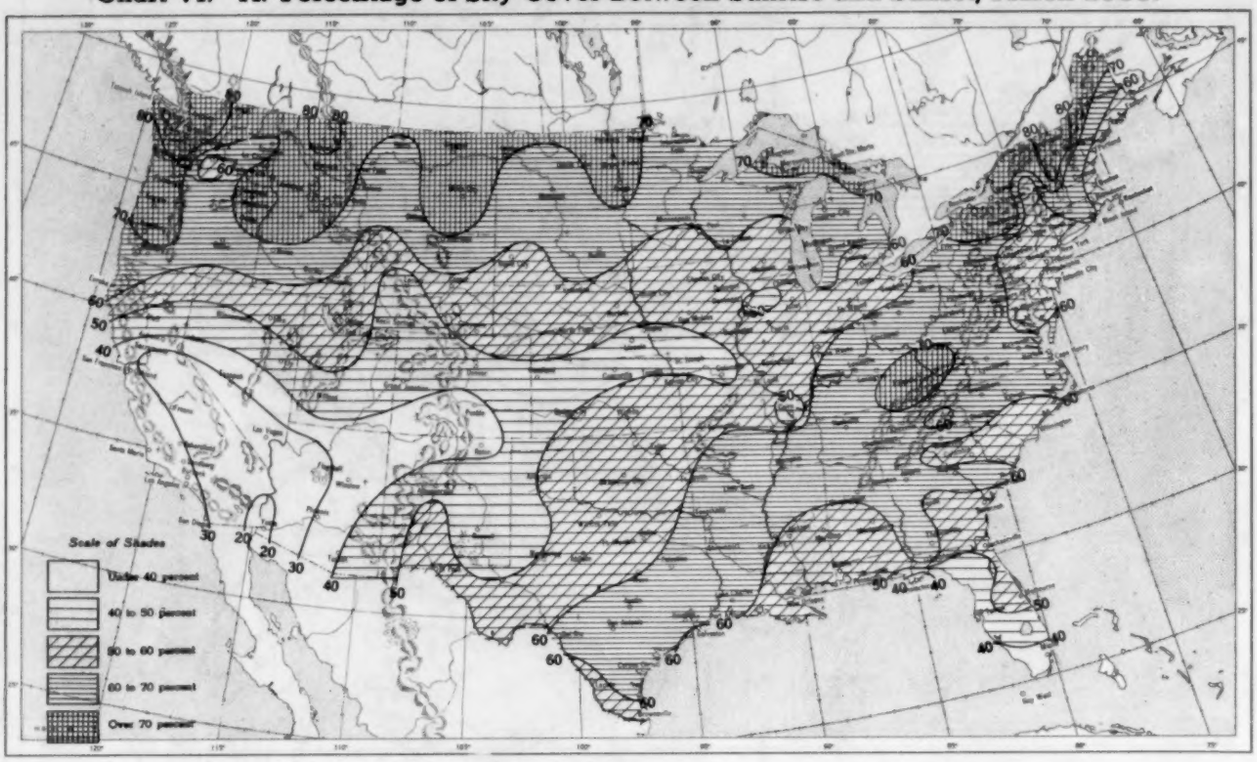

B. Percentage of Normal Sky Cover Between Sunrise and Sunset, March 1955.

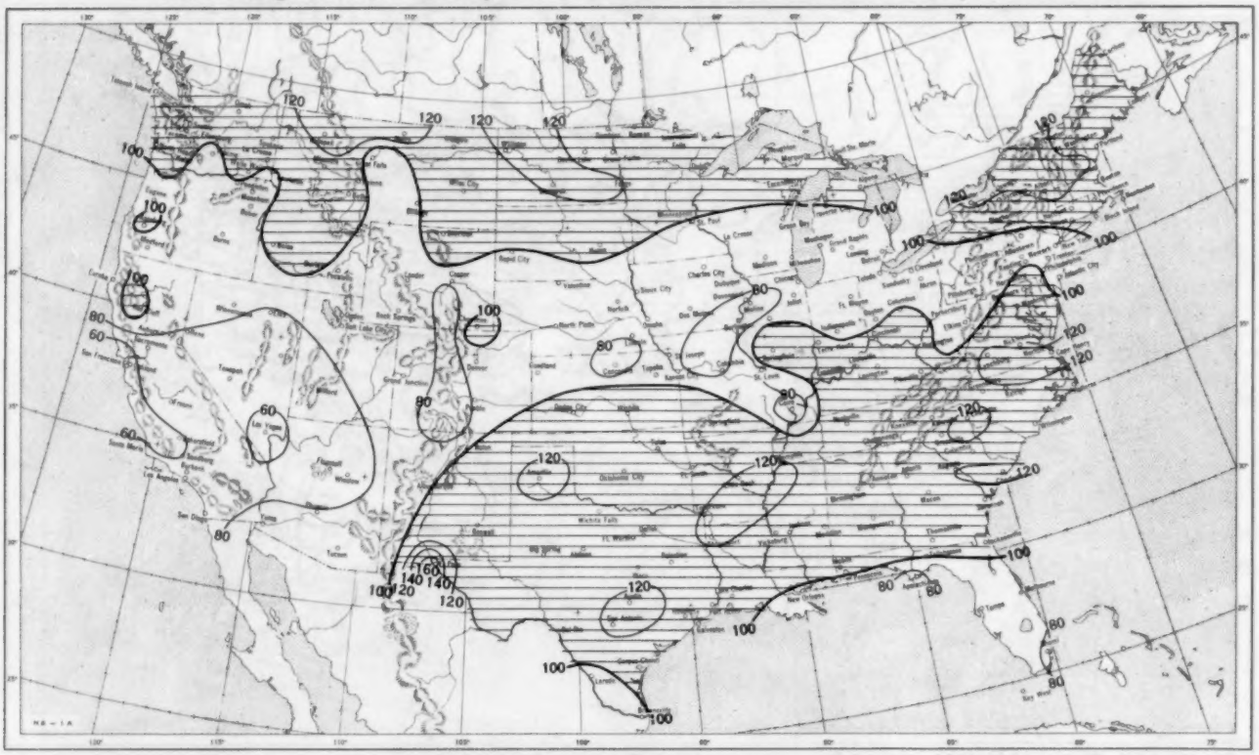

A. In addition to cloudiness, sky cover includes obscuration of the sky by fog, smoke, snow, etc. Chart based on visual observations made hourly at Weather Bureau stations and averaged over the month. B. Computations of normal amount of sky cover are made for stations having at least 10 years of record.

Chart VII. A. Percentage of Possible Sunshine, March 1955.

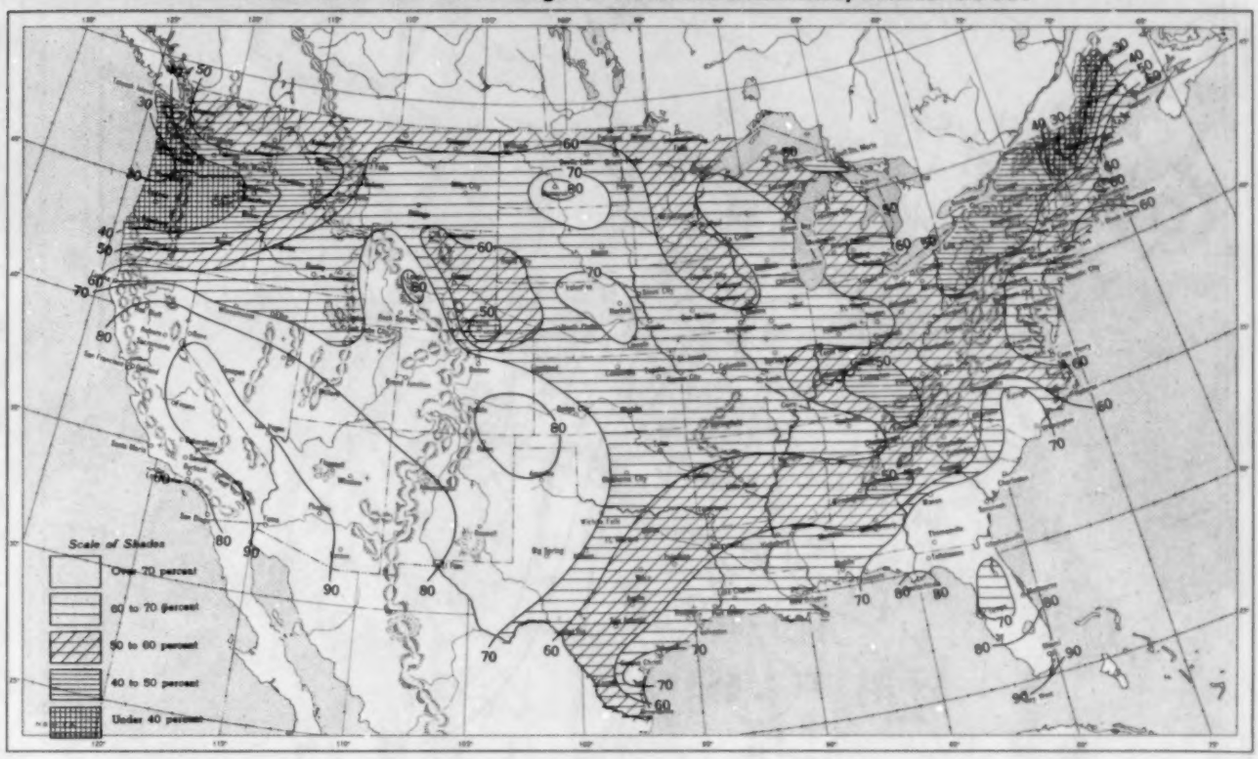

B. Percentage of Normal Sunshine, March 1955.

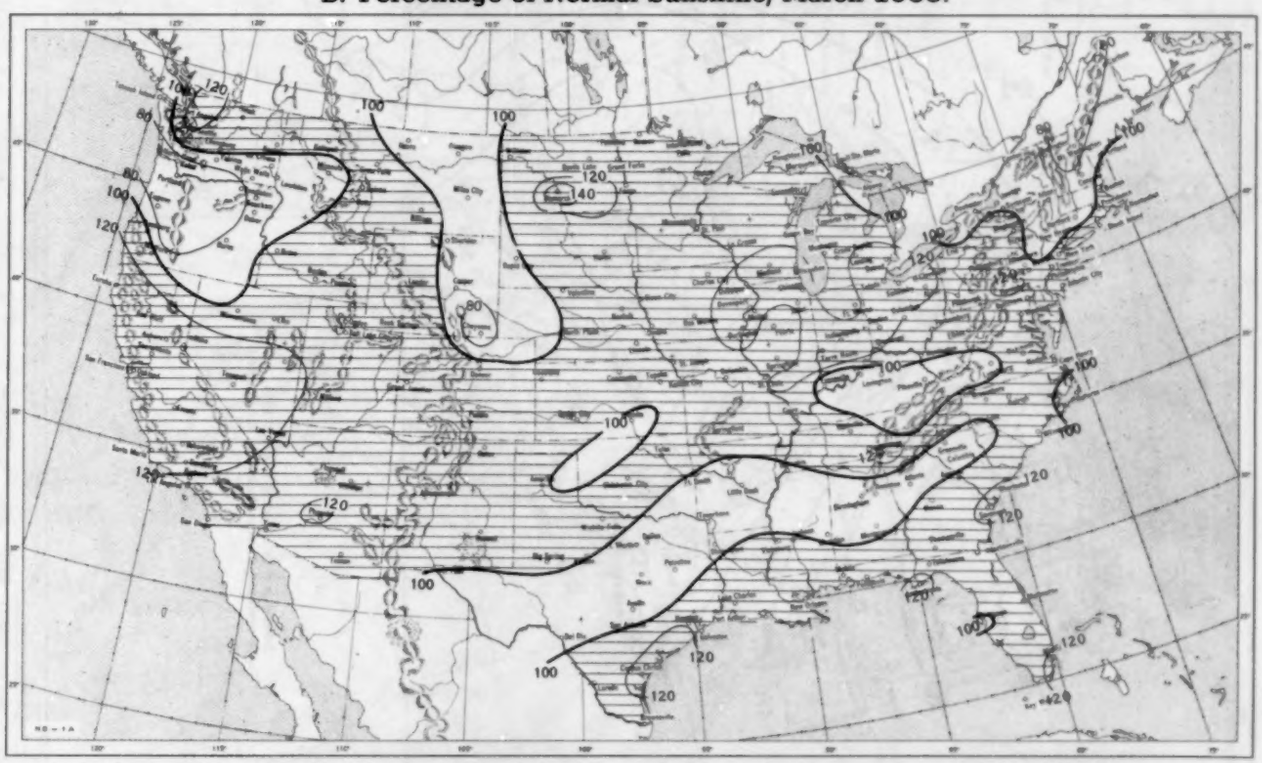

A. Computed from total number of hours of observed sunshine in relation to total number of possible hours of sunshine during month. B. Normals are computed for stations having at least 10 years of record.

Chart VIII. Average Daily Values of Solar Radiation, Direct + Diffuse, March 1955. Inset: Percentage of Normal Average Daily Solar Radiation.

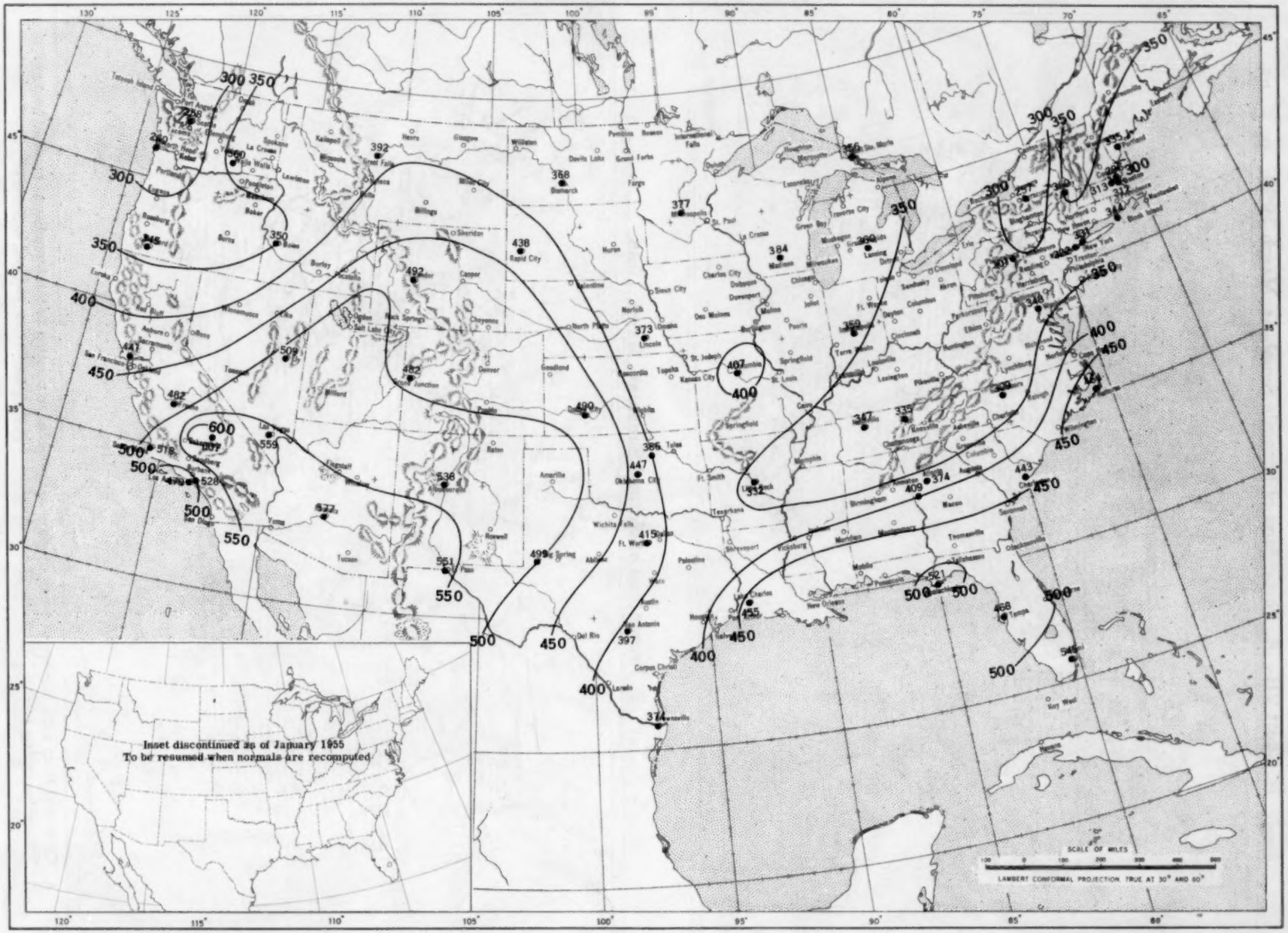
Inset discontinued as of January 1955
To be resumed when normals are recomputed
SCALE OF MILES
LAMBERT CONFORMAL PROJECTION, TRUE AT 30° AND 60°

Chart shows mean daily solar radiation, direct + diffuse, received on a horizontal surface in langleys (1 langley = 1 gm. cal. cm. $^{-2}$). Basic data for isolines are shown on chart. Further estimates are obtained from supplementary data for which limits of accuracy are wider than for those data shown.

Chart IX. Tracks of Centers of Anticyclones at Sea Level, March 1955.

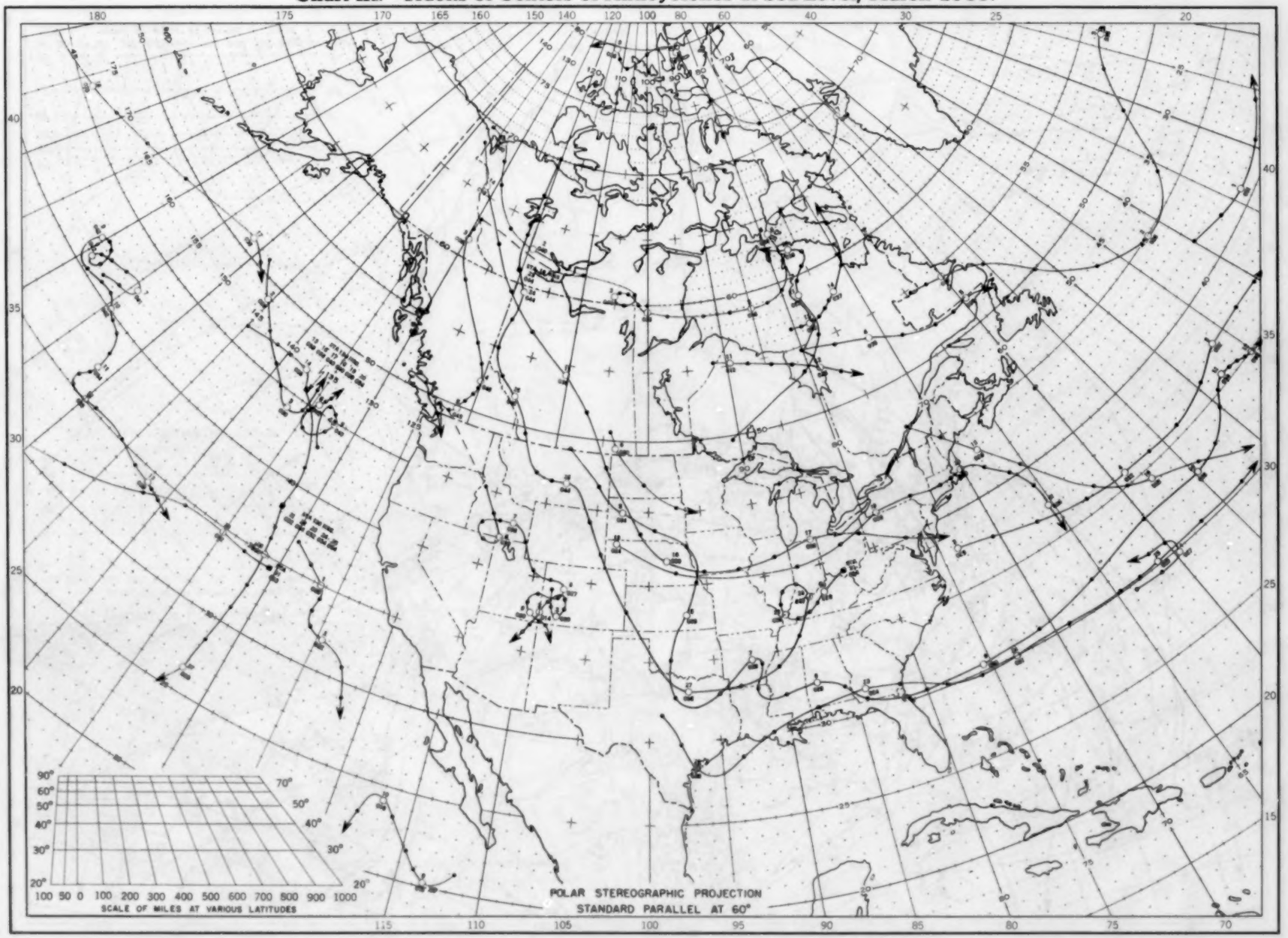
SCALE OF MILES AT VARIOUS LATITUDES
100 50 0 100 200 300 400 500 600 700 800 900 1000
POLAR STEREOGRAPHIC PROJECTION
STANDARD PARALLEL AT 60°

Circle indicates position of center at 7:30 a. m. E. S. T. Figure above circle indicates date, figure below, pressure to nearest millibar. Dots indicate intervening 6-hourly positions. Squares indicate position of stationary center for period shown. Dashed line in track indicates reformation at new position. Only those centers which could be identified for 24 hours or more are included.

Chart X. Tracks of Centers of Cyclones at Sea Level, March 1955.

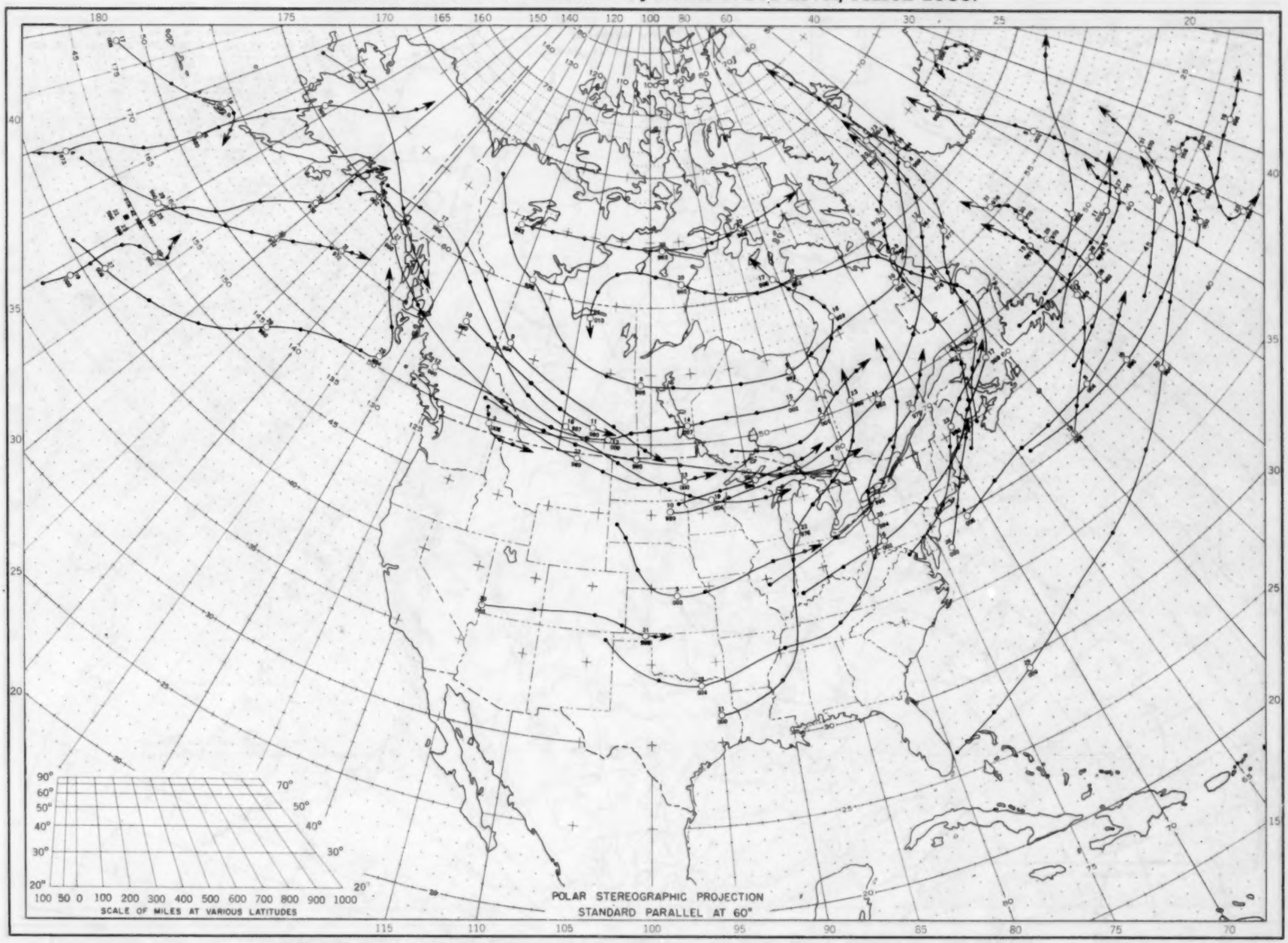

Circle indicates position of center at 7:30 a. m. E. S. T. See Chart IX for explanation of symbols.

Chart XI. Average Sea Level Pressure (mb.) and Surface Windroses, March 1955. Inset: Departure of Average Pressure (mb.) from Normal, March 1955.

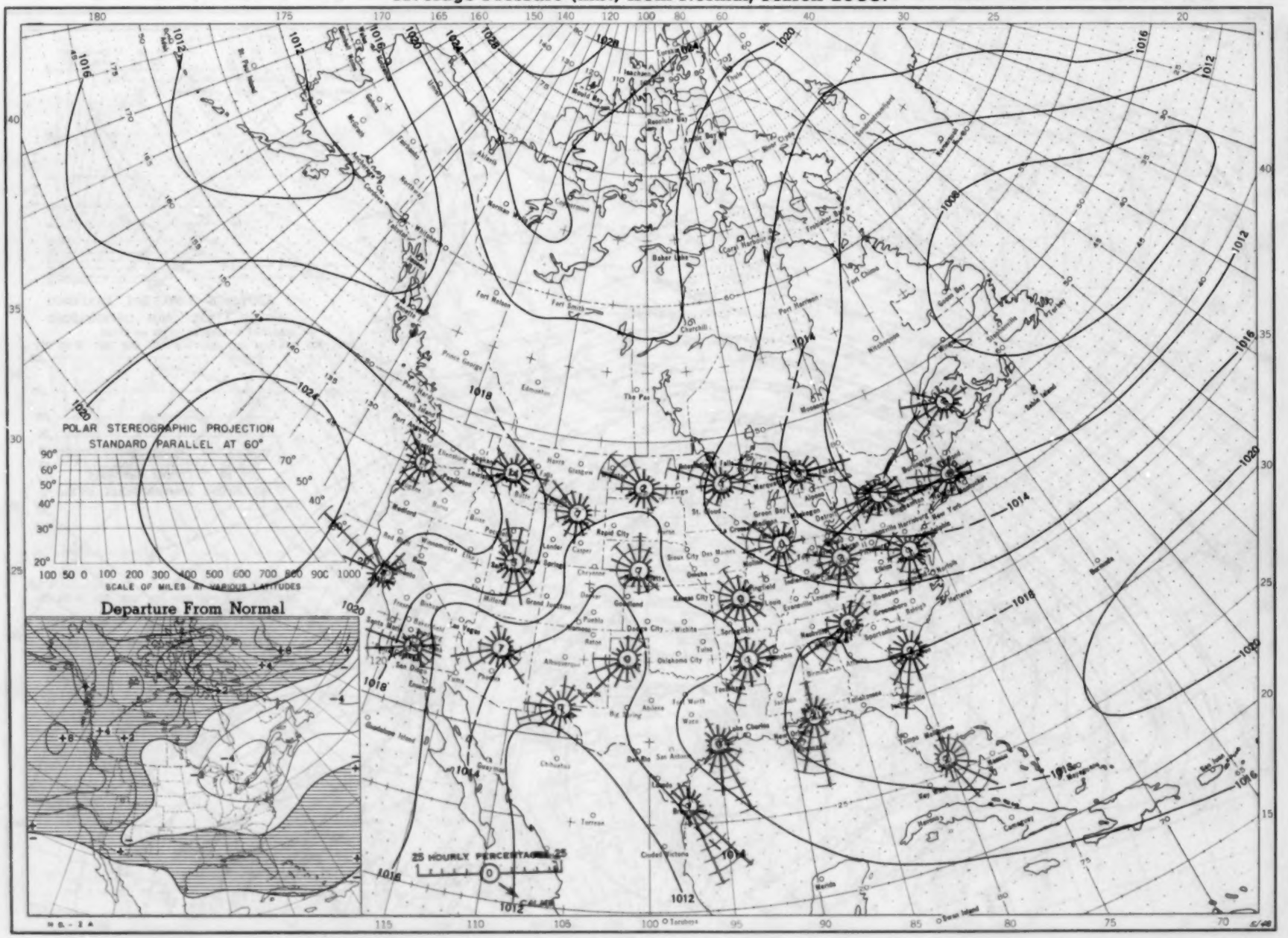

Average sea level pressures are obtained from the averages of the 7:30 a. m. and 7:30 p. m. E. S. T. readings. Windroses show percentage of time wind blew from 16 compass points or was calm during the month. Pressure normals are computed for stations having at least 10 years of record and for 10° intersections in a diamond grid based on readings from the Historical Weather Maps (1899-1939) for the 20 years of most complete data coverage prior to 1940.

Chart XII. Average Dynamic Height in Geopotential Meters (1 g.p.m. = 0.98 dynamic meters) of the 850-mb. Pressure Surface, Average Temperature in °C. at 850 mb., and Resultant Winds at 1500 Meters (m.s.l.), March 1955.

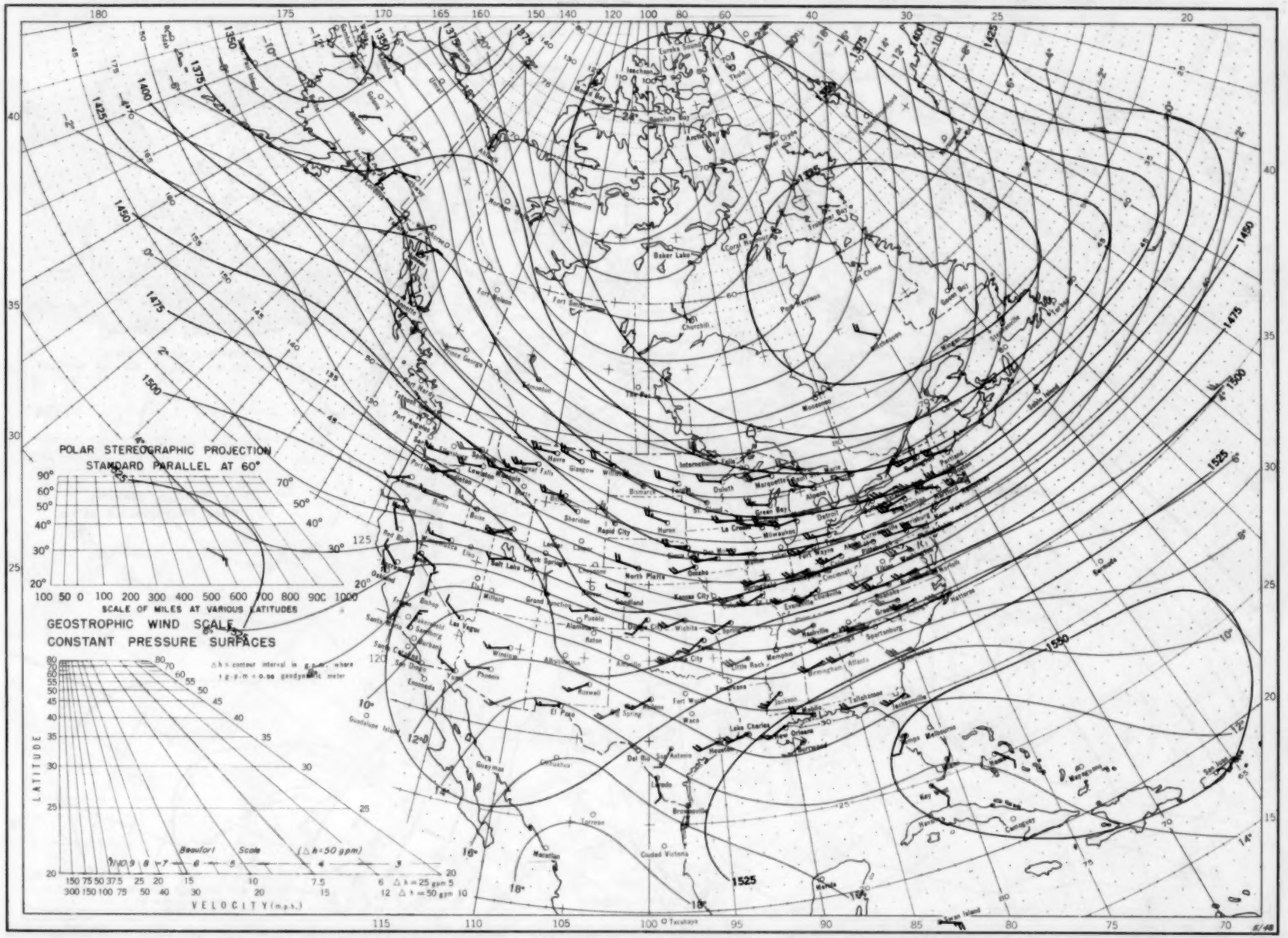

Contour lines and isotherms based on radiosonde observations at 0300 G. M. T. Winds shown in black are based on pilot balloon observations at 2100 G. M. T.; those shown in red are based on rawins taken at 0300 G. M. T. Wind barbs indicate wind speed on the Beaufort scale.

Chart XIII. Average Dynamic Height in Geopotential Meters (1 g.p.m.. = 0.98 dynamic meters) of the 700-mb. Pressure Surface, Average Temperature in °C. at 700 mb., and Resultant Winds at 3000 Meters (m.s.l.), March 1955.

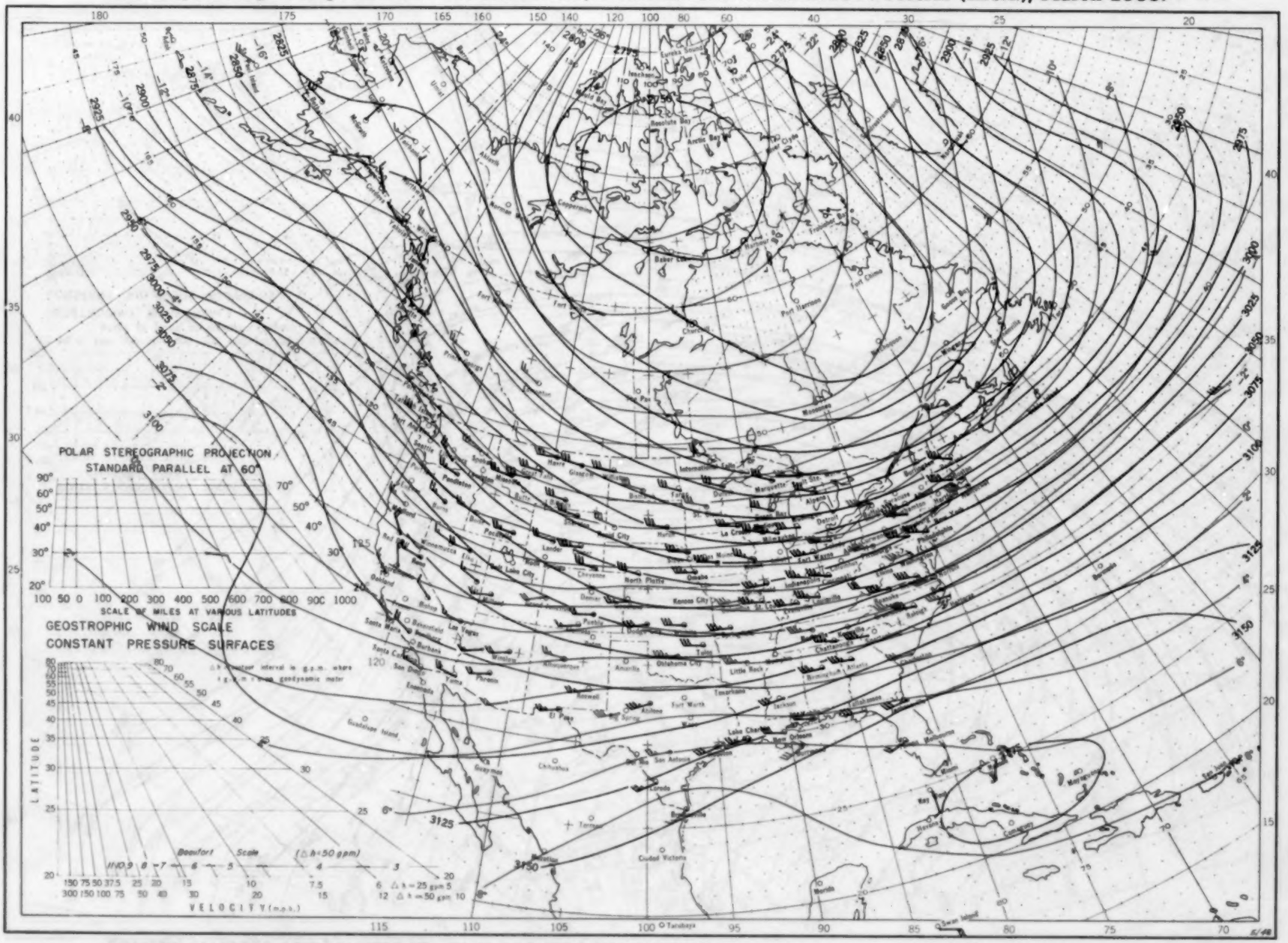

Contour lines and isotherms based on radiosonde observations at 0300 G. M. T. Winds shown in black are based on pilot balloon observations at 2100 G. M. T.; those shown in red are based on rawins taken at 0300 G. M. T. Wind barbs indicate wind speed on the Beaufort scale.

Chart XIV. Average Dynamic Height in Geopotential Meters (1 g.p.m. = 0.98 dynamic meters) of the 500-mb. Pressure Surface, Average Temperature in °C. at 500 mb., and Resultant Winds at 5000 Meters (m.s.l.), March 1955.

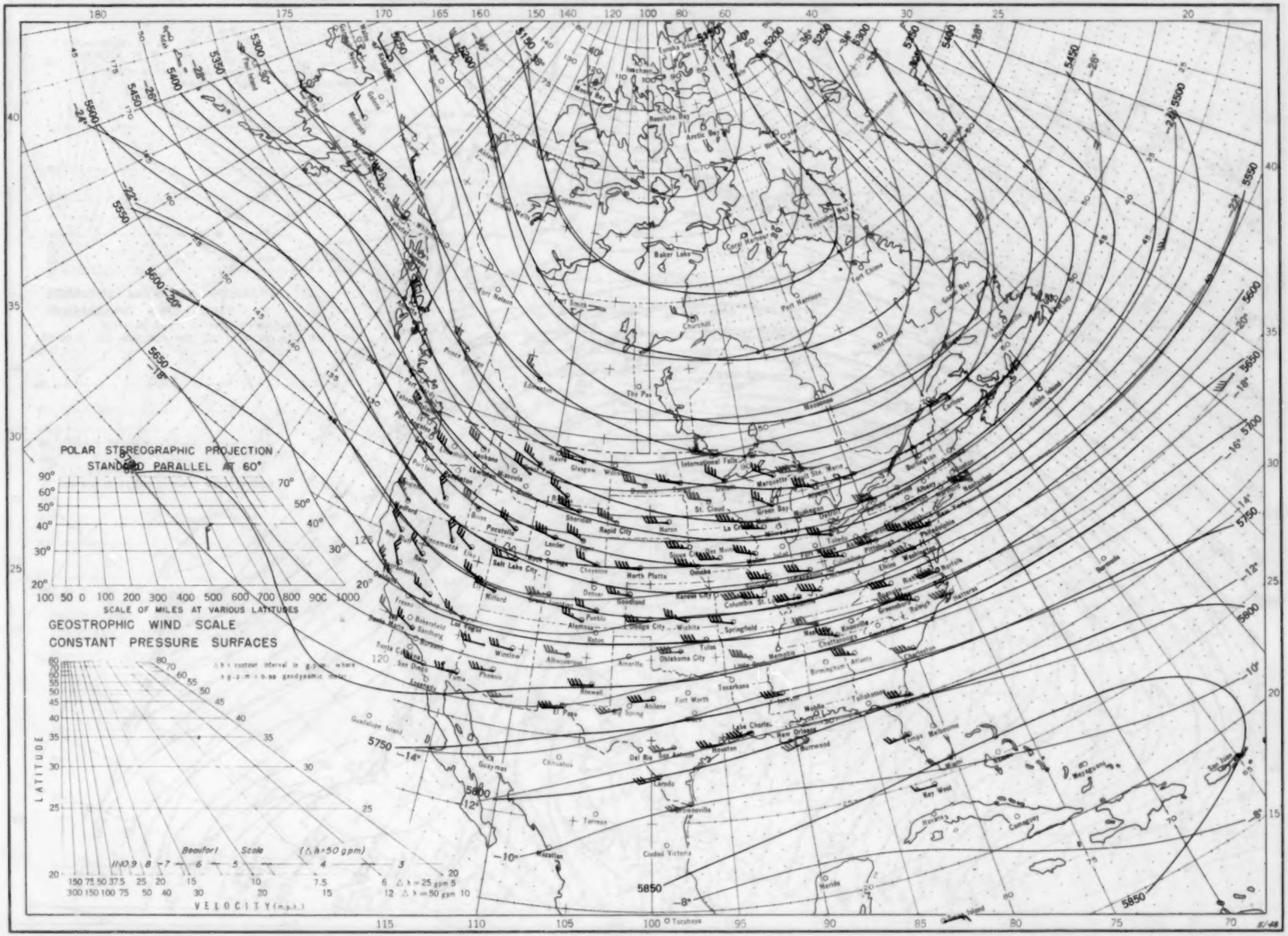

Contour lines and isotherms based on radiosonde observations at 0300 G. M. T. Winds shown in black are based on pilot balloon observations at 2100 G. M. T.; those shown in red are based on rawins at 0300 G. M. T. Wind barbs indicate wind speed on the Beaufort scale.

Chart XV. Average Dynamic Height in Geopotential Meters (1 g.p.m. = 0.98 dynamic meters) of the 300-mb. Pressure Surface, Average Temperature in °C. at 300 mb., and Resultant Winds at 10,000 Meters (m.s.l.), March 1955.

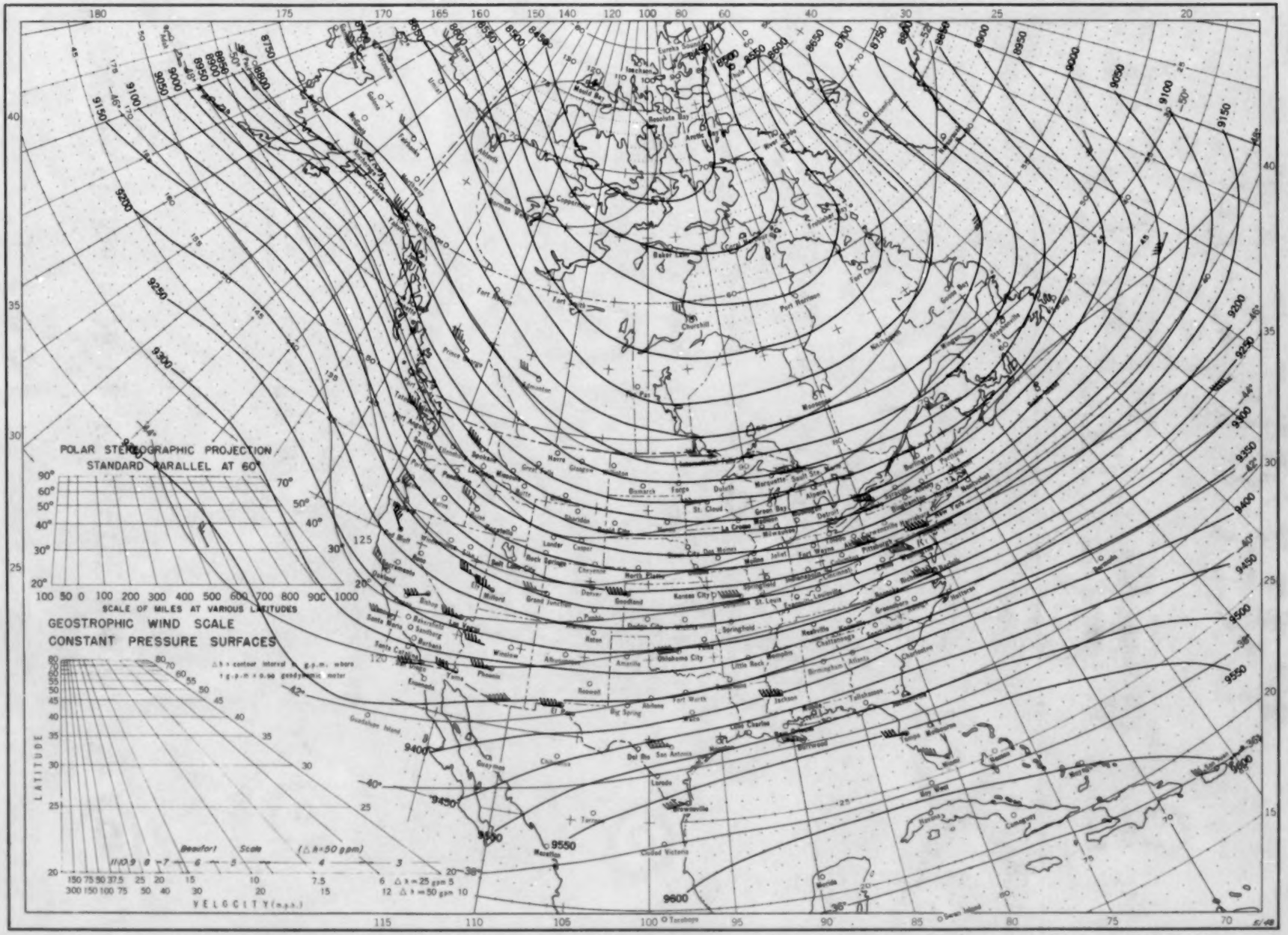

Contour lines and isotherms based on radiosonde observations at 0300 G. M. T. those shown in red are based on rawins at 0300 G. M. T. Winds shown in black are based on pilot balloon observations at 2100 G. M. T.; Wind barbs indicate wind speed on the Beaufort scale.